Università degli Studi di Cagliari

PHD DEGREE

Industrial Engineering

Cycle XXXII

Design, modelling, evaluation and comparison of energy systems for the production and use of renewable methanol using recycled CO_2

Scientific Disciplinary Sector

ING-IND/09

PhD Student:	Ing. Francesco Lonis
Coordinator of the PhD Programme	Prof. Ing. Francesco Aymerich
Supervisor	Prof. Ing. Giorgio Cau
Co-supervisor	Prof. Ing. Vittorio Tola

Final exam. Academic Year 2018 – 2019

Thesis defence: January-February 2020 Session

Francesco Lonis gratefully acknowledges Sardinian Regional Government for the financial support of her/his PhD scholarship (P.O.R. Sardegna F.S.E. - Operational Programme of the Autonomous Region of Sardinia, European Social Fund 2014-2020 - Axis III Education and training, Thematic goal 10, Investment Priority 10ii), Specific goal 10.5

Part of this thesis has been based on works and results published in the following peer-reviewed papers:

1. Lonis F, Tola V, Cau G. Renewable methanol production and use through reversible solid oxide cells and recycled CO_2 hydrogenation. Fuel 2019;246:500–15. https://doi.org/10.1016/j.fuel.2019.02.108

2. Lonis F, Tola V, Cau G. Integrated energy system for the production and use of renewable methanol via alkaline electrolysis and solid oxide fuel cells. Proceedings of the 11th International Conference on Applied Energy 2019. Accepted for publication, in Press

3. Lonis F, Tola V, Cascetta M, Arena S, Cau G. Performance evaluation of an integrated energy system for the production and use of renewable methanol via water electrolysis and CO2 hydrogenation. Proceedings (AIP Conference Proceedings) of the 74th ATI (Associazione Termotecnica Italiana) Conference 2019. 2019;020099. https://doi.org/10.1063/1.5138832

and works presented at the following conferences:

1. Lonis F, Tola V, Cau G. Renewable methanol production and use through reversible solid oxide cells and recycled CO_2 hydrogenation. 9th International Freiberg Conference on IGCC & XtL Technologies 2018, Berlin, Germany 2018

2. Lonis F, Tola V, Cau G. Integrated energy system to produce and use renewable methanol via alkaline electrolysis and solid oxide fuel cell. 11th International Conference on Applied Energy 2019 ICAE 2019, Västerås, Sweden 2019

3. Lonis F, Tola V, Cascetta M, Arena S, Cau G. Performance evaluation of an integrated energy system for the production and use of renewable methanol via water electrolysis and CO_2 hydrogenation. Associazione Termotecnica Italiana ATI Conference 2019, Modena, Italy 2019

Acknowledgements

I would like to thank my supervisor, Prof. Giorgio Cau, for the opportunity of undertaking this PhD in such an interesting topic, and his precious support and advice during the three-year PhD programme at the Department of Mechanical, Chemical and Materials Engineering (DIMCM) of the University of Cagliari. I would also like to thank my co-supervisor, Prof. Vittorio Tola, for his important contribution in the work carried out together.

I would like to thank Prof. Mercedes Maroto-Valer, my abroad supervisor at the Heriot-Watt University, for allowing me to carry out research in her research group.

I would like to thank the external reviewers, Prof. Chakib Bouallou and Prof. Jin Xuan, for the careful review of my thesis.

I would like to express my gratitude to all my colleagues and friends at the DIMCM and at Heriot-Watt University for the good time spent together and for being good friends, and to my PhD colleagues with whom I shared this experience: Daniele, Giuseppina, Maria Silvia, Nayeem, and especially Joseph for his comforting words and his contagious will to succeed in this challenge.

My sincere thanks to all my friends that were there for me during these three years.

A special thanks to Anna for her sincere love and the strong support she always gives me.

Infine, un ringraziamento speciale ai miei genitori, Guido ed Enrica, ai miei fratelli, Giovanni e Stefano, e ai miei parenti senza i quali non avrei raggiunto questo traguardo e senza cui non sarei diventato la persona che sono oggi.

Abstract

The topic of this PhD thesis is focused on the analysis of complex energy systems for the production of high-grade fuels such as methanol and dimethyl ether (DME) exploiting renewable energy sources (RES) for electrolytic hydrogen production and captured CO_2, in the context of a decarbonisation of the future society. The produced fuels might be used to generate electricity in a thermal engine (for instance reciprocating internal combustion engine or gas turbine) or for other uses such as transportation and heat or even as a chemical feedstock for different applications. Specifically, in this work the energy storage application is considered. Hydrogen is produced using RES and/or excess electric energy from the grid and converted to methanol by a methanol synthesis process based on CO_2 hydrogenation. The product is stored at ambient pressure. Subsequently, methanol is used in a fuel cell to produce electricity when required by the grid.
The energy system conceived to perform such a process is analysed mainly from the point of view of mass and energy balances of the components and sections constituting the system. Different layouts are studied to perform a comprehensive analysis of various solutions. Simulations of the single components are carried out mainly using the software Aspen Plus V8.8, MATLAB and MATLAB-Simulink. Electrochemical and mathematical models are implemented in the computational blocks of Aspen Plus to simulate the considered processes.
The general layout of the system consists of water electrolysis, CO_2 hydrogenation to methanol, methanol storage, methanol utilisation in a fuel cell, and a heat integration section to store or use the heat produced in the fuel cell. Water electrolysis via high temperature solid oxide electrolysis cells (SOEC) and alkaline electrolysis are considered, while the methanol synthesis section (MSS) is based on catalytic CO_2 hydrogenation and the fuel cell section is fixed as a high temperature solid oxide fuel cell (SOFC). SOEC and SOFC can be also considered as two operational modes of the same apparatus, namely reversible solid oxide cells (RSOC). A thermal energy storage (TES) system and an organic Rankine cycle (ORC) are also considered to boost the performance of the plant. In particular, the considered reference layout is composed of a SOEC to produce hydrogen that is sent to the MSS where CO_2 hydrogenation and methanol purification take place. Subsequently, when required, methanol is used in the SOFC to generate electricity and thermal energy as a by-product. Thermal energy contained in the SOFC exhaust gases is stored using a TES system in a latent heat packed bed of phase change materials (PCM). This energy is supplied back to the SOEC to vaporise water and optimise the energy requirements.
Variations on the reference layout allow getting a comprehensive view of different approaches and integrations. The SOFC system is the same in each considered solution, just like the MSS that is based on catalytic CO_2 hydrogenation and is not varied from one layout to the other. The SOEC, being a relatively new technology, is compared with the commercially and industrially affirmed alkaline electrolyser technology. When coupled to the alkaline electrolyser, the exhaust heat of the SOFC is used to run an ORC.
The performance indexes defined in this work allowed an objective comparison between the different solutions. Each main subsection was characterised by an efficiency consistent with literature data for similar systems. Depending on the chosen configuration, the optimal efficiency of the overall plant is found to be between 34 and 35% in case of commercially mature technology (AEL) and innovative technology (SOEC), respectively, while the power-to-liquids efficiency is between 57 and 71%. These values are consistent with both literature data regarding similar power-to-X technologies and with other energy storage technologies. Since the two main layouts are characterised by similar efficiencies, the one based on commercially ready technology (AEL) might be considered in a short-term perspective, while the one based on innovative technology (RSOC) might be considered in a long-term perspective.

Table of contents

Nomenclature

Acronyms			
AEL	Alkaline electrolysis/electrolyser	MSS	Methanol synthesis section
CAES	Compressed air energy storage	ORC	Organic Rankine cycle
CCUS	Carbon capture utilisation and storage	PCM	Phase change material
CRI	Carbon Recycling International	PEM	Polymeric electrolyte membrane
DME	Dimethyl ether	PHS	Pumped hydroelectric storage
EC	European Commission	PtG	Power-to-gas
ECCP	European Climate Change Programme	PtL	Power-to-liquids
EER	European Energy Roadmap	PtX	Power-to-X
EES	Electric energy storage	PV	Photovoltaic
FES	Flywheel energy storage	RES	Renewable energy sources
FT	Fischer-Tropsch	RSOC	Reversible solid oxide cell
GHG	Greenhouse gas	SMES	Superconducting magnetic energy storage
HEX	Heat exchanger	SOC	Solid oxide cell
LCA	Life cycle assessment	SOEC	Solid oxide electrolyser cell
LHTES	Latent heat thermal energy storage	SOFC	Solid oxide fuel cell
LHV	Lower heating value	TES	Thermal energy storage
LPG	Liquefied petroleum gas	TRL	Technology readiness level
MeOH	Methanol		

Equation symbols			
d_{an} , d_{cat}	Anode and cathode thickness [m]	η_{PtL}	Power-to-liquids efficiency
$D_{electrode}^{eff}$	Electrode effective diffusion coefficient [m^2/s]	φ_{AEL}	AEL-MSS corrective factor
D_{i-j}	Molecular diffusion coefficient (species i in species j) [m^2/s]	φ_{SOEC}	SOEC-MSS corrective factor
$D_{i,K}$	Knudsen diffusion coefficient for the species i [m^2/s]	F	Faraday constant [C/mol]
d_p	Mean pore size [m]	γ_{an} , γ_{cat}	Pre-exponential factors [A/m^2]
δ_{O_2}	Oxygen Knudsen diffusion vs. effective diffusion ratio	H_i	Lower heating value [kJ/kg]
E_0	Reversible potential [V]	J	Current density [A/m^2]
$E_{act,an}$, $E_{act,cat}$	Activation energy levels [J/mol]	$J_{0,i}$	Exchange current densities [A/m^2]
E_{eq}	Equilibrium voltage [V]	k_B	Boltzmann's constant [J/K]
$\dot{E}_{MSS}$	MSS inlet external power [kW]	k_i	Kinetic constants
E_{SOEC}	Electrolyser net voltage (SOEC) [V]	$M_{i,j}$	Molecular weight [g/mol]
E_{SOFC}	Cell net voltage (SOFC) [V]	$\dot{m}_i$	Mass flow rate [kg/s] or [kg/h]
$\varepsilon_{i,j}$	Lennard-Jones energy [K]	Ω_D	Diffusion collision integral
ξ	Tortuosity	p_c	Cell operating pressure [Pa]
η	Porosity	p_i	Partial pressure of species i
η_{act} / V_{act}	Activation overpotentials [V]	p_i^0	Electrodes mean pressure [Pa]
η_{conc}	Concentration overpotentials [V]	P_{AEL}	AEL electric power [kW]
η_{ohm} / V_{ohm}	Ohmic overpotential [V]	$P_{BOP,AEL}$	AEL auxiliaries power [kW]
η_{AEL}	AEL efficiency	$P_{BOP,MSS}$	MSS auxiliaries power [kW]
$\eta_{AEL,R}$	Rectified AEL efficiency	P_{SOEC}	SOEC electric power [kW]

η_F	Faraday efficiency	$P_{BOP,SOEC}$	SOEC auxiliaries power [kW]
η_G	System global efficiency	P_{SOFC}	SOFC electric power [kW]
$\eta_{G,ORC}$	System global efficiency with ORC	$P_{BOP,SOFC}$	SOFC auxiliaries power [kW]
η_{SOEC}	SOEC efficiency	R	Universal gas constant [J/(mol K)]
$\eta_{SOEC,R}$	Rectified SOEC efficiency	r_{CH_3OH} , r_{CO}	Methanol and CO reaction rates
η_{SOFC}	SOFC efficiency	ρ	Electrical resistivity [Ω m]
$\eta_{SOFC+ORC}$	SOFC + ORC efficiency	$\sigma_{i,j}$	Mean characteristic length [Å]
$\eta_{RSOC,G}$	Gross RSOC efficiency	T_c	Cell operating temperature [K]
η_{RSOC}	Net RSOC efficiency	Γ	Temperature coefficient
η_{MSS}	MSS efficiency	t_{el}	Electrolyte thickness [m]
$\eta_{MSS,C}$	MSS chemical energy conversion efficiency		

List of figures

List of tables

Chapter 1

Introduction

1.1 Motivation and objective

The constant increase in energy demand and the problems related to greenhouse gas emissions (GHG), and in particular CO_2, typical of the energy sources mainly adopted in this historical period, brought about the need for studying and developing new energy systems capable of reducing the threat they are responsible for. To reach this objective, the European Commission (EC) has been working to promote carbon friendly strategies across the Members since 1991. Among these strategies, the adoption of renewable energy sources (RES), the thrust towards energy efficiency and lower energy consumptions, taxation on conventional energy sources, and the development of a carbon market through the emissions trading system (ETS) have been adopted [1]. In 1992, the United Nations Framework Convention on Climate Change (UNFCCC) was established to prevent dangerous human interferences with the climate system by following a number of guidelines and commitments. In this context, 195 nations ratified the Convention with the objective of stabilising the GHG emissions and concentration levels to prevent important and irreversible anthropogenic changes in the environment [2]. To achieve the limits defined during the UNFCCC and the subsequent Kyoto Protocol in 1997, as well as other protocols and limits defined during the following years, the EC developed the European Climate Change Programme (ECCP) to define and coordinate the operations needed to achieve the objectives to prevent disastrous changes in the environment with the establishment of numerous working groups to identify options and potential approaches and technologies to reduce GHG emissions [3,4].
Nowadays, the main objectives to reduce climate change follow what is reported on the European Energy Roadmap (EER), firstly established in 2011. Considering 450 CO_2 ppm in the atmosphere as a threshold of no-return that should not be exceeded to maintain the mean global temperature below 2 °C by 2100, that in the pre-industrial period the average atmospheric CO_2 concentration was only 275 ppm, and that the last detection from the Mauna Loa Observatory, Hawaii, in September 2019 was approximately 409 ppm [5], the urgency of acting against this change is clear. The first universal and legally binding global climate deal was signed by 195 countries in December 2015 during the United Nations Climate Change Conference (COP21). The parties agreed to define the maximum limit of the increase in the average surface temperature well below 2 °C, accepting a maximum variation of +1.5 °C compared to the pre-industrial average temperature [6,7]. To achieve this objective, a reduction of GHG global emissions by 50% before 2050 is necessary. Nevertheless, the developed countries must reduce their emission by 80% compared to the emissions levels of 1990. The EU, according to the EER, has to reduce GHG emissions by 40% by 2030, 60% by 2040, and 80-95% by 2050 contemporarily with an increase in the energy production and consumption from RES and an improvement in energy efficiency [8]. Regarding the energy efficiency aspect, the European objective is to increase it by 20% by 2020 and by 32.5% by 2030. At the same time, RES share is set to 20% by 2020 and 32% by 2030. The reduction in the emissions should be done in every sector, from power to residential and tertiary, from industry to transport and agriculture. Figure 1.1 shows the reduction to be accomplished in each sector by 2050, and the present policy applied nowadays. The policy currently applied would lead to a reduction by only 40% by 2050.

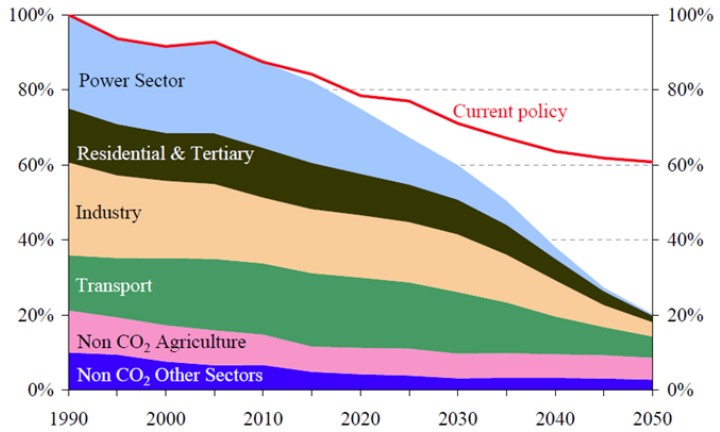

Fig. 1.1 – Emissions reduction by sector to be applied by 2050 - EER [8]

As shown in Fig. 1.1, the power sector is the sector where the highest reduction might be achieved, leading to almost a 0% share of GHG emissions by 2050. This is related to the technological and economical potential within this sector. The production of electricity exploiting RES such as solar, wind, water from hydroelectric dams, waves and tides, and biomass, the use of low-carbon technologies such as nuclear power, and carbon capture utilisation and storage (CCUS) in traditional power plants would allow a strong reduction in emissions coming from the power and energy generation sector.

The effort made to reduce now the future GHG emissions by turning to a low-carbon economy would guarantee a further improvement and growth in the European economy [9]. Clean and low or even free-carbon technologies development and applications would create a new industrial frame with new jobs and growth opportunities, would reduce the use of fundamental and valuable resources such as water, land, raw materials, and energy, the dependence towards imports such as oil and gas, and would increase the well-being of population by bringing about less pollution in the cities, with a reduction in health expenses related to pollution. Indeed, 91% of world's population lives in regions where the pollution levels exceed the World Health Organization guidelines, and outdoor air pollution causes 4.2 million deaths around the world every year [10]. Even though the expected transition would require enormous investments of approximately € 270 billion per year until the 2050, these costs are expected to be lower than those that will be paid in future due to irreversible climate change [8,11]. In 2017 only, economic costs for the damages caused by climate and weather-related disasters reached € 283 billion. In addition, in the future these disasters could affect two thirds of the European population, causing damages and problems in vast areas. Moreover, the development and deployment of carbon neutral technologies would reduce the costs related to energy consumption. The total savings achievable by moving towards a low-carbon society lie between € 175 and € 320 billion per year [8,11]. As reported in the EER 2050, the decarbonisation of the economy is technically and economically feasible and all scenarios that allow for reaching the expected emissions cut, result in a less expensive solution than sticking to the current policies [12,13].

Temperature increase would cause many different problems depending on the European region considered. Figure 1.2 shows the main European regions divided into how each region will be affected by the consequences of the climate change.

Fig. 1.2 – European regions and territories [11]

The main consequences by region would be [11,14]:

- The temperature of the arctic region would rise more than the global average. There would be a decrease in the sea ice coverage, in Greenland ice sheet and in permafrost areas. These changes would lead to an increased loss in biodiversity.
- The Atlantic region would face an increase in heavy precipitation events, leading to an increase in river flow and flooding phenomena. Increased risk of damages caused by winter storms and other climatic hazards.
- Across the mountain regions there would be a larger temperature rise than the European average, leading to a reduction in glaciers extent and volume. At the same time, there would be an upward shift of living beings and a higher risk of extinction of many species (both flora and fauna), leading to increased risk of forest pests, unstable soil and landslides. There would also be a variation in tourism flux due to the close of ski centres.
- In coastal zones there would be a rise in the sea level, an increase in the sea surface temperature as well as an increase in sea and ocean acidity. Therefore, marine species would migrate to the north, damaging the fishing industry and communities. Fish migrations would bring about marine dead zones. Water flooding would also cause the spread of water-borne diseases.
- Within the boreal region there would be an increase in heavy precipitation events and river flows, a decrease in snow, and in lakes and rivers ice cover. There would be a potential increase in forest growth leading to forest pests. Winter storms would damage the environment and reduce the crop yields. Some minor positive effect would be an increase in hydroelectric power availability and increased tourism flows.
- The continental region would be subjected to heat waves and heat extremes conditions, reduced summer precipitation and increased fire risk, while there would be an increase in river floods, and an increase in energy demand for cooling.
- The Mediterranean region would face the worst changes. A significant increase in heat extremes, accompanied by decreased precipitation, and so diminished river flows, would bring about an increased risk of droughts, biodiversity loss, and forest fires. Water sources would become a new reason of competition and conflict also because of the increase in agricultural demand. At the same time, a reduction in crop yields would determine more severe agricultural problems. Consequently, there would be a reduction in livestock production, causing a reduction in food availability. Population would suffer from higher mortality rate due to heat waves and heat extremes. Increased temperature would facilitate the spread of southern disease vectors. There would be a decrease in the

potential for energy production (e.g. from hydroelectric power plants) and a simultaneous increase in energy demand for cooling. Socio-politic tensions would arise due to scarce resources across the Mediterranean territories, leading also to a higher vulnerability due to spillover effects from outside Europe. Therefore, most economic sectors would be affected negatively.

Given these changes in the environmental, social, and economic conditions across Europe, it is clear how the costs for the low-carbon transition will be lower than those determined by the damages linked to climate change.

Figure 1.3a shows the share of GHG emissions by economic sector. Power and heat generation covers the largest portion, followed by agricultural and other land use, industry and transportation. Figure 1.3b shows the share of global GHG emissions by type of GHG. Both figures show the information reported in the Mitigation of Climate Change report of the Intergovernmental Panel on Climate Change from data regarding the 2010 emissions [15]. The largest amount of emissions is related to carbon dioxide from fossil fuel and industrial processes and various land use for a total share of 76%.

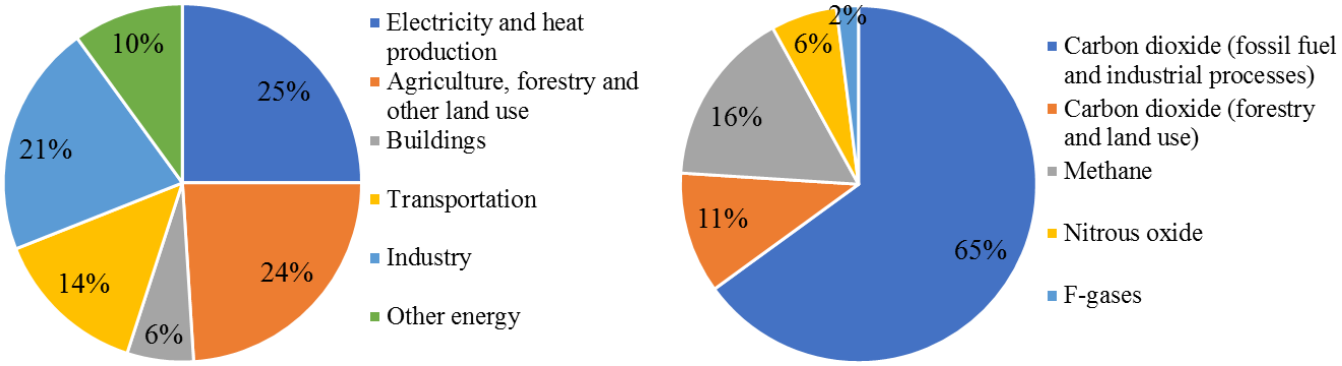

Fig. 1.3 – Global GHG emissions share by economic sector (a, left) and type of gas (b, right) [15]

Among the main GHGs (Fig. 1.3b) CO_2 emissions are the largest and each one of the main sectors is responsible for its share (Fig. 1.3a). Hence, it is important to study and develop a solution capable of solving the problem globally in each of these sectors.

The use of fossil fuels is strongly settled in many different sectors. They are used for electricity production, heating, and chemical manufacturing, as well as transportation in the main means of transport (road, air, naval), and in industry (from chemical production to metallurgic processes and minerals extraction and processing). Agricultural and other land use emissions are related to cultivation, livestock, and deforestation. Approximately, 75% of emissions comes from the use of fossil fuels or derivatives while the remaining share is related to land use and similar. It is clear how the huge amount of GHG emissions, coming mainly from fossil fuel utilisation, might be reduced by deploying clean fuel technologies with the aim of reducing the utilisation of fossil resources.

Given the large share of emissions related to the use of fossil fuels for both energy and chemical compounds production, substituting their use with renewable fuels and their derivatives would help mitigate the negative effect of the CO_2 in atmosphere. Generally, these renewable fuels and products are those manufactured using RES and captured CO_2 following the approach of power-to-gas (PtG), power-to-liquids (PtL), and in general power-to-X (PtX) in which clean electric energy is exploited to produce liquid fuels (PtL) or other type of fuels and chemical compounds (PtG, PtX). These fuels might be used to establish a closed carbon cycle through which clean electricity coming from RES is used to produce hydrogen from the electrolysis of water. The renewable hydrogen is then converted to other valuable products by reacting with CO_2. In this way, both a clean production of H_2 and a re-utilisation of CO_2 are accomplished, reducing the harm given by the conventional hydrogen production ways (96% of today's hydrogen comes from fossil fuel, for instance from methane reforming from which 48% of the present hydrogen comes [16]) and by CO_2 emissions in the atmosphere. Not only would this solution help obtain raw materials (such as methanol and dimethyl-ether

DME) for further industrial processing or fuels to be used directly, but also it would help balance the electricity production given by RES. Ideally, this technology would allow the creation of a closed carbon utilisation cycle while boosting renewable energy penetration in the existing electric system. Figures 1.4 and 1.5 show two different representations of this concept. The first one is related to the project MefCO_2 (Methanol fuel from CO_2) [17] while the second one refers to the world's largest commercial renewable methanol production plant, the Carbon Recycling International (CRI) George Olah Plant [18]. The images represent the re-utilisation of CO_2 coming from flue gases of point sources (i.e. industrial processes), such as cement production facilities or fossil fuel power plants, or even from the atmosphere. Carbon dioxide is captured and stored, and it is subsequently used to produce methanol through the reaction with renewable hydrogen produced exploiting RES.

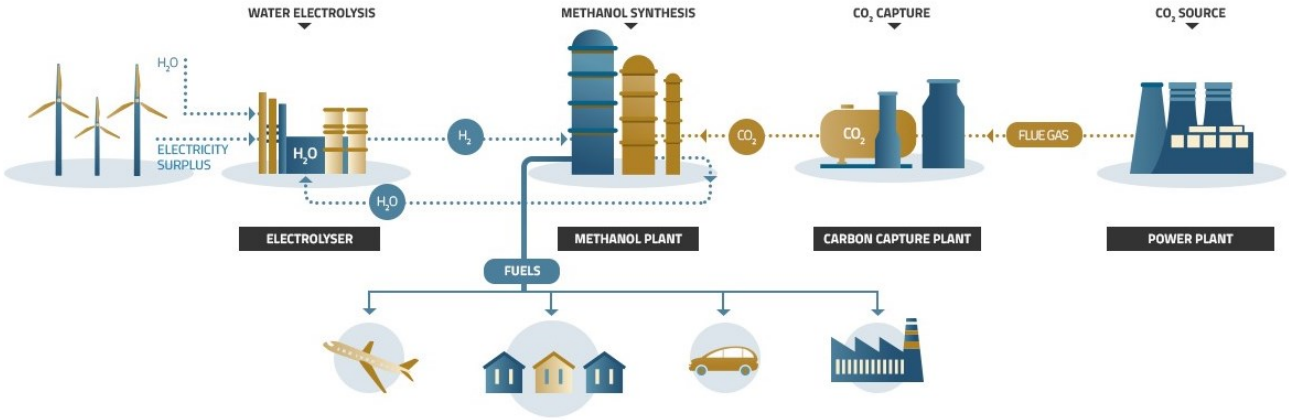

Fig. 1.4 – MefCO_2 (Methanol fuel from CO_2) - Synthesis of methanol from captured carbon dioxide and surplus electricity [17]

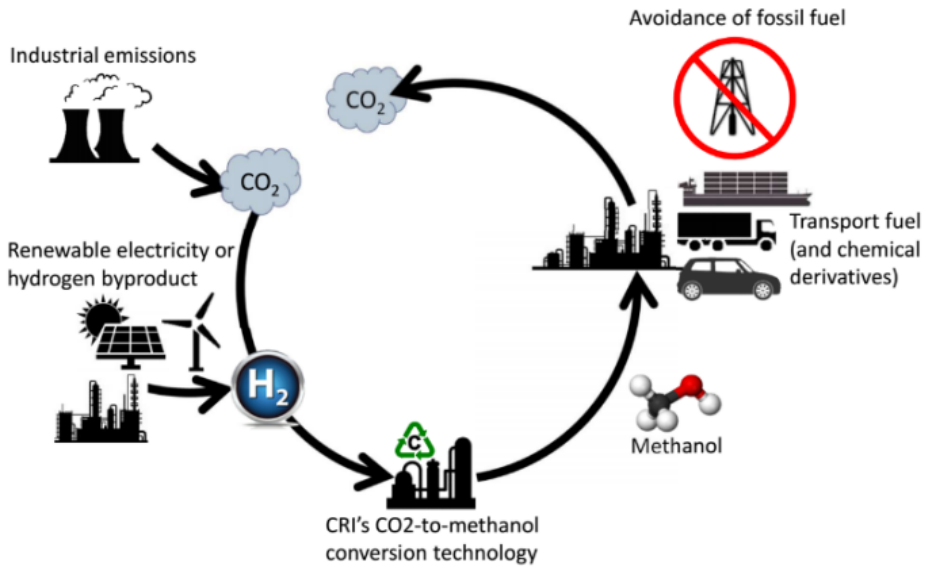

Fig. 1.5 – Renewable methanol: A Tera-Watt-Hour Scale Renewable Power and Energy Strategy - P. Wuebben [19]

Using RES in such a way is one of the opportunities to perform an electric energy storage (EES) where peak or excess energy is stored in chemical media to be subsequently used to level out the energy demand curve throughout the day, with a load levelling and peak shaving approach. In this context, renewable fuels might play a fundamental energy storage role in a future clean economy. Indeed, a low carbon economy where RES prevail among the other sources must ensure an adequate electric grid stability throughout all the possible

conditions of operation guaranteeing enough reliability. Even though the consumption of such chemicals would release back the CO_2 previously stored, a closed carbon cycle where the CO_2 is used cyclically to build back the chemical compounds via EES would ideally solve the problems related to the use of fossil fuels, holding at the same time their advantages. Indeed, any type of fuel obtained via CO_2 recycling and RES is characterised by the beneficial aspects of both clean energy sources and fossil fuels: on the one hand, low-carbon technology with zero or near-zero CO_2 emissions (solar, wind, hydro, etc.); on the other hand reliability, density, and intensity typically found in fossil fuels without the counterpart of remarkable CO_2 emissions [20]. Moreover, not only would the production of fuels such as methanol allow the energy independence towards fossil fuels, but also it would determine a sort of chemical independence, where further conversion of methanol to other compounds (e.g. DME) would guarantee the production of low carbon chemicals.
In this thesis the main objective is to analyse different plant configurations to simulate the conversion of electricity into high quality chemicals, such as methanol. Systems based on commercially mature or innovative technologies are analysed throughout the development of models to simulate each subsection and process and evaluate the performance of the overall system. The analysis carried out in this thesis allowed the evaluation of the effectiveness of such innovative solutions as energy storage systems or as a source of clean chemical compounds, usable in many different sectors. The evaluation of the performance indexes was considered as the first step to take before developing more accurate models (for instance dynamic models). Indeed, only after obtaining a good preliminary performance would it be sensible to perform a more accurate analysis of the specific behaviour under real world conditions.

1.2 Thesis overview

The thesis is structured in 5 chapters (including the introductory chapter) and a concluding chapter, each divided in paragraphs.

A brief description of the content of each chapter is reported here:

- Chapter 2: A brief description of the types of energy storage and the framing of the power-to-methanol technology is presented. Methanol properties, the production ways, its usefulness, and the potential applications and users in a present perspective and considering a future economy based on clean methanol are described.

- Chapter 3: The overall generic configuration of the plant and the main processes and sections are analysed in this chapter. A comprehensive description of the processes is carried out with the help of schemes and tables. All the main technologies considered and adopted in this thesis are described thoroughly. This chapter reports an overview and description of the water electrolysis processes, the technology of the solid oxide cells, the methanol synthesis process, and the organic Rankine cycle. In addition, an overview of the specific configurations and how the different technologies are coupled together is provided.

- Chapter 4: The models used to evaluate the performance of the system are defined in this chapter. The models were developed in Aspen Plus, using its graphical interface of interconnected streams and blocks to simulate the real processes, and MATLAB and MATLAB-Simulink. Special models for the solid oxide cells (electrolyser and fuel cell), the alkaline electrolysis process, the methanol reactor and the entire methanol synthesis sections (comprising the distillation subsection), and the organic Rankine cycle, were developed, both using the graphical interface and the Fortran interface of Aspen Plus. The models were validated using data found in literature and the validation results are reported in this chapter.

- Chapter 5: Different system configurations are analysed and compared, mainly considering two systems based on a commercially mature technology and on an innovative technology to conduct the electrolysis of water. The electrolytic hydrogen, along with CO_2, is used to produce methanol. A description of each system and of the main sections constituting each layout is carried out. Performance indexes to evaluate the efficiencies of the subsections and of the overall systems are defined and used as objective judgement parameters to evaluate and compare the effectiveness of the different solutions.

- Chapter 6: Main conclusion and future research opportunities are highlighted.

Chapter 2

Energy storage, renewable fuels, and methanol

2.1 Introduction

Energy storage is an important way to get the maximum out of the load diagram throughout the days, the weeks and the seasons by storing the excess energy during the off-peak moments and by releasing it during peak moments. In this way the load diagram can be levelled out, obtaining a more constant energy production output, optimising the operation of conventional power plants (the base load) and, at the same time, reducing the waste of excess and unmanageable energy produced by RES. On the one hand, there would be the optimisation of fossil fuels utilisation with the increase in efficiency and decrease in fuel consumption. On the other hand a better exploitation of RES without penalising the conventional power plants [21]. The classification of energy storage technologies depends on how the energy is stored, i.e. the form in which the energy is accumulated. Any type of renewable energy can be stored. Wind, hydro and oceans, solar, biomass, geothermal will all play a fundamental role in the reduction of fossil fuels utilisation and in the decarbonisation of the future society. The main branches are shown in Table 2.1 [22].

Table 2.1 – Classification of energy storage technologies by how the energy is stored

Mechanical	Pumped hydroelectric – PHS Compressed air – CAES Flywheel – FES
Electrochemical	Secondary battery (Lead-acid; NaS; Li-ion) Flow battery (Redox flow/hybrid flow)
Electrical	Capacitor, supercapacitor Superconducting magnets – SMES
Thermochemical	Reversible solid-gas reactions
Chemical	Hydrogen (Fuel cell/Electrolyser) Liquid/Gaseous fuels
Thermal	Sensible/Latent heat storage

Each type of energy storage has its own advantages and disadvantages. For example, considering the mechanical storage form, PHS and CAES are both mature technologies characterised by high energy and power capacity, long life span and low specific cost for large scale applications. However, both require special construction sites (PHS requires proper sites for the two reservoirs, CAES requires proper geological sites such as salt mines, large caverns, etc.), and are characterised by high capital costs and long construction times [23]. Typically, mechanical energy storage is characterised by large capacity and power, high initial investment costs and geographic limitations (considering the PHS and CAES). The electrochemical storage has high efficiency, but short storage period directly related to the dimensions of the batteries. On the contrary, the chemical storage is characterised by long storage period, not being affected by self-discharge processes or material decomposition, but low efficiency. The main advantages and disadvantages of the different ways to store energy can be found in literature [21–24]. Figure 2.1 shows the power delivered and the energy contained in each of the main media used to store electric energy. Each technology is characterised by different values of power and energy content, leading to different preferred applications and utilisation. For example, systems such as supercapacitors, SMES, and FES contain only small quantities of

energy, but they can deliver this energy extremely quickly with the ability to follow the tiny variations of the load diagram instantly. Systems like PHS or CAES, on the contrary, store a remarkable quantity of energy that can be delivered in a range spanning from a few hours to several days. In a future perspective, the integration between all the technologies reported in Table 2.1 and Fig. 2.1 will be fundamental to guarantee power and energy delivery that matches the electric grid requests perfectly.

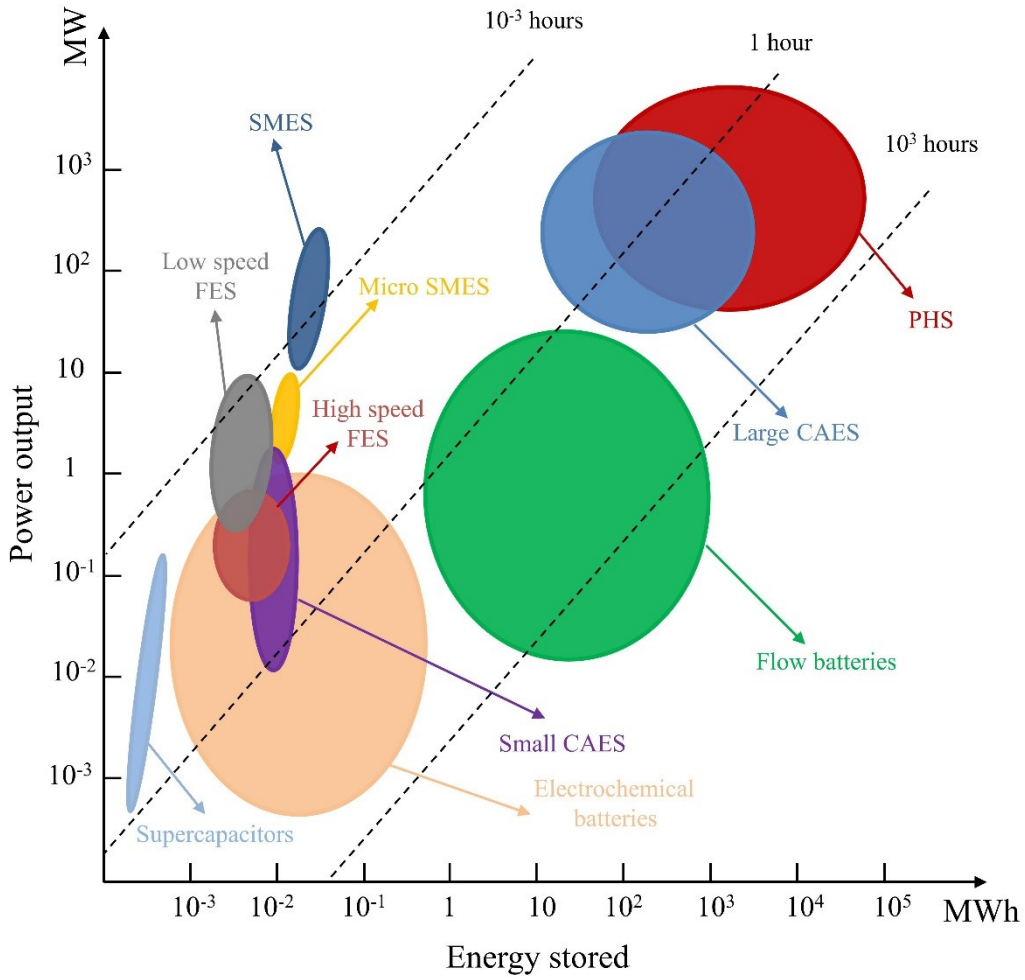

Fig. 2.1 – Electrical energy storage technologies by power output and energy stored (adapted from [24])

Among the conventional EES shown in Fig. 2.1, other ways of storing energy are the thermochemical, chemical and thermal (Table 2.1). Thermochemical storage is based on a variety of solid-gas reversible chemical reactions. Typically, the forward reaction is endothermic, and heat is used (and stored) to separate a chemical compound (solid) in its constituents (a solid and a gaseous species). Then the constituents are stored separately to avoid reconversion into the original compound. When the stored heat is needed, the two reactants are recombined and the backward reaction takes place, releasing the heat that was previously stored in the forward reaction. Typical compounds employed are metal hydrides (e.g. MgH_2, $NaMgH_3$, Mg_2FeH_6, Mg_2NiH_4, CaH_2, etc), metal hydroxides (e.g. $2LiOH$, $Ca(OH)_2$, $Mg(OH)_2$, $Fe(OH)_2$, etc.), metal carbonates (e.g. $CaCO_3$, $FeCO_3$ etc.), and others (e.g. $MgSO_4 \cdot 7H_2O$, $CaSO_4 \cdot 2H_2O$, etc.) [25–27]. The thermochemical storage is particularly suitable to store heat because the gaseous species can be easily separated from the solid species during the forward reaction. In addition, this technology can be employed for both short and long-term heat storage [25]. Energy storage via chemical compounds allows the conversion of electric energy into chemical energy that is stored in different media (hydrogen, methane, methanol, DME, syngas, etc.). To produce these chemical compounds, the main building blocks are hydrogen and carbon, that can be recovered from carbon monoxide and carbon dioxide. Such an electric energy storage is advantageous

because it allows the accumulation of energy in a long-term stability material, that is usually stored, transported, distributed and used easily. For instance, methanol is a liquid at ambient conditions. Hence, it is readily storable, transportable and usable without serious changes in the existing infrastructure. Nowadays, hydrogen is produced mainly from the reforming of natural gas (48%) and oil (30%), and from coal gasification (18%) [16,28,29]. These production processes, if not accompanied by carbon capture and storage (CCS) equipment, release CO_2 in the atmosphere contributing to the climate change problem. Instead of producing hydrogen from the conversion of fossil fuels, water electrolysis exploiting renewable electricity or nuclear energy might be used. Indeed, even though this process is characterised by high electricity consumption and high production costs, using renewable energy would lead to a completely carbon-free and clean production process [16]. If renewable hydrogen is reacted with captured CO_2 from industries and power plants, or directly from the atmosphere, various clean chemical compounds similar to those typically derived from fossil fuels can be produced. These clean chemicals and their derivatives would be useful in many different sectors. Usually, fuels produced from renewable electricity, hydrogen and captured CO_2 are known as "renewable fuels". Finally, thermal energy storage (TES) allows the increase in energy savings and process efficiency by storing heat to be used in substitution of higher quality energy (i.e. electricity) that would be used to produce the heat required by the process if the TES was not applied.
In the present work, chemical energy storage and TES are mainly considered. The first to convert electricity from RES into a long-lasting, easy-to-handle and use chemical, and the second to accumulate and re-use heat, instead of wasting it and providing it ex novo.

2.2 Renewable resources and fuels

Almost every RES comes from the Sun directly or indirectly, which is an unlimited source of energy. Solar radiation can be used to produce both electricity and heat and is considered as the main RES being responsible for many others. Winds are mainly originated by the temperature gradients across regions and continents. Biomasses exist because they harvest energy directly from the Sun, converting CO_2, water, and soil substances into nutrients. Hydroelectric power is related to irradiation and heat coming from the Sun, due to the evaporation and precipitation cycles involving oceanic water. Other notable RES are geothermal, tidal, waves, and sea currents. In an optic of a future power grid where the electric energy is almost exclusively produced from RES and where at the same time the conventional fuels are still needed (chemical industries, transportation, heat etc.), the production, storage and reuse of renewable fuels would be the basis of a strong backup power, coupling both the advantages of RES and fossil fuels.
Renewable fuels are usually referred as those produced by exploiting RES and, typically, CO_2. Among these fuels are included different types of biofuels. Ethanol, also known as ethyl alcohol, is a biofuel produced mainly through fermentation processes of glucose from different molecules such as sugar, contained in cane sugar, sugar beet, and sweet sorghum; starch, present in grains, tapioca, and cassava; cellulose, found in wood, switch grass, and corn stover. Ethanol is used in numerous different sectors such as industry where it is employed as a solvent, in food processing, for medicine production in sterilisation processes, in agriculture, and in the transportation sector as a fuel blended with gasoline allowing the improvement of vehicle emissions and power [30]. As with these, biodiesel is another renewable fuel produced from vegetable oil, animal fats, and other wastes such as cooking oil. These substances undergo a process called transesterification, a catalytic process through which almost the total production of biodiesel is carried out worldwide. Biomasses are considered as a biofuel, with a theoretical net zero CO_2 emissions, because during the plant lifetime the CO_2 captured from the atmosphere is fixed to the plant structure and it comes back to the environment when the biomass is burnt. Of course, given all the processes involved in biomass growth, collection, and transportation, it is not straight to assess the effective carbon neutral cycle of biomass use. Hydrogen, when produced from RES and water, is one of the most interesting renewable fuel due to its extremely high lower heating value (LHV) (120 MJ/kg_{H_2}) and the opportunity to be used directly in fuel cells, without the limitations of the second law of thermodynamics and harmful CO_2 emissions. Even though

the energy density is the highest among energy vectors, the net energy density after the storage processes is only approximately 0.70-0.80 MJ/kg_{H_2} (cf. Table 2.4 in Par. 2.4.1). In addition, large scale deployment of hydrogen technology would be too expensive due to the necessary revolution in the transportation and use infrastructures. Moreover, hydrogen storage and handling are characterised by difficulties and problems such as the need of extremely high pressure or extremely low temperature for its storage in liquid form. Thus, different energy vectors such as methanol or DME have been receiving a growing attention in the last few years. Indeed, also methanol and DME, when produced from RES and captured CO_2 can be considered to all effects as renewable fuels.

2.2.1 Renewable energy sources cost

To manufacture a clean and low-carbon fuel, it is mandatory to produce hydrogen from carbon neutral technologies instead of sticking to hydrogen produced from fossil fuels (cf. Par. 2.1 and Par. 3.2.1). Rather than converting natural gas to hydrogen via steam reforming processes (or other fossil resources with other processes), clean and renewable hydrogen must be supplied to the PtX plant. Typically, the highest cost share in a PtX process that involves water electrolysis for the hydrogen production, is covered by the electrolysis itself. Indeed, water electrolysis requires a considerable amount of electricity (roughly 80% of the energy of the entire PtX process), and so it results feasible only when the cost of electricity from RES is low enough to guarantee competitiveness to fossil derived hydrogen. Nowadays (IRENA 2018 database based on data from 2017 [31]), within the G20 countries, the levelised cost of electricity generation from fossil fuels ranges between 0.050 and 0.170 USD/kWh, depending on the technology and region considered, whereas RES production cost in Europe, without considering incentives and CO_2 tax costs, already has dropped between 0.080 (onshore wind power) and 0.150 (offshore wind power) USD/kWh. Regarding the global weighted average costs, onshore wind was below 0.100 USD/kWh already in 2010, and it is predicted to reach the lowest fossil fuel price limit of 0.050 USD/kWh by 2020 with a cumulative deployment of 712 GW. Offshore wind has always been more expensive than the inland counterpart, with an average cost starting from 0.150 USD/kWh in 2010 and increasing to approximately 0.200 in 2013 due to accelerated deployment and installations in deeper waters. Following the general reduction trend of RES cost, offshore wind power generation will have dropped to 0.080 USD/kWh by 2020 with a cumulative power deployment in the order of 31 GW. Initially, photovoltaic (PV) had the highest cost in 2010 (approximately 0.350 USD/kWh), but the cost has drop sensibly in the last few years with a predicted cost of 0.060 USD/kWh by 2020 with a cumulative power deployment in the order of 650 GW. Concentrated solar power remains the most expensive RES with a cost of 0.280 USD/kWh in 2016 but a predicted cost of 0.080 USD/kWh by 2020 and a cumulative power of 12 GW. Hydroelectric power production cost is already equal to or below the production cost of electricity via fossil fuels anywhere in the world, with a capacity of 1121 GW as of 2016 (excluding pumped hydro). From this data, it is clear how the large-scale deployment and use of RES is economically feasible and convenient, and that the costs are foreseen to decrease even more in future, especially when fossil fuel electricity production is correctly taxed, and RES are incentivised.

2.3 CO_2 and power-to-X

Numerous different approaches can be considered regarding EES. One of these is to use the electricity to produce different kinds of fuels and chemicals via different processes, recycling CO_2 and making it react with H_2. Carbon dioxide can be used as a feedstock for fuels and chemicals production, being carbon the building block of the organic matter. Milani et al. [32] comprehensively showed how CO_2 can be used to produce several products and to address a variety of sectors directly or indirectly. For instance, CO_2 can be directly used in refrigeration systems, in wastewater treatment, in solvents production, in the food industry, to produce dry ice, in enhanced oil recovery processes. CO_2 can also be turned into methanol or it can be dry-reformed to syngas composed of CO and H_2. Then, methanol or syngas can be converted to a variety of

derivatives such as solvents, synthetic liquid fuels and other products. In this way, CO_2 is indirectly used as the building block of these chemical compounds.
Numerous authors studied different production chains in various PtX plants, obtaining a variety of results and performance indexes strongly dependent on the chosen process and approach. Table 2.2 reports some of the numerous works found in literature regarding PtL processes and their efficiencies. Mignard and Pritchard [33] considered the potential of converting excess renewable electricity produced in British off-shore wind farms, and in general in RES plants detached from the main grid, into chemicals as a source of fuels for different applications. A convenient way to store and transport electricity in regions where a strong grid connection is not available is mandatory to guarantee the penetration of RES even in rural and isolated zones. Using hydrogen as an energy vector and carrier for such a scope would not be feasible, due to the necessary changes in the existing transportation and use infrastructure. Three different processes were considered by the authors: methanol synthesis from synthesis gas via catalytic hydrogenation; synthesis of mixed alcohols, such as ethanol (C_2H_5OH) and other higher alcohols through a chain growth process carried out with Fischer-Tropsch (FT) conversion; methanol to gasoline process on zeolite catalyst, via the Mobil process. Mass and energy balances were applied to the flowsheets and schemes of each process and the conversion efficiency was calculated for each of them, considering pumps, CO_2 extraction and liquefaction, and feed compression. Efficiencies (chemical energy content vs electricity needed to obtain that chemical energy) were found between 45 and 61% depending on the analysed process and the obtained products. O'Brien et al. [34] explored the production of synthesis gas performing the co-electrolysis of water and CO_2 using energy and heat coming from nuclear power plants. High temperature electrolysis coupled to nuclear energy would be one of the main players in a future economy based on large scale hydrogen production, where remarkable quantities of hydrogen will be used both in the chemical industry and as a base chemical species to produce synthetic fuels. Simulations were carried out using a commercial software, by developing a complex flowsheet for the evaluation of the main parameters from which the performance of such a system depends on. Not only did the authors consider the co-electrolysis of H_2 and CO_2, but also, they analysed the production of liquid fuel from the obtained syngas via a FT process. Efficiency spans from 31 to 43-44%, depending on the considered operating temperature. The work pointed up how the total efficiency drops under extremely low values (i.e. 20%) when the plant operates at a low utilisation factor, corresponding to high irreversibility and consumption in the auxiliaries. Graves et al. [35] focused on the production of liquid fuels coupling CO_2 direct air capture to high temperature electrolysis solid oxide electrolysis cells (SOEC) and FT synthesis. Carbon dioxide capture was simulated via solid adsorbent and humidity swing processes, which was found to be the least energy demanding technique, whilst high temperature SOEC allowed the co-electrolysis of CO_2 and water to obtain syngas in a single device. The authors also carried out an economic analysis finding the feasibility of this approach when considering a constant electricity supply. The overall electricity-to-liquids efficiency was approximately 70%. Albrecht et al. [36–38] considered numerous ways of producing synthetic fuels. In [36], an SOC (solid oxide cell) reversible system, capable of working in different modes, was coupled to a FT process to produce syngas and convert it to different types of fuels such as gasoline, kerosene, and diesel. The authors considered a system composed of gas storage facilities to store syngas and tail gas to be used in both the FT reactor and in a combined cycle to maximise electricity production. The reference operating mode consisted of a steady state PtL plant using SOEC fed with RES and FT to produce liquid fuels continuously, while tail gases were used to produce electricity to reduce the consumption of electricity from the grid. The second system was based on a flexible reversible SOC capable of working in both SOEC and SOFC (solid oxide fuel cell) mode, where the system was switched between the two operating modes in the best way to optimise the system performance. Efficiency of 37% and 44% were obtained in the reference and in the flexible case, respectively. In the other two works ([38,39]), the same authors analysed the efficiencies of different synthetic fuel production chains, where syngas obtained following different approaches was converted to liquid fuels: biomass-to-liquids, biomass and power-to-liquids, power-to-liquids. The X-to-liquids efficiencies (defined as the ratio between the energy content of

the produced fuel and all the energy flows entering the system) were equal to 36.3 (biomass-to-liquids), 51.4 (biomass and power-to-liquids), and 50.6% (power-to-liquids). The corresponding overall plant efficiencies, comprising also the by-product electricity and the useful heat exploited in a heat market (steam production and district heating), were 82.6, 65.0, and 66.8%. Fasihi et al. [40] explored a value chain design for the production and transport of synthetic fuel such as diesel fuel using a hybrid PV-wind system coupled to electrolysers and a hydrogen-to-liquids facility. The system allowed for storing RES electricity into liquid fuels that were obtained via a FT process. The authors focused on achieving production costs equal to those typical of fossil fuels, supposing to install the plant in the best complementing solar-wind sites and considering direct air CO_2 capture via air scrubbers, not to have limitations given by CO_2 availability. The resulting fuel was composed of naphtha, jet fuel, and diesel in percentages equal to 15, 25, and 60% respectively. The overall efficiency was found to be 65%. Schmidt et al. [41,42] considered various case scenarios for the production of methanol and other synthetic fuels considering low and high temperature electrolysis, and CO_2 coming from direct air capture or concentrated sources. The obtained fuels are characterised by different LHV depending on their final composition. The authors came up with PtL efficiencies expressed as the ratio between fuel output and electricity input (gate-to-gate efficiency) in a range from 39 to 64%. Low temperature electrolysis and direct air CO_2 capture are the most energy demanding processes. In low temperature electrolysis almost all the energy must be supplied as electricity (while in high temperature electrolysis part of the electric energy might be substituted by heat). Therefore, electricity consumptions tend to be high. Direct air CO_2 capture is more energy demanding than concentrated source capture since, given the relatively low CO_2 concentration in air (≈ 400 ppm) it is necessary to process a remarkable amount of air to gather the needed CO_2. When the same technology is adopted, the overall efficiencies to produce methanol or other liquid fuels are almost the same. Table 2.2 shows a summary of some of the research carried out within the PtX field, highlighting the main process considered in each work, the obtained efficiency, and the fuel characteristics.

Table 2.2 – Findings on PtX process efficiency

Reference	Process	Efficiency	Fuel characteristics
Mignard 2006 [33]	H_2 compression (30 to 400 bar)	61%	Hydrogen
	Methanol	50-51.5%	Methanol
	Mixed alcohols via FT	45-47%	Ethanol, methanol, higher alcohols
	Methanol to gasoline via Mobil process	42%	Gasoline
		46%	Gasoline, LPG
O'Brien 2008 [34]	Power to syngas and liquid fuels via FT	43-44%	Syngas and liquid fuels
Graves 2011 [35]	Water, CO_2 co-electrolysis, FT	70%	Gasoline, diesel, alcohols, DME etc.
Albrecht 2016 [36]	SOEC and FT (constant electricity input)	37%	Gasoline, kerosene, diesel (LHV 29 MJ/kg)
	SOC and FT (reversible system, not constant electricity)	44%	Gasoline, kerosene, diesel (LHV 23 MJ/kg)
Fasihi 2016 [40]	Hydrogen to liquids (RWGS, FT, hydrocracking)	65%	15% naphtha, 25% jet fuel, 60% diesel
Albrecht 2017 [37,38]	Biomass to liquids	36.3%	Liquid fuels (LHV 44 MJ/kg)
	Power and biomass to liquids	51.4%	
	Power to liquids	50.6%	

Schmidt 2016 [41]	Low temperature electrolysis		
	Methanol (CO_2, H_2O co-electrolysis) (CO_2 direct air capture)	42%	Methanol
	Methanol (CO_2, H_2O co-electrolysis) (CO_2 concentrated)	54%	
	Liquids via FT (CO_2 direct air capture)	42%	Liquid fuels (LHV 43 MJ/kg)
	Liquids via FT (CO_2 concentrated)	53%	
	High temperature electrolysis		
	Methanol (CO_2, H_2O co-electrolysis) (CO_2 direct air capture)	47%	Methanol
	Methanol (CO_2, H_2O co-electrolysis) (CO_2 concentrated)	63%	
	Liquids via FT (CO_2 direct air capture)	47%	Liquid fuels (LHV 43 MJ/kg)
	Liquids via FT (CO_2 concentrated)	64%	
Schmidt 2018 [42]	Methanol (CO_2, H_2O co-electrolysis) (CO_2 direct air capture)	39%	Methanol
	Methanol (CO_2, H_2O co-electrolysis) (CO_2 concentrated)	48%	
	Liquids via FT (CO_2 direct air capture)	39%	Liquid fuels (LHV 42 MJ/kg)
	Liquids via FT (CO_2 concentrated)	47%	

As shown in Table 2.2, different processes are characterised by different products and efficiencies. Even among similar processes and final products, differences in efficiency might be relatively large. This is because each author made different hypothesis and assumptions in his work.

In the present work, other approaches and system layouts were studied and different results from those reported here were found. Nevertheless, as well as these cited research works, the findings demonstrate the overall effectiveness in terms of performance and future technology application in a carbon free economy.

In general, a few main reactions can be considered for the conversion of CO_2 to other C-compounds. Since CO_2 is an extremely stable molecule due to the double covalent bond between the carbon atom and the oxygen atoms, CO_2 must undergo reduction reactions in which the thermodynamic and kinetic stability of carbon dioxide are overcome. Some of these reactions are (2.1)-(2.6) [43]:

$$CO_2 + H_2 \leftrightarrows CO + H_2O \quad (2.1)$$

$$CO_2 + 3H_2 \leftrightarrows CH_3OH + H_2O \quad (2.2)$$

$$CO_2 + CH_4 \leftrightarrows 2CO + 2H_2 \quad (2.3)$$

$$CO_2 + H_2O \leftrightarrows CO + H_2 + O_2 \quad (2.4)$$

$$CO_2 + 4H_2 \leftrightarrows CH_4 + 2H_2O \quad (2.5)$$

$$CO_2 + H_2O \leftrightarrows -CH_2 - + \frac{3}{2}O_2 \quad (2.6)$$

These equations represent the reverse water gas shift reaction (2.1), CO_2 hydrogenation to methanol (2.2), methane reforming with CO_2 (2.3), CO_2 and water electrocatalytic reduction (2.4), CO_2 hydrogenation to methane (2.5), and the generic CO_2 conversion to methylene ($-CH_2-$) (2.6), which is used to create longer chain hydrocarbons in FT processes. Methylene combustion, as a representative of the many existing long chain hydrocarbons, is reported in reaction (2.7).

$$2(-CH_2-) + 3O_2 \rightarrow 2CO_2 + 2H_2O \quad (2.7)$$

The combustion of 1 kg_{-CH_2-} brings about the emission of 3.14 kg_{CO_2}.

Power-to-liquids can also be used to produce clean jet fuel that can be obtained both by following a methanol pathway (i.e. further conversion of methanol) or a FT pathway (i.e. syngas conversion to chain hydrocarbons). Jet fuel is composed of long chain hydrocarbons based on methylene, which is reported in the left term of reaction (2.7). Power-to-liquids fuels are characterised by ease of deployment and usage, high energy density, remarkable global renewable potential, almost carbon neutrality (GHG emissions near to zero in the production process), low water and land demand compared to biofuels. In addition, renewable synthetic fuels can strengthen local economies valorising the regions with high wind and solar availability while providing grid ancillary services and reducing the emissions both at the ground level and at high altitude (when considering renewable jet fuel). Among the disadvantages are the cost of fuel production, especially to produce hydrogen via a clean pathway (i.e. water electrolysis), the renewable CO_2 supply since direct air capture is not yet a competitive technology, and the absence of an option to have zero emissions (even though PtL fuels come from RES, their combustion releases back the stored CO_2 and other pollutants in the atmosphere). Among the concerns and threats there are the dependence on engine architecture (fixed LHV, flammability limits, etc.), on conventional CO_2 sources to perform the fuels synthesis, and the population acceptance of extensive renewable power plants spread across regions to provide the necessary energy to produce the fuels [41,42].

2.4 Power-to-methanol and CO_2 to methanol

2.4.1 Why methanol?

Methanol is the simplest alcohol. Owing to its physical and chemical properties, it is a compound that is easy to handle, transport, store, and use. However, due to its flash point of 9 °C and the ignition temperature of 440 °C, safety problems might arise, and so specific guidelines must be followed. At ambient pressure it has a fusion temperature of -97.8 °C and a boiling temperature of 64.6 °C, while under normal conditions (0°C and 101325 Pa) it has a density of 810.3 kg/Nm^3 (approximately 792 kg/m^3 at 20 °C). It is a highly volatile and flammable liquid and its vapours form explosive mixtures with air. It can be blended with water in any percentage reducing the risk of accumulation in groundwater, in the soil, and in the air. Since it is miscible with water easily, it is rapidly decomposed by the action of bacteria. Thus, accidents, leakage, and spills are not particularly harmful for the environment. Indeed, in water methanol dissolves to low concentration quickly. Even though groundwater contamination depends strongly on the nature and magnitude of the release, in a scenario of significant methanol release its concentration is likely to drop quickly due to biodegradation. Compared to methanol, conventional gasoline and diesel fuel released in the environment persists longer and has more far-reaching effects. For comparison, methanol is characterised by a half-life in groundwater environment of only 1-7 days while benzene, a common constituent of gasoline, has a half-life

between 10 and 730 days. Hence, methanol is safer and less dangerous for the environment. In addition, methanol is often considered as a toxic and dangerous substance to human health, however it is neither carcinogenic nor teratogenic in contrast with gasoline and diesel fuels [44–47]. Methanol LHV is approximately 19.9 MJ/kg, which is not particularly high when compared to other common liquid fuels. Nevertheless, methanol is characterised by a higher latent heat of vaporisation compared to that of gasoline, improving an engine efficiency when blended with gasoline. Furthermore, it was found that using methanol in diesel engines allowed the reduction in the engine size by almost 40% along with an increase in power by 30%. Moreover, the lack of carbon-carbon bonds leads to a near to zero soot formation during the combustion process, while the absence of sulphur and the lower flame temperature lead to cleaner exhaust gases from the point of view of SO_x and NO_x [48]. Finally, it is easier to store and transport than hydrogen and natural gas, since it can be simply stored in conventional tanks at ambient conditions. For the sake of comparison, Table 2.3 reports the LHV of some of the most common liquid and gaseous fuels [49].

Table 2.3 – Lower heating values for different fuels

Fuel	LHV [MJ/kg]	Fuel	LHV [MJ/kg]
Methanol	19.9	Kerosene	43.0
Ethanol	26.7	Gasoline	43.4
Dimethyl ether	28.9	Butane	45.3
Butanol	34.4	Liquefied petroleum gas (LPG)	45.5
Methyl tertiary butyl ether (MTBE)	35.1	Propane	46.4
Biodiesel (methyl ester)	37.5	Natural gas	47.1
Biodiesel (vegetable oils)	37.8	Ethane	47.8
Heavy fuel oil	38.2	Liquefied natural gas (LNG)	48.6
Light fuel oil	39.0	Methane	50.0
Diesel	42.6	Hydrogen	120.0

Compared to other chemical storage media, namely lead accumulator and Li-ion batteries, methanol storage is an excellent candidate as a chemical battery because of its high energy density of 19.9 MJ/kg. Indeed, state of the art batteries are characterised by an energy density of only 0.11 (lead accumulator) and 0.5-3.6 MJ/kg (Li-ion batteries) [50,51]. Furthermore, the production of such chemical accumulators is extremely pollutant owing to the extraction and use of rare metals.

Among the potential renewable fuels, methanol has some peculiar characteristics. It is a well-known chemical compound that in the last few decades has increased its importance worldwide as a hydrogen carrier, as a fuel [52,53] and, more generally, as a multiuse chemical and energy feedstock [51], even leading to the prospect of a future methanol economy [54–56]. Indeed, methanol can be easily used, transported and stored without significant changes in the existing infrastructures (vehicle engines, fuel transport and distribution systems), being similar to commonly used fuels such as gasoline or diesel fuel. On the contrary, switching to a hydrogen economy, with the mass production and utilisation of pure hydrogen, would need for a revolution in the fuel infrastructure [54]: the deployment of new design for vehicles and refuelling stations would be necessary, along with convenient systems to store and transport the hydrogen from the production facilities to the utilisation regions. Methanol is a better energy storage medium than the most important hydrogen storage technologies, namely high-pressure storage in composite cylinders (up to 300 bar) and metal hydride cylinders. The benefits of methanol production as a hydrogen storage medium are substantial when considering both indirect methanol use (i.e. production of hydrogen via a reforming process) and direct methanol use as a fuel. Table 2.4 shows the comparison between hydrogen and methanol storage from the point of view of the energy density, the storage efficiency, and the net energy density [57,58].

Table 2.4 – Hydrogen and methanol storage efficiency comparison			
Storage method	Energy density	Storage efficiency [%]	Net energy density
H_2 in composite cylinders (300 bar)	119.9 [MJ/kg]	0.60	0.72 [MJ/kg]
	33.3 [kWh/kg]		0.20 [kWh/kg]
H_2 in metal hydride	119.9 [MJ/kg]	0.65	0.78 [MJ/kg]
	33.3 [kWh/kg]		0.22 [kWh/kg]
H_2 from methanol (indirect use)	119.9 [MJ/kg]	6.90	8.27 [MJ/kg]
	33.3 [kWh/kg]		2.30 [kWh/kg]
Methanol in plastic tanks (direct use)	19.9 [MJ/kg]	95	18.90 [MJ/kg]
	5.54 [kWh/kg]		5.26 [kWh/kg]

Both methanol storage pathways are significantly more efficient than hydrogen storage and have a remarkably higher net energy density. The hydrogen efficiencies (first three rows of Table 2.4) are expressed as percentage of mass of hydrogen in the storage media. In the fourth case (methanol direct use) methanol is used in a direct methanol fuel cell achieving the highest storage efficiency. Methanol indirect use (i.e. methanol reforming to hydrogen and hydrogen oxidation in a fuel cell) is approximately ten times more efficient than pure hydrogen storage, but it is almost fourteen times less efficient than methanol direct use as a fuel. However, the overall energy density is slightly more than two times lower than that of methanol direct storage and use (8.27 against 18.9 MJ/kg). From these values, it is clear how methanol as a hydrogen carrier is more efficient than storing hydrogen directly.

Following the increase in climate change concern due to CO_2 emissions, the analysis and development of innovative systems for the production and utilisation of renewable methanol, for example methanol produced from RES and recycled CO_2, is an interesting option to reduce the environmental impact caused by the consumption of fossil fuels in the energy, transportation and industrial sectors. Indeed, methanol is already commonly used as a feedstock for petrochemicals in the methanol-to-olefins processes (formaldehyde, acetic acid, DME, propylene, ethylene, various solvents, etc.), for heat or steam generation, in both maritime and ground transportation sectors [59] and for power generation in gas turbines or fuel cells. Moreover, due to the progressive increase in RES exploitation, a massive contribution of energy storage is fundamental to improve the overall penetration, usability and dispatchability of RES. In this context, methanol as an energy carrier might help solve the main issues related to renewable sources, improving their reliability and reducing the impact of intermittency and variability on the grid [60]. Also, coupling methanol production plants to conventional power plants would reduce the fluctuation caused by the penetration of RES, smoothing the load profile and increasing the overall efficiency of the entire electric grid, thereby boosting the convenience of RES utilisation [61]. In addition, in comparison to other energy carriers, such as syngas produced following the power-to-gas routes, the power-to-methanol (the conversion of hydrogen produced using electricity into a valuable chemical) provides a more profitable way to convert electric energy [60].

While methanol from fossil fuels is currently carried out in centralised production plants and distributed to the users, a renewable power-to-methanol approach would be based on small to medium scale plants (with a foreseen production in the range of 50-100 kt/year [48]) in a decentralised approach where the production facilities would be near to both the feedstock source and the final users. Power-to-methanol employing captured CO_2 is at a TRL (technology readiness level, i.e. a scale used to estimate the maturity of a technology [62]) of 6-7 (out of a maximum of 9) [63]. Currently, the largest demonstrative power-to-methanol plant based on alkaline electrolysis, RES and captured CO_2 is being operated in Iceland (CRI George Olah Plant) with a production of approximately 4000 t/year of methanol, a recycling of 5500 t/year of captured CO_2, and an electricity consumption of 6 MW_{el} [18,48,64]. In the future, it is planned to expand

the plant capacity up to 40000 t/year [65]. To produce 1 t of methanol, 1.38 t of CO_2 are recovered from the flue gases of the geothermal plant located nearby. Renewable water electrolysis, assisted by industrial H_2 source, produces a total of 0.19 t of hydrogen. Hydrogen and CO_2 are compressed and reacted with a synthesis conversion efficiency of 99%. A distillation step allows the separation of 0.59 t of water from 1 t of methanol, that contains a chemical energy of 5.58 MWh_{LHV}. When hydrogen production is performed using RES, the methanol production pathway employed by CRI reduces the life-cycle carbon footprint of each MWh_{LHV} of chemical energy by about 90-99% compared to European conventional gasoline or diesel fuel. Compared to the natural gas methanol production process, renewable methanol allows a reduction of the overall CO_2 emissions by 1.53 t per t of produced methanol [48]. The overall efficiency (defined as the ratio between the LHV of methanol and the electricity used to produce it) of a power-to-methanol plant is approximately 61% [60]. CRI has achieved many records with the operation of the George Olah Plant. Indeed, it has been the first company to: a) produce transport fuel using CO_2 from an industrial source, b) use a multi-MW alkaline electrolyser skid to produce hydrogen in a PtL application, c) deliver a renewable fuel of non-biological origin to the European market by blending the produced methanol with gasoline and biodiesel, and d) receive a certification for producing a renewable fuel from non-biological sources [19,48].
Other approaches in the production of methanol are the exploitation of hydrogen contained in off-gases coming from industrial plants such as coke oven gas or gases from ethylene production and chlor-alkali electrolysis, or even the hybridisation between the production of hydrogen from water electrolysis using an excess of RES and hydrogen extracted from rich tail gases. These technologies are already available at the commercial stage with a production scale up to 100 kt/year [48].
Nowadays, methanol production is based almost exclusively on fossil fuels and is carried out in large centralised plants capable of producing more than 1 million t/year by steam reforming of natural gas or gasification of coal and residual oil. Typically, fossil fuelled methanol plants have a daily production capacity spanning from 1500 t/day to up to 5000 t/day, emitting 1 t of CO_2 per t of methanol when exploiting natural gas and up to 3.5 t of CO_2 per t of methanol when exploiting coal [48]. Any type of fossil fuel can be reformed or partially oxidised to produce syngas which is subsequently converted into methanol via CO and CO_2 hydrogenation. Fossil fuels characterised by a rich carbonaceous composition such as natural gas, coal, coke, petroleum, heavy oils, and asphalts are transformed into syngas, namely a mixture of hydrogen, carbon monoxide and carbon dioxide, that is turned into methanol over heterogeneous catalysts following the catalytic CO (2.8) and CO_2 hydrogenation reactions (2.9) and the reverse water gas shift reaction, (2.10).

$$CO + 2H_2 \leftrightarrows CH_3OH \tag{2.8}$$

$$CO_2 + 3H_2 \leftrightarrows CH_3OH + H_2O \tag{2.9}$$

$$CO_2 + H_2 \leftrightarrows CO + H_2O \tag{2.10}$$

Methanol production from syngas in industrial processes is performed at very high pressure and high temperature, depending on the chosen catalyst. The most common commercial catalyst used in the CO_2 hydrogenation to methanol conversion is $Cu/ZnO/Al_2O_3$. Optimal operating conditions span from 200 to 270 °C and 50 to 100 bar, with a carbon molecules yield conversion to methanol of approximately 99.5%. Typical composition of commercially available catalysts is Cu 50-55 wt%, ZnO 21-26 wt%, and Al_2O_3 5.5-10 wt%, depending on the manufacturer [66]. In an industrial process, syngas enters the catalytic reactor, is converted into a mixture of methanol, water, and unreacted gases following reactions (2.8)-(2.10). The mixture is processed to separate methanol and water from the unreacted gases. Crude methanol, composed of water and methanol mainly, is purified in a distillation column where methanol is the distillate leaving from

the top while water leaves the column from the bottom. Residual CO_2 contained in the methanol stream is further separated and recycled back to the reactor, or vented [67].
Methanol is also one of the main chemicals used in the industrial sector. Numerous different compounds and derivatives are obtained by its refining. Among the chemicals obtainable from methanol are: formaldehyde, acetic acid, MMA (methyl methacrylate), MTBE (methyl tert-butyl ether), DME, gasoline, MTO/MTP (methanol-to-olefins/methanol-to-propylene) derivatives, biodiesel [50]. All these derivatives are used to obtain a variety of different end use products such as resins, chemical additives, olefins, more complex fuels, and others. Considering the potential sectors where these chemicals are employed, it is clear how many of them are involved and could benefit from the production of renewable methanol, reducing overall indirect emissions that would be otherwise coming from substances originally produced from fossil resources, such as plastic materials. Some examples of benefitting sectors are: construction; automotive; electronics and appliances; paints, coatings, and insulations; pharmacology; packaging; solvents. Figure 2.2 shows a summary of the derivatives obtainable from methanol processing. Many of these final products are obtained by the conversion of DME, which can be obtained via catalytic methanol dehydration.

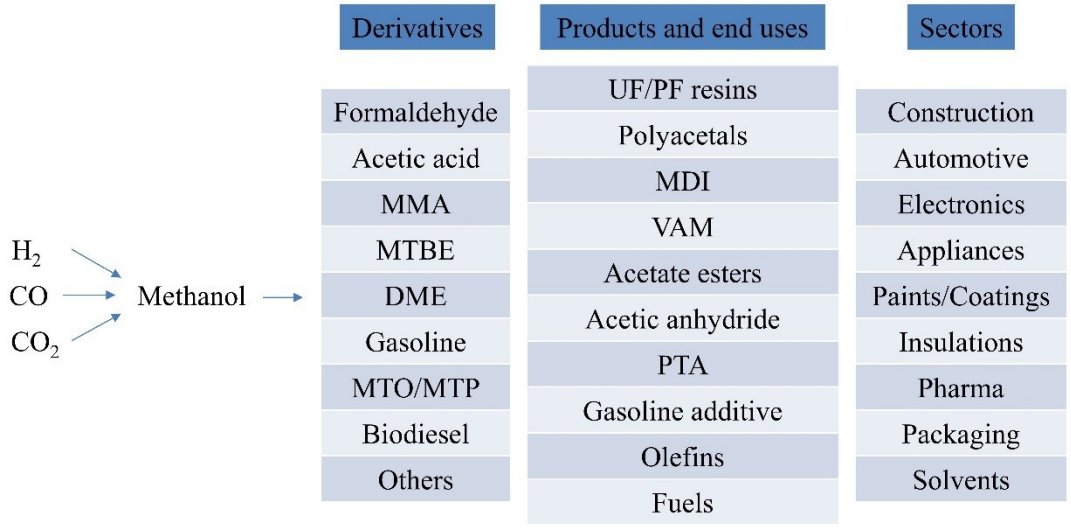

Fig. 2.2 – Methanol derivatives, products, and sectors of application (adapted from [50])

Among the chemicals reported in Fig. 2.2, formaldehyde, MTO/MTP products, gasoline and other fuels, and acetic acid, covered approximately 27, 18, 12, and 9% of the methanol use in 2015, respectively. Figure 2.3 shows the share of methanol end use in 2010 and 2015 [68]. The wide potential use of methanol in many sectors, its ease of storage, transportation, and use with negligible losses owing to its chemical stability make it one of the most promising way to store and use renewable energy in excess. It is predicted that by 2040, the energy produced by the installed RES will be remarkably larger than the total storage potential. Since the storage of energy via chemical compounds such as methanol, or other liquid fuels, requires simple tanks (without using expensive or harmful materials such as those employed in electrochemical batteries), it is clear how this road should be seriously taken into account [50].

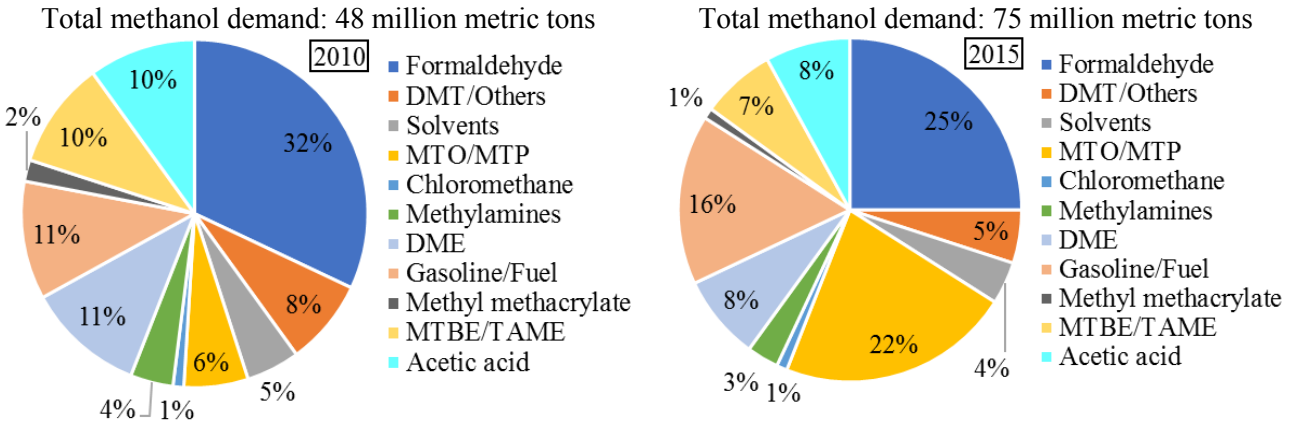

Fig. 2.3 – Methanol share by end use in 2010 (left) and 2015 (right) [68]

Worldwide, the global methanol demand increased from 48 million metric tons in 2010 to 75 million metric tons in 2015 [68]. The main variations in the share of methanol by end use regard the reduction in formaldehyde (from 32 to 25%) and a substantial increase (from 6 to 22%) in the MTO/MTP applications. Another important change regards the increase in the gasoline blending applications, from 11 to 16%. In the same year, 40% of the global demand was attributed to energy applications [69].

As previously mentioned, methanol production is mainly based on the conversion of synthesis gas, that can be obtained from different feedstocks, from both fossil or renewable sources. Among fossil resources are numerous substances such as coal, lignite, natural gas, shale gas, oil, and oil refinery wastes. This route is the most exploited nowadays. Among renewable resources, wood, agricultural wastes, biogas, and biomass in general might be used. In addition, RES can be used to produce clean hydrogen that is reacted with CO_2 via catalytic reactions. Each of these ways to manufacture methanol is characterised by different technology solutions, costs, and complexity. Depending on the availability of different resources, one solution or another would be greater or lesser attractive than others. However, given the increase in conventional feedstock costs, the limitation of natural resources, and the climate change problem, a growing interest towards the use of CO_2 as a building block of the chemicals of the future is spreading. Not only would such a system be suitable for medium-large centralised power stations (similarly to the one in Iceland [18,64]), but also it would be applicable in an perspective of decentralised RES-based stations with direct air CO_2 capture. Numerous ways of separating and capturing CO_2 from both flue gases and the atmosphere exist, but they are not the focus of this thesis. Leung et al. [70] worked on a review regarding carbon capture and storage technologies.

Many studies show that renewable methanol produced using sustainable pathways, such as captured CO_2 and RES or even biomass and RES (as well as other PtL approaches such as FT conversion), is characterised by a favourable GHG balance compared to those of fuels manufactured using fossil resources. For instance, Matzen and Demirel [71] carried out a life cycle assessment (LCA) study on the production of renewable methanol (and DME) using electrolytic hydrogen produced by wind power, and atmospheric CO_2, that had been previously fixed in biomass, released during an ethanol fermentation process. The system boundary considered by the authors consisted of a wind farm and an electrolyser, a hydrogen compression stage, as well as CO_2 processing from biomass (biomass growing, harvesting and transportation, and fermentation), the methanol production and conversion into DME section and the use of the produced fuel. Both methanol and DME produced using the renewable process described in the work were demonstrated to be more sustainable than petroleum-based processes. The analysed process is characterised by a reduction in GHG by 82-86%, a minimisation of other pollutants (e.g. SO_x, NO_x, and others), and an induced reduction in fossil fuel consumption by 82-91%. Schmidt et al. [41,42] worked out that the production of jet fuel using a PtL approach via both a methanol or a FT pathway (exploiting wind and PV energy) is more sustainable than other production pathways, both via fossil fuels or biomass. The jet fuel production via methanol conversion is based on the conversion of CO and CO_2 in the reactor. To produce jet fuel from methanol a few

intermediate steps must be performed, namely DME synthesis, olefin synthesis, oligomerisation, and hydrotreating. A FT-based process requires an intermediate step of conversion of CO_2 to CO via the reverse water gas shift reaction, since hydrogen and carbon monoxide react to produce the crude fuel of the FT process. The raw product is refined through hydrocracking, isomerisation, and distillation. While FT-derived aviation fuel can be blended with conventional jet fuel up to 50%, synthetic jet fuel derived from methanol still cannot be blended and it is awaiting approval within the ASTM standard. Table 2.5 shows the specific GHG emissions of the main processes considered by the authors. Renewable PtL option results as the nearest to a carbon neutral solution compared to both the reference process based on fossil fuels and biomass-based processes.

Table 2.5 – Specific GHG emissions of various jet fuel production pathways [41,42]

Jet fuel production	GHG emissions $[g_{CO_2,eq}/MJ_{fuel}]$
Crude oil	87.5
Crude oil (low sulphur)	89.1
Oil sand	103.4
Oil shale	121.5
Natural gas (gas-to-liquids)	101.0
Coal (coal-to-liquids)	194.8
Switchgrass (biomass-to-liquids)	17.7
Soybean oil (hydroprocessed esters and fatty acids)	37
Palm oil (HEFA)	30.1
Rapeseed oil (HEFA)	54.9
Jatropha oil (HEFA)	39.4
Algae oil (HEFA)	50.7
PtL (wind/PV, methanol or FT)	≈1

Nowadays, considering the GHG emissions related to renewable power plants deployment (material sourcing and construction), PtL processes show a reduction of emissions above 70% compared to the conventional jet fuel production. In a future perspective, with the wide diffusion of RES it will be possible to reach a reduction of GHG emissions higher than 95% compared to the reference jet fuel production process. This order of magnitude for the GHG reduction has been already achieved in the CRI George Olah Plant (cf. Par. 2.4.1). The GHG reduction can be achieved only when the electricity mix comes from RES. Indeed, since electricity production from coal-fired plants and natural gas-fired plants is characterised by a specific emission of CO_2 in the order of 800-1300 g_{CO_2}/kWh_{el} and 380-600 g_{CO_2}/kWh_{el}, respectively, even with a modest share of fossils in the electricity mix, PtL processes would become unsustainable [42]. In addition, water consumption is almost zero compared to the water needed in biomass-based processes. For instance, methanol produced from PtL requires only 1.33 l_{H_2O} for each jet fuel equivalent litre ($l_{jet\text{-}fuel\text{-}eq}$) produced, against a water amount varying in a range from 500 (algae oil produced in open ponds with water recycling) to almost 20000 $l_{H_2O}/l_{jet\text{-}fuel\text{-}eq}$ (jatropha oil) depending on the considered biomass [41]. Indeed, biomass must be cultivated using a remarkable amount of water while in a PtL process the consumed water is directly correlated to the stoichiometry of the water electrolysis reaction and to the amount of fuel produced during the process. Finally, PtL processes are characterised by a higher jet fuel yield and achievable air mileage per unit of area resulting in lower land demand and utilisation. This aspect is favourable for a reduced competition between the use of land for energy and food production [41,42].

2.4.2 Methanol to dimethyl ether

Another important conversion process that can be taken into account is the methanol to dimethyl ether process. Dimethyl ether is the simplest ether and a colourless gas, typically used as a precursor to several organic compounds. It is an extremely flammable gas that forms explosive mixtures when mixed with air, characterised by a flash point temperature of -42.2 °C and an autoignition temperature of 240 °C. At ambient pressure it melts at approximately -141.5 °C and it boils at -24.8 °C. Hence, adequate storage conditions are necessary to keep it in the liquid form at ambient conditions. Typically, DME is kept in the liquid state applying pressure up to 5 bar. The density of DME is approximately 2.1 kg/Nm^3 (0 °C, 101325 Pa). Even though it is soluble in water, biodegradation in both soil and water is a slow process. It is a rather clean fuel with no presence of sulphur and NO_x, so it can be used as household gas to cook and heat, or as a fuel in diesel engines and gas turbines, as well as fuel cells, with no need for gas exhaust treatment. Used in diesel engines, it guarantees the same efficiency as conventional fuels. However, due to its low LHV, about half of that of diesel fuel (Table 2.3), a tank twice as large as that of a diesel-fired engine is required. The combustion of DME in a diesel engine is clean without production of soot. Hence, it would be an interesting substitute to reduce particles production during combustion. DME is also employed to produce olefins and synthetic hydrocarbons. Finally, the existing infrastructure of LPG can be readily used to store and transport the DME [72–75].

Dimethyl ether production processes and advantages are similar to those of methanol. It is a chemical compound that is usually produced from synthetic gas obtained from natural gas reforming, coal gasification, or biomass conversion. Synthetic gas can be either turned into dimethyl ether via a two-step or a single step process. In the former, methanol produced from synthetic gas is sent to a second catalytic reactor to undergo a dehydration process described by reaction (2.11). In the latter, methanol synthesis and methanol dehydration are carried out in the same reactor filled with a bifunctional catalyst such as $Cu/ZnO/\gamma\text{-}Al_2O_3$ that can perform both processes. It is a feasible pathway because the conditions for the methanol and DME synthesis reactions are similar. Indeed, dimethyl ether synthesis needs for a pressure in the range of 30-100 bar and a temperature between 210 and 290 °C, ranges similar to those typical of the methanol synthesis process. Methanol synthesis occurs on $Cu/ZnO/Al_2O_3$ while methanol dehydration on an acidic catalyst modified with $\gamma\text{-}Al_2O_3$ or $ZSM-5$ catalyst (zeolite-based catalysts). The combination of these two reactions in one single process and reactor, allows more favourable reaction thermodynamics and kinetics. By varying the ratio between the two catalysts it is possible to obtain a final products with DME content ranging from 5 to 95% [76]. Reactions (2.11)-(2.13) show the main reaction mechanism depending on the initial composition of the synthesis gas. Reaction (2.11) represents the methanol dehydration process.

$$2CH_3OH \rightarrow C_2H_6O + H_2O \tag{2.11}$$

If the reactor inlet contains only CO and H_2, then the overall reaction (2.12) takes place. The formed CO_2 can be recycled in the process where syngas is produced.

$$3CO + 3H_2 \rightleftarrows C_2H_6O + CO_2 \tag{2.12}$$

Otherwise, with CO, CO_2, and H_2 as the feedstocks, reactions (2.10) and (2.13) are carried out.

$$2CO + 4H_2 \rightleftarrows C_2H_6O + H_2O \tag{2.13}$$

The conventional and most diffused way to perform DME synthesis is the two-step process, presently used by companies such as Haldor Topsøe, Toyo Engineering, Oberon Fuels, BioDME and Lurgi. The main advantage of this approach is that a methanol production facility can be modified and expanded by connecting a second reactor to the existing system, with low capital investment. With this approach, an existing methanol production plant can be retrofitted to produce DME only when required by adding the DME synthesis section. Another benefit is that the acidic catalyst used in the dehydration process has a limited activity towards the water gas shift reaction. Hence, during the second step only a marginal quantity of CO_2 is generated from reaction (2.10). On the other hand, in the one-step process the catalyst used to

produce methanol is highly active towards reaction (2.10). Considering a process aimed at the reduction of CO_2 impact, the lower the CO_2 released from the process, the better. On the other hand, the one-step process is characterised by a theoretical higher DME yield because the presence of a bifunctional catalyst changes the equilibrium between reactions (2.8) and (2.9) leading to a higher methanol yield and so a higher DME yield. Syngas conversion to DME results in higher equilibrium conversion than that of the syngas to methanol process, because of the strong synergy between the reactions (2.8)-(2.10) and (2.11) [67].

Chapter 3

System configurations and main processes

3.1 Overall system configuration

This thesis is focused on the analysis of different configurations of an energy storage system, using different technologies, to produce chemical compounds exploiting RES, hydrogen and recycled CO_2. Following the information provided in Chapter 2, the main chemical species considered is methanol.

The innovative energy system studied in this work is conceived to produce methanol coupling water electrolysis technology to a chemical conversion reactor and a fuel cell. With the integration with proper components (cf. Par. 2.4.2), also dimethyl ether production can be performed. Such a system would be ideally used to contribute to decarbonizing the atmosphere by storing excess renewable energy as chemical energy in liquid fuels and turning it into electricity during lack of renewable energy, or as a source of fuels and chemicals for a variety of applications in different industrial sectors. Indeed, PtL processes can favour the penetration of RES and the exploitation of renewable energy via the production of chemicals, if renewable hydrogen and recycled CO_2 are employed. As an energy storage system, the excess of renewable electricity is stored as a chemical compound to level out the load diagram and reduce the overall losses within the grid system.

Figure 3.1 shows a simplified functional scheme of the overall system and of the main subsections considered and studied in this work.

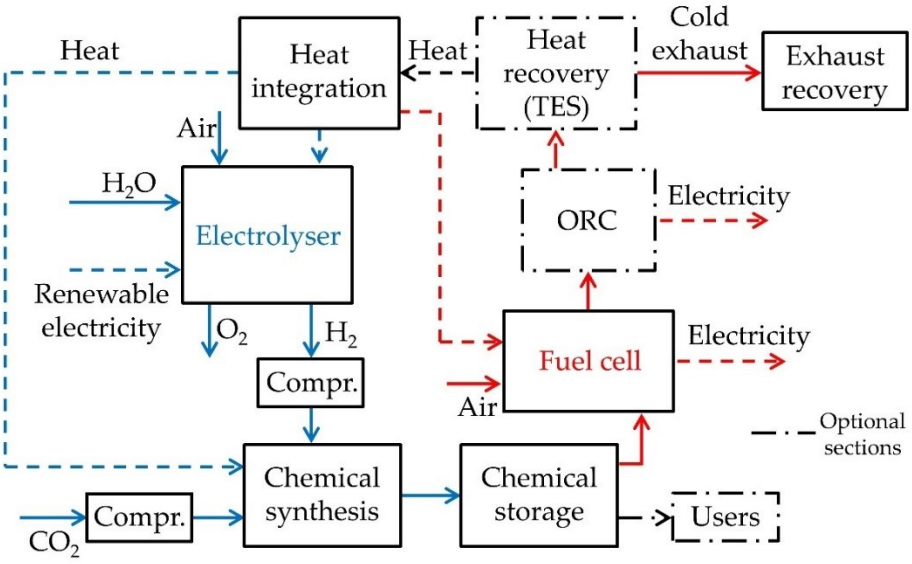

Fig. 3.1 – Simplified functional scheme of the possible overall systems

Blue and red objects represent the two main processes carried out in the described system. The streams related to the electrolysis operation are depicted in blue, while in red are those related to the fuel cell operation. More generic processes such as the compression sections, the chemical synthesis and storage blocks, and the heat recovery are represented in black.

Different configurations of the general system depicted in Fig. 3.1 were analysed to evaluate the performance of a power to methanol energy storage plant. In general, as depicted in the scheme, the main subsections for

the operation of the system are an electrolyser, a chemical synthesis and a storage section, a fuel cell and a heat recovery section. The electrolyser is fed with RES to produce hydrogen from water. Electrolytic hydrogen is directly sent to the chemical synthesis section where the chemical conversion and the purification processes take place. Prior to the chemical synthesis, CO_2 and H_2 are compressed to the chemical synthesis operating conditions. Thus, the hydrogen production process and the chemical synthesis are directly connected and occurs in series under the same operating process ("charge phase"), since the feedstocks (namely hydrogen and carbon dioxide) are directly sent to the chemical reactor. The chemical compounds produced in this process are stored under proper conditions to be used subsequently. The stored chemicals can be either used in a fuel cell to produce electricity when needed ("discharge phase"), or used in other end user applications, such as fuel for transportation or chemical feedstock in the chemical industry. To produce electricity, methanol (and if considered, DME) is reformed to syngas, composed of hydrogen and carbon monoxide that are oxidised in the cells. Otherwise, considering different end user applications, the fuels are stored in liquid phase and then transported where needed, using the existing handling, transportation, and distribution infrastructure. Considering the electricity production process, the residual gases (mainly composed of hydrogen) exiting the fuel cell are burnt in a post combustor to increase the temperature of the hot exhaust gases. An organic Rankine cycle (ORC) system fed by the hot exhaust gases coming from the fuel cell section can be considered as well. Indeed, the introduction of an ORC would improve the energy output of the system by exploiting the fuel cell heat that otherwise would be wasted. However, the advantage of an ORC depends on the amount of heat effectively available in the exhaust gases that strongly depends on the configuration and technologies considered for the other sections. To reduce the thermal energy requirements within the sections, to improve the self-sustainability of the system, and to boost the overall performance, a heat recovery section (thermal energy storage system, TES) is necessary. Indeed, excess heat produced in fuel cell mode (charge phase) can be stored during the discharge phase and used back during the charge phase. The presence of the TES allows a deferred use of the stored heat. Finally, the heat integration block depicted in Fig. 3.1 comprises the heat exchangers and heaters needed to guarantee the correct operation of the system. The figure also shows the main material, heat, and electricity streams entering and exiting each section.

The main technologies considered are:

- alkaline water electrolysis cells
- solid oxide electrolyser cells
- methanol synthesis reactor and distillation
- solid oxide fuel cells
- organic Rankine cycle
- phase change material thermal energy storage (PCM-TES).

The main variation between the configurations consists of the electrolysis and fuel cell sections, where a commercially mature technology (namely alkaline water electrolysis) is compared to another not yet fully developed technology (i.e. solid oxide cells and reversible solid oxide cells), that is believed to have achieved commercial readiness by 2030 [77]. Each technology will be briefly described in the following, and a description of the main specific configurations analysed in this work will be reported.

3.2 Water electrolysis

Since in this work hydrogen is produced via water electrolysis processes, the three main technologies employed today are described, namely alkaline electrolysis, proton exchange membrane electrolysis, and solid oxide electrolysis. The production of hydrogen from liquid water requires an amount of energy at least equal to the formation enthalpy of 285.9 $\mathrm{kJ/mol}$, corresponding to 15.87 $\mathrm{MJ/kg_{H_2O}}$ and to 3.55 $\mathrm{kWh_{el}/Nm^3_{H_2}}$. The actual power absorbed by an industrial water electrolysis plant is in the range 4.5-5.0 $\mathrm{kWh_{el}/Nm^3_{H_2}}$ [29]. Water splitting occurs at the cathode and anode following reactions (3.1) and (3.2), respectively:

$$2H_2O + 2e^- \rightarrow H_2 + 2OH^- \quad (3.1)$$

$$2H_2O \rightarrow O_2 + 4H^+ + 4e^- \quad (3.2)$$

Water can be split in an electrolysis process both as liquid or as steam, depending on the operating temperature that is related to the technology used. Low temperature water electrolysis is the typical approach used in alkaline and proton-exchange membrane cells, while high temperature steam electrolysis is typical of solid oxide cells technology. High temperature electrolysis allows the reduction of the decomposition voltage by partially substituting electric power with heat, reducing the need for high quality energy.

3.2.1 Worldwide hydrogen production and use

As previously stated (cf. Par. 2.1), nowadays hydrogen is mainly produced from fossil fuels via the reforming of natural gas (48%) and oil (30%), and coal gasification (18%), while only 3.9% comes from water electrolysis and 0.1% from other sources [16,28,29]. Approximately 70 million t of hydrogen are used each year worldwide, mostly for oil refining, chemical production such as fertilisers, ammonia, and urea, and steel treatment where it is used as a reducing agent. Ammonia synthesis accounts for 55% of the hydrogen consumption, refineries require roughly 25% of the total produced hydrogen, and methanol production covers approximately 10% of the hydrogen usage. Over the last decade, methanol has gained an important share of hydrogen consumption worldwide, with an increase in its production from 35 to 45 million $t/year$. The typical fossil methanol plant capacity is 5000 t/day, corresponding to a hydrogen consumption of approximately 265 $kt/year$ [78]. Other applications (such as hydrogen mobility, FT hydrocarbons production, and others) cover the remaining 10% [29,79]. Specifically, in Europe 90% of the hydrogen is consumed in the industrial sector (roughly 7 million $t/year$) where 63% is used in chemical production, 30% in refineries, 6% in metal processing, and the remaining 1% in other applications. Within the chemical sector, 84% of the hydrogen is used to produce ammonia, 12% methanol, 2% polyurethane, and 2% nylon [78].

3.2.2 Alkaline electrolysis

Alkaline electrolysis of water (AEL) is a low temperature process based on the use of a base such as KOH or $NaOH$, mixed with water to improve the water splitting process. Among these two, KOH is preferred over $NaOH$ solutions because it guarantees higher conductivity [80]. The liquid electrolyte contains both the electrodes that are separated by a membrane, or diaphragm, crossed by OH^- ions during the electrolysis [81]. At the anode side, reaction (3.3) (oxygen evolution reaction) takes place:

$$4OH^- \rightarrow O_2 + 2H_2O + 4e^- \quad (3.3)$$

while at the cathode side, reaction (3.4) (hydrogen evolution reaction) takes place.

$$4H_2O + 4e^- \rightarrow 2H_2 + 4OH^- \quad (3.4)$$

The energy carrier in both reactions (3.3) and (3.4) are the hydroxide OH^- ions [82]. Figure 3.2 shows a simplified representation of the operating principle of the PEM electrolysis process.

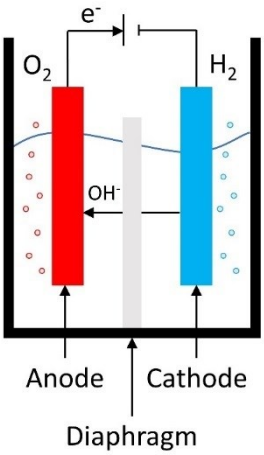

Fig. 3.2 – Simplified representation of the operating principle of AEL electrolysis (adapted from [83])

The energy consumption of water electrolysis is strictly related to the cell voltage. Typical voltages applied to commercial AEL are in a range from 1.8 to 2.4 V. The current density is another important value in cell operation. In AEL it is usually set between a lower limit of 1000-2000 $\mathrm{A/m^2}$ and an upper limit of 3000-4000 $\mathrm{A/m^2}$ and determines the rate at which the hydrogen is produced [77,84,85]. Hydrogen purity reaches values as high as 99.5 vol.% [77]. At the stack level, the energy consumed in an AEL is in a range from 4.2 to 5.9 $\mathrm{kWh_{el}/Nm^3_{H_2}}$ [77]. Usually, operating temperature is set between 60 and 90 °C to avoid an excessive evaporation of the alkaline solution and the breakdown of the membrane. However, the higher the temperature, the lower the electricity and the higher the heat required, while the total energy demand slightly increases, as shown in Fig. 3.3 [86–88]. Figure 3.3 shows the energy required by an ideal electrolyser as a function of temperature (left) and pressure (right), at standard pressure and temperature, respectively. The general equation describing the curves in Fig. 3.3 is Eq. (3.5):

$$\Delta H = \Delta G + T\Delta S \tag{3.5}$$

where ΔH is the thermal energy available from the reaction, also known as enthalpy of formation, and ΔG is the Gibbs energy of formation. The difference between these two, i.e. $T\Delta S$, is converted to (fuel cell operation) or provided as (electrolysis operation) heat. Considering the water electrolysis process, ΔH is higher than ΔG, so the reaction is endothermic, and heat must be supplied as $T\Delta S$. Increasing the temperature leads to a reduction in the electricity, namely ΔG, allowing the substitution of high quality energy with a lower quality energy, namely heat [89].

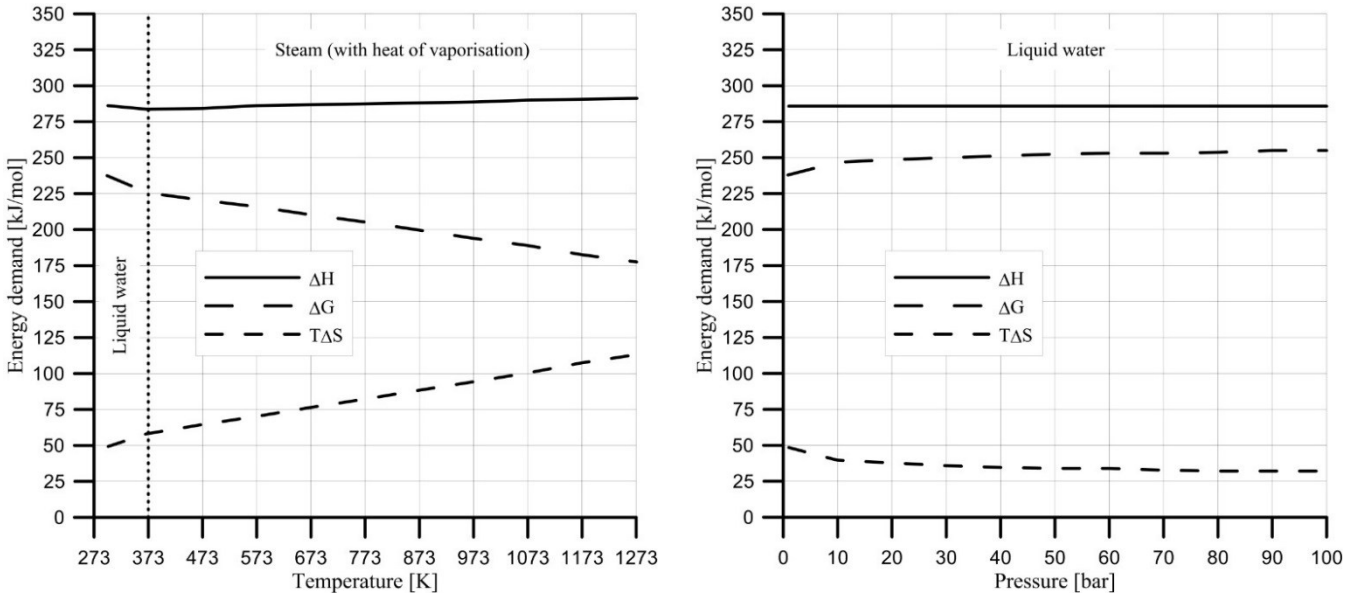

Fig. 3.3 – Energy consumption of an ideal electrolyser as a function of temperature (left) and as a function of pressure (right) (adapted from [88])

On the one hand, an increase in operating temperature would lead to a lower consumption of high-quality energy (i.e. electricity). On the other hand, regarding the AEL, to a higher temperature corresponds a greater water evaporation rate and greater problems of thermal management and stability of the electrolyte materials. Pressurised operation up to 35 bar is doable and causes a reduction in bubbles size, reducing the ohmic losses related to bubbles formation. In spite of this advantage, the efficiency gain is marginal [85]. Nevertheless, operating at high pressure might be useful to reduce energy requirements in subsequent processes such as hydrogen handling or further chemical conversion. Moreover, the AEL is characterised by a thermal balance voltage at which the cell is in thermal equilibrium, a condition at which the temperature of the cell is constant without active management. The thermal balance voltage is related to the temperature and pressure values. If, at a given pressure, the voltage applied to the cell is lower than the corresponding thermal balance voltage, the cell temperature will drop until it reaches a lower equilibrium temperature [82]. At this voltage, which is different from the thermoneutral one, it is not necessary to provide additional heat to the cell. Higher pressures reduce the thermal balance voltage and so guarantee efficient operation without providing additional heat, even with voltages between 1.5 and 1.7 V [82]. Material choice and optimisation are two other important aspects for durable, stable, and reliable cells. For instance, electrolyte concentration is important to determine the electrolyte resistance. Electrode materials must be stable and must be characterised by high electrochemical activity and high resistance to alkali corrosion. Nickel shows a good compromise between these specifics, resulting a long-lasting and inexpensive electrode material. Finally, water purity is especially important in alkaline electrolysis since accumulations and deposits of impurities on the electrodes and membrane would lead to reduced performance and limitations in mass and electrons transfer. Power consumption for alkaline electrolysis plants spans between the order of the kW to several hundred MW (depending on the number of modules arranged in series and parallel) [85,90].

Typical commercial alkaline water electrolysers are characterised by an electrical energy consumption not higher than 70 kWh_{el}/kg_{H_2}, while a well optimised system, working at nominal condition, absorbs between 43 and 53 kWh_{el}/kg_{H_2} [55,91–93]. Generally speaking, in literature the electric consumptions for commercial AEL are reported in a range from 47 to 67 kWh_{el}/kg_{H_2} (4.2 to 6.0 $kWh_{el}/Nm^3_{H_2}$) [94,95]. Commercial alkaline electrolyser modules have reached a size up to 3.2 MW_{el} with a production of 760 $Nm^3_{H_2}/h$. The modules can be arranged in complex systems that guarantee modularity, not only favouring the building of both decentralised and centralised plants but also reducing the problems related to part load operation, which causes a significant increase in electricity consumption when the electrolyser is not

operated under nominal conditions [96,97]. Alkaline electrolysers are characterised by great durability in the order of 70000-100000 hours, corresponding to a lifespan of 9-15 years [97].
Current alkaline electrolysers are not perfectly suitable to be coupled to intermittent RES to produce clean hydrogen due to poor performance at low current density. Low current density operation brings about difficulties and problems from the point of view of flexibility in following RES load, thermal management, power/voltage matching, and safe operation conditions (with intermittent operation and low current density, the rate of permeation of hydrogen and oxygen is higher than the rate of production and these two gases might mix, determining hazardous conditions) [95,98,99]. Nevertheless, new materials and manufacturing technique developed at DLR (German Aerospace Center – Deutsches Zentrum für Luft- und Raumfahrt) allow long-term stability over intermittent operation, that had been demonstrated during several years of testing and operation [100]. AEL systems are suitable to work in a range from 15 to 100% of the nominal load, with start-up times of 1 and 10 minutes when warm and cold, respectively, ramping speed upward and downward of 0.2-20%/s and shutdown period between 1 and 10 minutes. Even though constant progresses are made to improve AEL flexibility, at present these values are still not perfectly applicable in RES load following. Nevertheless, RES hydrogen production via AEL would be feasible and efficient if the system is connected to the grid. In this way the electrolyser would be fed with a constant nominal power input by coupling RES and grid power. This scenario is of particular importance in the case of wind source, that is the most intermittent RES [95].
To evaluate the heat balance of an alkaline electrolysers five main factors should be considered. These are related to cells overpotential (due to current flow and kinetic losses), water vaporisation, heat transfer to the environment, heat needed to provide refilling water at the right temperature, and the energy related to hydrogen and oxygen recombination inside the cell [82,101].

3.2.3 Proton exchange membrane electrolysis

Proton exchange membrane electrolysis cells (PEMEL or PEM) were not analysed in this work. However, since it is one of the three main water electrolysis technologies, a brief description of its characteristic is reported here for the sake of completeness. The electrolysis mechanism in PEM is different from AEL, since the process occurs through a gas-tight polymeric membrane usually made of Nafion [102]. The reactions involved in PEM electrolysis are (3.6) (at the anode, where water is split) and (3.7) (at the cathode, where hydrogen is released).

$$2H_2O \rightarrow O_2 + 4H^+ + 4e^- \tag{3.6}$$

$$4H^+ + 4e^- \rightarrow 2H_2 \tag{3.7}$$

Figure 3.4 shows a simplified representation of the operating principle of the PEM electrolysis process.

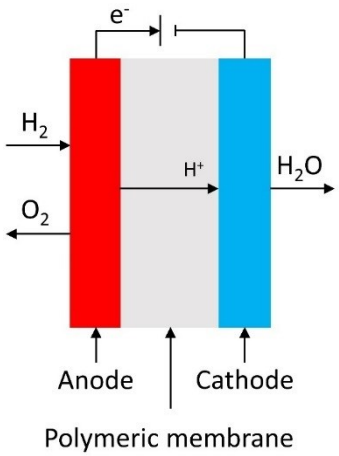

Fig. 3.4 – Simplified representation of the operating principle of PEM electrolysis (adapted from [83])

PEM typical voltage is similar to that of AEL, ranging between 1.8 and 2.2 V while current densities span from 6000 to 20000 A/cm^2, remarkably larger than the maximum AEL current densities [77]. The operating temperature is usually set between 50 and 80 °C due to the use of polymeric membranes that lose their conductivity because of dehydration processes [103]. State of the art systems are characterised by a maximum hydrogen output of 30 Nm^3/h absorbing 174 kW_{el} [97]. In some applications, high pressure operation is feasible with values up to 85 bar, resulting in lower compression energy and costs in subsequent processes. The produced hydrogen is purer than AEL hydrogen with purity levels as high as 99.99 vol.%. Electrical energy absorption is in a range from 4.5 to 7.5 $kWh_{el}/Nm^3_{H_2}$ (50.4-84.1 kWh_{el}/kg_{H_2}). Stack lifetime is lower than 20000 hours, resulting a less competitive solution than AEL [88,104,105]. However, for transient operation based on RES, PEM cells are more suitable than AEL. Indeed, they can be operated in a range from 0 to 160% of the nominal load, with a start-up time from 1 second to 5 minutes, a ramping speed of 100%/s (i.e. system response in the order of a few milliseconds) and a shutdown time in the order of seconds [77,106].

Compared to AEL, the disadvantages are mainly related to shorter lifetime (approximately half or even less), lower nominal efficiency, higher investment costs, and high degradation rate. Nevertheless, PEM are particularly suitable to be coupled to RES because, along with high flexibility and transient operation response of few milliseconds, are characterised by higher efficiency in part load operation than at nominal conditions, and operation at low current densities does not cause formation of flammable mixtures [88,106–108]. In addition, PEM electrolysis technology is still expensive due to the use of noble metals. In particular platinum oxides are largely used and R&D effort is aimed at the use of carbon-supported catalysts that are platinum free [104,109,110]. PEM electrolysis systems are facing a rapid growth and expansion towards commercialisation because of the promising performance in RES storage applications [107].

PEM operation is usually exothermic due to the overpotentials inside the cells. Under this condition, it is not necessary to provide external heat since all the needed thermal energy is produced inside the cell [111].

3.2.4 Solid oxide electrolysis

In the last few years, SOEC technology has been receiving a growing attention as a high efficiency device to produce hydrogen from water electrolysis. SOECs are typically developed from existing SOFC, using established materials and geometries employed for the fuel cell variant. Moreover, it is possible to operate a SOFC in SOEC mode with minor or no modifications. SOCs are built using porous ceramic materials (for the electrodes and the electrolyte) such as a mixture of Ni-YSZ-LSM (Nickel – Yttria Stabilised Zirconia – $La_{0.8}Sr_{0.2}MnO_3$) that allows working at very high temperature without the need for expensive catalysts typically employed in AEL and PEM systems. In a SOEC, the reactions occurring at the cathode ((3.8)) and at the anode ((3.9), (3.10)) are:

$$2H_2O + 4e^- \rightarrow 2H_2 + 2O^{2-} \quad (3.8)$$

$$2O^{2-} \rightarrow O_2 + 4e^- \quad (3.9)$$

$$O + O \rightarrow O_2 \quad (3.10)$$

Oxygen ions flow from the cathode to the anode across the electrolyte, releasing the current and the oxygen molecules. Figure 3.5 shows a simplified representation of the operating principle of the solid oxide electrolysis process.

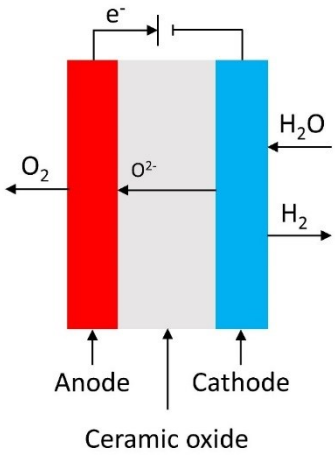

Fig. 3.5 – Simplified representation of the operating principle of SOC electrolysis (adapted from [83])

Typical operating temperatures of SOEC (and SOFC) are in a range from 600 to 1000 °C, with a production rate of 1 Nm^3/h_{H_2} and a maximum size of a few hundreds of kW. SOCs are usually operated in a voltage range from 0.7 to 1.5 V and a current density from 3000 to 20000 A/m^2. Typical power consumption is higher than 3.2 $kWh_{el}/Nm^3_{H_2}$ (35.9 kWh_{el}/kg_{H_2}) at the stack level and increases up to more than 3.7 $kWh_{el}/Nm^3_{H_2}$ (41.5 kWh_{el}/kg_{H_2}) at the system level. State of the art stacks achieve a power of 150 kW [77].

While in the case of the AEL and PEM cells the temperature cannot be higher than 90-100 °C, because of the evaporation of the water mixture in the AEL, or the failure of the polymeric membrane in the PEM, SOCs can be operated at a very high temperature, benefitting the most from the behaviour showed in Fig. 3.3. Indeed, the main advantage when using these cells is that the electricity requirement is lower, and a remarkable portion of the total energy needed in the electrolysis process can be provided as heat. Moreover, high temperature favours the kinetic mechanism of the reactions and minimises the electrochemical losses. Nevertheless, working at high temperature has its own drawbacks, such as significant mechanical and thermal stress, that bring about a reduced lifespan of the stack. Owing to this type of stress, material and assembly must be wisely chosen and performed. Hence, due to the high temperature operation, material degradation is a major problem leading to stack lifetime shorter than 10000 hours [77]. Furthermore, to avoid a premature drop in the electrode performance, some modifications in the oxygen electrode derived from SOFC must be applied [112].

Among numerous SOC design, the typical shapes are the tubular and planar with the latter being the most commonly employed [112,113]. The main differences between the two configurations are related to the difficulties in construction (higher for the tubular), the mechanical resistance (higher for the tubular, since the circular pattern reduces the mechanical stresses), and gas distribution (better for the planar, since the gases between the plates is distributed better within the inner channels). Because of its ease of construction

and manufacturing, and since SOECs are typically derived from planar SOFCs, the planar shape is becoming the reference geometry for such systems. Thus, the planar geometry was considered in this work.
Finally, in this thesis the SOEC technology was chosen over PEM because Schmidt et al. [77] foreseen an evolution of the two technologies happening at the same pace in the next ten years. Thus, SOECs were chosen because of the lower energy consumption and the higher efficiency.

3.3 Solid oxide fuel cell

SOFC is a clean and highly efficient technology, employed in various energy conversion applications, that can be fed with a variety of fuels. Commercial SOFCs for stationary applications are typically available in a range from 10 kW to 1 MW depending on how the stacks and modules are arranged, but research is pushing towards larger size to deploy systems for even larger stationary applications [112,114,115]. Typical operating conditions (i.e. voltage and current densities) are those reported in Par. 3.2.4 for generic SOCs.
As reported in Par. 3.2.4, SOFCs are manufactured using porous ceramic materials. Compared to a SOEC, in a SOFC the anode and cathode definitions are inverted. However, this is only a convention since each electrode is optimised to perform one of the two main reactions in the hydrogen production/oxidation process. Hence, while in a SOEC the cathode is where the water splitting takes place, in a SOFC the electrode where water is formed is called anode. In both cases, the cathode and the anode represent the positive and the negative electrodes of the cell, respectively. Reactions (3.11) and (3.12) are carried out at the SOFC anode and cathode, respectively:

$$2H_2 + 2O^{2-} \rightarrow 2H_2O + 4e^- \tag{3.11}$$

$$2O_2 + 4e^- \rightarrow 2O^{2-} \tag{3.12}$$

The oxygen ions cross the electrolyte, from the cathode to the anode, to react with hydrogen, producing electricity and forming water. Typically, the fuel feeding a SOFC can be reformed either in an external reformer placed outside the SOFC stack boundaries or in an internal reformer directly connected and in contact with the SOFC. Nevertheless, owing to the high operating temperature of the SOFC, this type of cell can also be directly fed with a variety of hydrocarbons, such as natural gas, without an external reformer and are less influenced by fuel impurities. For instance, ceramic materials are not subjected to carbon poisoning, a phenomenon that causes the deactivation of the catalysts employed in low temperature fuel cells. Furthermore, SOFCs are characterised by the advantages already reported for SOECs (i.e. better reactions kinetic than low temperature operation, and low electrochemical losses), leading to higher energy output than other fuel cells. Finally, SOFC can be operated in both electrolyser and fuel cell modes without substantial differences in performance level. Hence, a renovated interest has recently risen on the use of a single SOC operated as a reversible solid oxide cell (RSOC) in cyclic operation, to perform water electrolysis and fuel oxidation in the same device [116–118]. Indeed, SOFC (and SOC in general) are characterised by cell and stack design flexibility, multiple fabrication options, multi-fuel capability, and a wide range of operating temperature that allows the use of the system in several applications [112].

3.4 Reversible solid oxide cell

RSOC systems incorporate both SOFC and SOEC operation modes in a single unit. Using a single RSOC capable of operating in both modes, instead of two separate SOEC and SOFC, allows saving investment costs on some appliances and components and at the same time addressing numerous different markets with only one system (i.e. energy storage, distributed power generation, power to gas or liquids, hydrogen production, etc.) [99,119,120]. Nevertheless, to improve competitiveness, the optimisation of RSOC materials is required to guarantee a proper system stability in both operating modes [121,122].

Typically, SOEC and RSOC are derived from existing SOFC, using the materials employed in the SOFC manufacturing [112,121,123,124]. Also, the mathematical models describing the SOEC and RSOC are slightly modified versions of SOFC models [125–127]. Even though some differences should be taken into account, at the best of author's knowledge, the papers analysed and cited above regarding RSOC did not consider any particular difference between SOFC and SOEC both from the materials point of view and the electrochemical models when considering a single RSOC. In addition, no major advantages in SOFC and SOEC usage over a single RSOC were highlighted. Since the technology employed in SOFC and RSOC is the same, the operating temperature range is also the same, spanning from 600 to 1000 °C. As already mentioned, typical materials employed in the manufacturing of SOCs are:

- yttria stabilised zirconia (YSZ) used as the main substance for the electrolyte;
- different types of perovskites (namely LSM, lanthanum strontium manganese oxide, and LSCF, lanthanum strontium cobalt iron oxide) for the oxygen electrode;
- a cermet (a composite material made of ceramic and metal materials) of Ni/YSZ as the main component of the hydrogen electrode;
- highly conductive material used for the interconnections, to assemble stacks via interconnected cells such as LSC (lanthanum strontium chromium perovskite) or stainless steels.

To be effective, an RSOC should work efficiently, guaranteeing good performance, reversibility and stability, in both operating modes, and in cyclic operation. RSOC material sets are usually optimised to work in a small temperature range [124]. Even though both SOEC and SOFC are characterised by relatively low stability and high degradation rate over time, Graves et al. [128] demonstrated with a 4000-hour test that a SOC reversibly cycled between SOEC and SOFC mode, does not incur in degradation and, on the contrary, its ohmic resistance slightly decreases. This means that the performance of the cell improves over time instead of diminishing. The RSOC behaved just like a rechargeable battery and its suitability for large scale RES storage was demonstrated. Also Chen et al. [129] found out that the cyclic operation of an RSOC allows the avoidance of degradation in the cell.

3.5 Methanol and dimethyl ether synthesis and distillation

Another important section in the overall system is the chemical synthesis system, that turns the hydrogen, produced in the electrolysis section, and the recycled CO_2 into valuable fuels and chemicals. In the chemical synthesis section, the purification of the products takes place as well. Methanol synthesis, as well as dimethyl ether synthesis, occurs in a reactor filled with a commercial catalyst (cf. Par. 2.4.1 and 2.4.2) where adequate conditions are maintained to optimise the chemical yield and conversion. The feedstocks (hydrogen and carbon dioxide) enter the reactor and are converted into chemicals such as methanol (and/or dimethyl ether). The products, typically composed of water, methanol, hydrogen and CO_2, are purified from the unreacted species and incondensable gases via flash processes. The unreacted species are recycled back to the reactor inlet to boost methanol production. The liquid outlet from the last flash, called crude methanol, is sent to a distillation column where the purification steps take place and methanol is separated by water and residual CO_2. The unreacted CO_2 leaving the distillation column is recycled to the reactor inlet to improve methanol conversion.

In a similar way, when considering the dimethyl ether produced in a two-step process (cf. Par. 2.4.2), purified methanol is brought at the DME reactor conditions and enters the reactor where the dehydration reaction (2.11) takes place. Usually, the products exiting the DME reactor are purified in two subsequent distillation columns, where the separation between DME, MeOH and water is carried out. Typically, in the first column DME is separated from the other species (mainly water and methanol) while methanol and water are separated in the second column. The unreacted methanol exiting the second distillation column is recycled to the reactor inlet to boost dimethyl ether production.

3.6 Organic Rankine cycle system

Organic Rankine engines exploit low-grade thermal energy more efficiently than conventional steam cycles, that are not always technically and economically feasible. Main manufacturers are Turboden, Ormat, and Maxxtec, while the typical installed power ranges from 100 kW_{el} to up to 50 MW_{el}. Table 3.1 reports the share of installed units and installed power by these three manufacturers [130].

Table 3.1 – Share of installed units and power

Manufacturer	Installed units	Installed power
Turboden	45%	8.6%
Ormat	24%	86.0%
Maxxtec	23%	3.4%

Organic Rankine engines work following the ORC. These engines are used for power generation when the heat source is in a temperature range from 80 to 350 °C, guaranteeing the most convenient solution for electricity production providing high performance, flexibility, and low capital costs compared to gas and steam cycles when these are applied to the same range of operation (low temperature and/or limited thermal power availability). Working fluids employed in ORC have properties suitable for the low-temperature application: lower boiling point, higher vapour pressure and higher molecular mass than water, that determine lower rotation speed and pressure and no liquid phase during expansion, which in turn reduces the erosion of the turbine components and so the maintenance costs. Moreover, an ORC system is characterised by a reduced environmental footprint: there is no production of waste water and there is little soil consumption due to the compact design. The main subsystems in an ORC plant are: a turbine, where the working fluid expands and produces electricity through a generator coupled to the turbine; heat exchangers typically of the shell and tubes type; a condenser to cool the working fluid using air or water; a feed pump to bring the organic fluid to the maximum pressure of the cycle [131,132]. Figure 3.6 shows the thermodynamic cycle and a simplified scheme of a typical ORC plant.

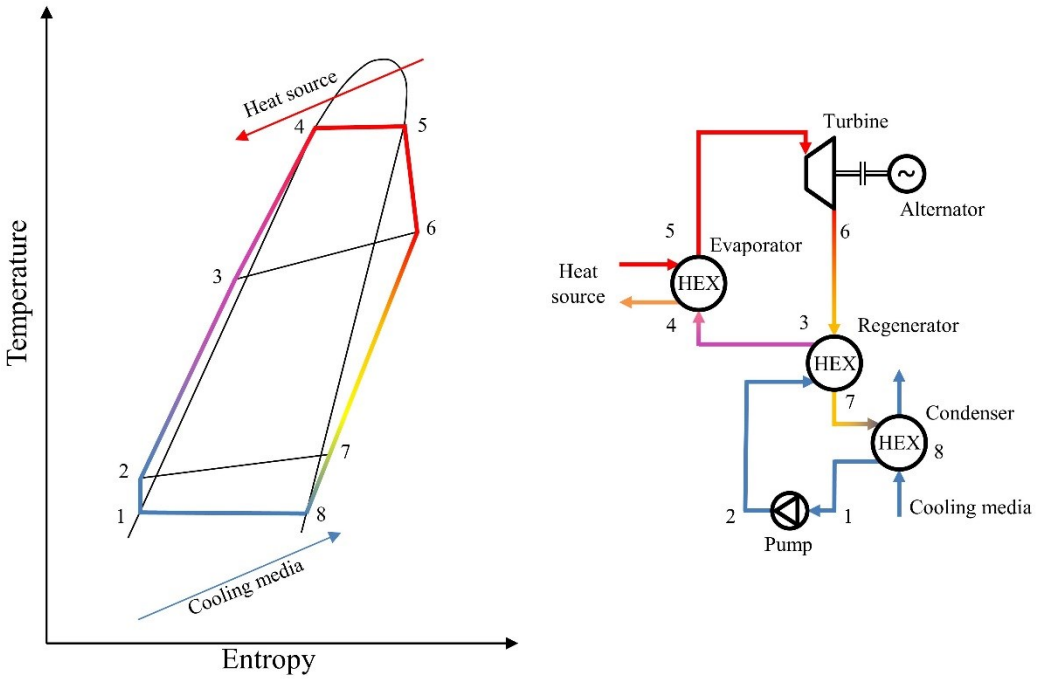

Fig. 3.6 – Organic Rankine cycle and simplified plant scheme (adapted from [132])

In general, a heat source releases its energy to the working fluid in an evaporator (4-5 in the simplified scheme of Fig. 3.6) that is sent to the turbine coupled to an electric generator (5-6). When the primary heat source is at high pressure, an intermediate thermal oil circuit might be used to perform the heat transfer to the working fluid via an ambient pressure loop, reducing the system complexity and cost. The hot working fluid expands in the turbine to a pressure slightly higher than the condensation one. The turbine exhaust heat is exploited to preheat the working fluid in a regenerator (6-7, 2-3). The residual heat is dissipated in a condenser using a cooling medium such as air or water (7-1). The cold working fluid is brought to the maximum cycle pressure via the feed pump (1-2) and the cycle begins again. The configuration shown in Fig. 3.6 represents a single pressure level cycle. Depending on the configuration, the operating conditions, and the working fluid, not only might the primary heat exchanger be composed of an evaporator but also by an economiser and a superheater. This configuration is usually applied to large subcritical plants, while a configuration with a once-through heat exchanger is mandatory in the case of supercritical cycles. Subcritical cycles are employed in large geothermal plants, biomass combustion processes, waste heat recovery, and domestic cogeneration. Superheating is convenient only when the maximum temperature of the heat source is significantly larger than the critical temperature of the working fluid. Otherwise there would be a reduction in the power output owing to a reduction of the mass flow rate. Superheating is effective when the critical temperature is lower than the maximum heat source temperature, because the average temperature tends to increase while the heat source is used at best. In supercritical cycles the maximum pressure is higher than the critical one and the fluid phase change happens in a smooth and gradual way that prevents discontinuity in the variation of the thermodynamic properties. Supercritical cycles reach higher efficiency than corresponding subcritical cycles, but they also work at higher pressures. Therefore, more sophisticated and expensive components, such as heat exchangers with thicker walls or special types of pumps, are necessary. Other types of ORC are the multi pressure level cycles and the trilateral cycles, which can achieve higher efficiencies but are rarely adopted due to remarkable system complexity [133]. ORC working fluids tend to decompose at high temperature, hence the maximum allowed temperature is usually in a range from 350 to 400 °C. Above these values, the organic fluids lose stability and decompose [134].
Organic Rankine cycle systems are useful when a corresponding steam cycle, working under the same conditions, would have a low efficiency due to low temperature heat, typically below 350 °C. Between an ORC and a steam Rankine cycle (SRC) there are several differences since the properties of the two types of fluids differs significantly [130].

3.7 Phase change material thermal energy storage

Thermal energy can be stored as sensible heat or as latent heat, depending on the chosen storage material and its properties. Typically, latent heat thermal energy storage (LHTES) systems are used in applications such as ORC or in small to medium scale CSP plants, as well as in other industrial applications such as solar cooling systems, fuel cells, heat recovery in hydrogen storage within metal hydrides, food industry and others, where the thermal source providing the heat is below 250-300 °C. Nevertheless, depending on the chosen PCM, this temperature limit might be even higher. Phase change materials are commonly used to store and release a large quantity of energy as latent heat, during the phase change process. In LHTES systems, the storage materials undergo a phase transition. Indeed, latent heat change is remarkably larger than the sensible heat change of a substance, so exploiting this mechanism allows the storage of a significantly larger amount of thermal energy than it would be stored by exploiting only the sensible heat. Usually, LHTES systems are characterised by high thermal energy storage capacity per unit mass compared to that of sensible heat systems. However, they can only be operated in small temperature ranges because the heat transfer in the transition phase occurs at almost constant temperature. Nevertheless, they are considered as an efficient alternative to sensible TES systems.
Different types of PCM can be considered, depending on the type of phase change and how the energy is stored. Indeed, the thermal energy might be stored in solid-solid, solid-gas or liquid-gas, and solid-liquid

PCMs. In solid-solid PCMs, the stored energy brings about a change in the crystalline structure of the material, that takes place with a low volume change. Solid-gas and liquid-gas PCMs are characterised by a greater heat of vaporisation than the corresponding heat in the solid-solid counterpart and by a greater volume variation that leads to difficulties in the design of the PCM containers. Solid-liquid PCMs are the best compromise: they are characterised by large heat of vaporisation and relatively low volume variation from one phase to the other, coupling the two main advantages of the other PCMs.

3.8 Specific overall system configuration

While in Fig. 3.1 a generic scheme of the overall system configuration was presented (cf. Par. 3.1), in this paragraph a series of specific system configurations are described. A system based on alkaline water electrolysis, with and without an ORC, and a system based on RSOC are presented in the following.

3.8.1 Alkaline electrolysis and solid oxide fuel cells without ORC

A first power to methanol system, depicted in Fig. 3.7, based on a commercially mature technology, namely alkaline water electrolysis, was analysed. The system produces methanol following the methanol synthesis reactions described in Par. 2.4.1 (reactions (2.8)-(2.10)).

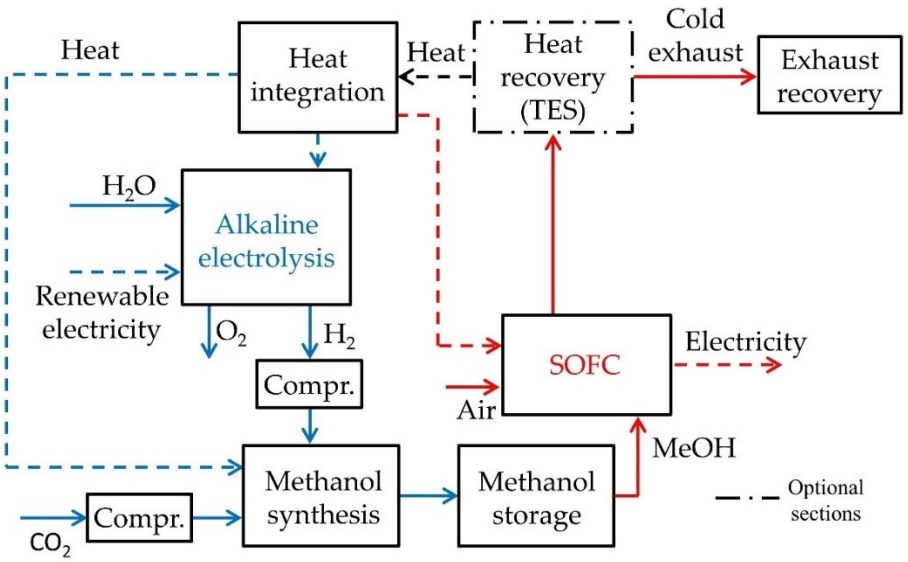

Fig. 3.7 – Simplified functional scheme of the overall system based on alkaline electrolysis without ORC

In electrolysis mode, when there is an excess of renewable energy, water and electricity feed the AEL cells where water is split into its constituent (i.e. hydrogen and oxygen). Subsequently, hydrogen and carbon dioxide are compressed in two different train of compressors to the methanol synthesis operating conditions (cf. Par. 2.4.1). On a commercial catalyst ($Cu/ZnO/Al_2O_3$), the reactants are turned into methanol that is purified in a distillation column (included in the "Methanol synthesis" block). Pure methanol is stored in tanks under ambient conditions and used back in fuel cell mode when there is lack of electricity or, in general, when needed. Methanol is reformed prior to produce electricity in the SOFC. The resulting gas, that is mainly composed of hydrogen, is oxidised and electricity is produced. Residual gases containing unreacted hydrogen and carbon monoxide are burnt, and residual heat of the exhaust might be stored in the heat recovery section to be used during hydrogen production within the electrolysis process or for other applications such as hot water production.

3.8.2 Alkaline electrolysis and solid oxide fuel cells with ORC

Figure 3.8 shows the same system reported in Par. 3.8.1 with the introduction of an ORC. As it will be shown in the section regarding the evaluation of the system performance reported in Chapter 1, it was found that the thermal energy released by the SOFC was significantly larger than that required in the electrolysis process. Hence, to reduce the dimensions of the TES system and increase the electricity production of the overall system during the discharge phase, the ORC was inserted between the SOFC and the PCM-TES. In this way, the hot gases exiting the cell can be exploited to produce electricity and boost the system performance. Depending on the chosen configurations and plant solutions, residual heat from the SOFC can be integrally used to produce electricity in the ORC.

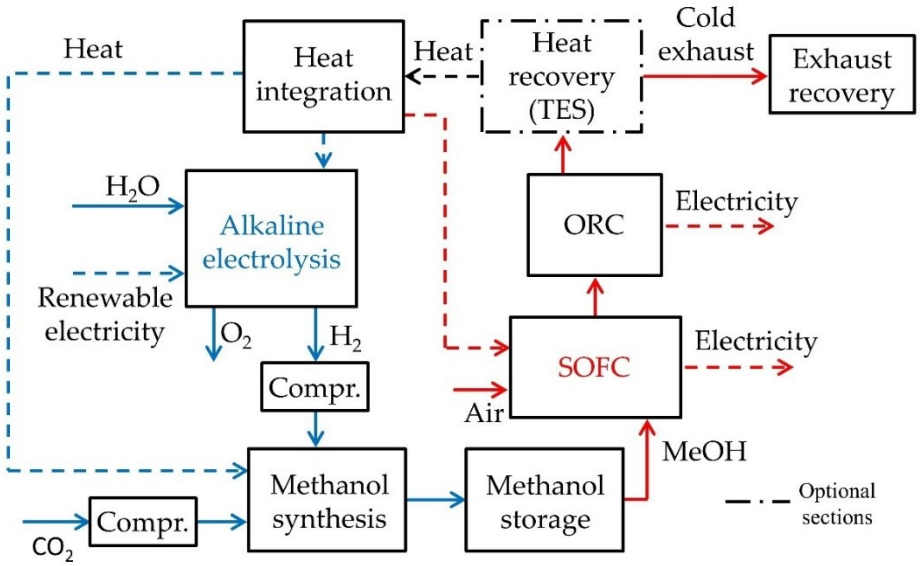

Fig. 3.8 – Simplified functional scheme of the overall system based on alkaline electrolysis with ORC

Both the AEL and the ORC are commercially ready technologies, allowing the immediate development of an energy storage system based on these technologies and on CO_2capture and recycle.

3.8.3 Reversible solid oxide cells

Another configuration considered in this work is based on reversible solid oxide cells, a relatively new technology characterised by high efficiency owing to high temperature operation (cf. Par. 3.2.4, 3.3, 3.4). RSOCs are developed from the more mature SOFC technology, that has achieved a power production in the order of a few MW [114]. However, due to optimisation in materials and construction, state of the art SOFCs capable of working as an RSOC to also produce hydrogen are limited to a power production of 30-50 kW in fuel cell mode and a power consumption in electrolysis mode of 150 kW [135]. Nevertheless, in this work a comparison between 1 MW-systems was carried out, supposing that in few years the RSOC systems will reach the capabilities of the state of the art of standalone SOFC.

Figure 3.9 shows the simplified functional scheme of the power to methanol system based on RSOC as it was studied in this work. Instead of two different devices to perform the water electrolysis and the production of electricity (namely an AEL and a SOFC or a SOEC and a SOFC), only one device is used with the RSOC configuration. Since the excess of renewable energy and the need of electricity are usually deferred throughout the day, it is possible to use one single device, such as the RSOC, that is switched from one mode to the other depending on the electricity availability. The general concept is similar to that of the AEL-based system. The RSOC operates at high temperature and the heat released by the SOFC is used to perform the electrolysis during the hydrogen production process. The heat is stored in a PCM-TES system. Since all the heat released by the SOFC is stored and then provided to the electrolysis process, there is no

residual heat available that allows the introduction of an ORC. Thus, compared to the systems described previously, the RSOC-based system is simpler due to the absence of the ORC and the use of a device capable of working in two different modes.

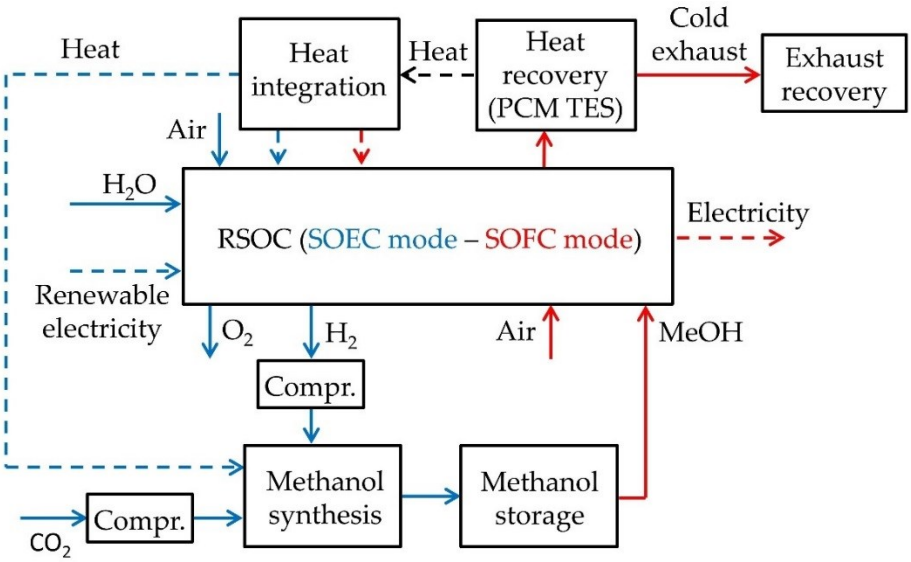

Fig. 3.9 – Simplified functional scheme of the overall system based on RSOC

Even though extensive R&D is mandatory to increase the size and capabilities of RSOC, in a future perspective it is a promising technology to perform energy storage via chemical compounds.
Although single sub-systems have been analysed thoroughly in literature and some studies on similar integrations have been proposed, to the best of authors' knowledge a power-to-methanol process based specifically on AEL or RSOC, CO_2 hydrogenation, heat recovery through a low temperature TES and an ORC has not yet been assessed. As shown in Chapter 4, complete and comprehensive electrochemical models of the AEL and the RSOC (in both SOEC and SOFC operating modes) were developed and implemented in Aspen Plus V8.8. A kinetic model was also developed to simulate the methanol synthesis section (MSS), as well as an ORC model. Whilst other papers analysed similar systems based on hydrogen storage, or coupled to methanation, or employing water and CO_2 co-electrolysis processes, the main novelty of this study is the conversion of electrical energy further towards methanol in a future methanol economy perspective and the comparison between a commercially mature technology (i.e. alkaline water electrolysis) and an innovative technology (namely, reversible solid oxide cells). Besides, the integration with a low temperature PCM-TES system results in a different and new approach compared to the high temperature energy storage systems proposed in literature. Thermal integration between the sections was carried out to verify the feasibility of a self-sustainable system that not only consists of electrolytic hydrogen production, but also of further hydrogen conversion and utilisation for electricity production or industrial applications.

3.9 Previous studies on complex PtX systems

In the context of complex systems to store energy using PtX technologies, heat integration and optimisation of RSOCs for the production and use of methanol represents a recent area of research and a technological development of growing interest. In literature, several papers have focused on methanol production from hydrogen via RES and recycled CO_2 using either conventional or innovative water electrolysis. Leonard et al. [136] analysed a system composed of a CO_2 capture section (studied in a previous work by the same authors [137,138]), a water/CO_2 co-electrolysis section via high temperature SOEC (850 °C) and a methanol synthesis section. This study showed an increase in the overall system efficiency from 40.1 to 53.0% via a proper heat integration. Yuan et al. [139] analysed a hybrid system consisting of a wind turbine, water

electrolysis, hydrogen and oxygen storage, coal-based methanol production (via gasification) and methanol fuel cells. The system provides a stable wind power supply, produces a constant methanol flow rate, and reduces the overall CO_2 emissions of the process. An excess of wind energy feeds the electrolyser to produce hydrogen. Hydrogen and oxygen are stored, and hydrogen is used to produce electricity in a fuel cell. Methanol is produced continuously using coal, hydrogen and oxygen, even in the absence of wind. Indeed, the coupling between the subsections that compose the system provide flexibility even when the intermittency of the wind power does not allow the matching of the requested energy. The authors developed a control scheme to optimise the system. Such an approach would be useful to perform a stable methanol production even when the provision of RES is intermittent, through the integration of conventional energy sources or electricity coming from the grid. Mermelstein and Posdziech [120] analysed a complex RSOC system to produce, store, and reuse hydrogen in a long-term perspective. The system was able to serve different purposes: renewable hydrogen production, power-to-gas, energy storage, grid balancing, and power generation via distributed fuel production. The system was composed of a fuel cell, a steam generator, a desalination unit and a hydrogen storage system. The system had been tested for approximately 1000 hours in both operating modes, to simulate the behaviour under real load conditions. The system achieved an efficiency of 60.5%$_{LHV}$ in SOEC mode and 49.4 %$_{LHV}$, consistent with typical values of such systems. Di Giorgio and Desideri [140] studied a system for EES with the aim of hindering the issues related to the intermittency of RES. The system was composed of an RSOC and was studied by analysing different high temperature (1050 K) TES technologies, including both latent and sensible heat storage, to optimise the energy balance. The authors developed a special methodology to predict the theoretical roundtrip performance of the system. Santhanam et al. [126] analysed a conceptual RSOC system considering a high temperature TES system based on PCMs to supply heat during electrolysis operations to quantify the theoretical limit of the roundtrip efficiency for both an ideal reactor and a commercially available reactor at different operating pressures. The RSOC was operated at different temperatures in SOFC (850 °C) and SOEC (800 °C) mode. The system, based on the selected commercial reactor, achieved a roundtrip efficiency of 55% at 1 bar and of 60% at 30 bar. Mottaghizadeh et al. [141] comprehensively studied a complete self-sustaining system consisting of an RSOC coupled to a methanation process and a high temperature (850 °C) TES system based on PCM, looking for optimal thermal integration and balance of plant using the software Aspen Plus. The model was based on a commercially available RSOC characterised by a planar design. Endothermic reactions of the electrolysis process were promoted by the thermal energy previously stored during fuel cell operation. A roundtrip efficiency of 54.3% was calculated considering reference conditions, with an increase to 60.4% by working at 25 bar and by improving the system design to make it thermally self-sustaining. Ferrero [142] carried out a comprehensive analysis of electricity storage using power-to-gas technology based on RSOCs to produce methane from RES, evaluating the optimal operating conditions. Soltanieh et al. [143] studied the coupling between a natural gas Matiant power plant [144] and a methanol production unit along with a CO_2 capture process based on oxy-fuel combustion, and alkaline water electrolysis. Even though the produced methanol cannot be defined as renewable, all the CO_2 emitted by the conventional power plant is captured and turned into approximately 230 kt/year of methanol. Matzen and Demirel [71] analysed the production of methanol and DME exploiting wind power to feed a water electrolysis process, and using CO_2 captured from an ethanol fermentation plant. The analysis was carried out employing several models developed in Aspen Plus. An LCA was carried out to verify the environmental impact of these processes and the fuel production phase was found to be the most critical from the LCA point of view. Nevertheless, the environmental feasibility of the whole production process was assessed. Indeed, both renewable fuels led to a reduction of 82-86% in GHG emissions and to a reduction in fossil fuel depletion of 82-91% compared to the corresponding conventional production routes. Other research on different types of PtX systems, to produce chemicals employing a variety of technologies and processes, have been already reported in Par. 2.3 and Table 2.2.

From the point of view of the economic feasibility, already in 2006 Guan et al. [119] carried out a comprehensive analysis of different system configurations based on SOCs. They analysed SOEC, SOFC, and RSOC modes evaluating different costs aspects to define which was the best way to run both a centralised and a distributed system. In addition, a comparison between alkaline, PEM, and SOC electrolysis was carried out. The study demonstrated the potential advantage of operating through a SOEC (from the point of view of the cost of hydrogen) when this technology reaches a maturity level similar to that of AEL and PEM (expected in 2030 [77]). The main advantage is related to the lower operating voltage that reduces the overall cost associated with the system main feedstock (the electricity). Lower voltages and lower power consumption bring about higher efficiencies than conventional electrolysis processes. Nevertheless, only with extensive research, development, and deployment of such technology it would be possible to achieve the expected results. Akikur et al. [145] analysed an integrated system based on RSOC driven by PV and concentrated solar power capable of working in different ways to harmonise electricity production with solar energy and hydrogen production. Hydrogen is directly stored and used without further conversion to methanol or other chemical compounds. When solar radiation is low, the RSOC is used in SOFC mode to provide electricity and heat. When solar radiation is high, the RSOC produces hydrogen in SOEC mode while the PV section provides electricity. During night time, the RSOC is used in SOFC mode to produce electricity from the hydrogen that was produced and stored previously. Following a meticulous economic analysis based on 2014 costs for components and appliances, the system cost of electricity was found equal to 0.068 USD/kWh (68 USD/MWh) which is approximately the same as the electricity cost of other RES [31] (cf. Par. 2.2.1). Hank et al. [146] analysed numerous different scenarios regarding the production of renewable methanol via H_2 production through PEM electrolysis and CO_2 hydrogenation in the German market. At present, renewable methanol production is not competitive compared to methanol obtained from fossil fuels, due to the low cost of fossil resources and the use of large-scale plants. In the future, large utilisation factors, large-scale plants, exploitation of existing concentrated CO_2 sources (as it is done in the CRI methanol plant), and proper CCU taxation (CO_2 emissions avoidance cost) would lead to a competitive solution compared to conventional methanol production ways. The decrease in costs is expected in the next one or two decades, also due to RES expansion, growth, and cost reduction. Considering the contemporary improvement in SOC technology expected within the same time span, as reported in [77] and [147], renewable methanol production will be a suitable substitute to conventional production ways.

Chapter 4

Modelling of the main processes

4.1 Introduction

The sections and processes considered in this thesis were mainly developed using the software Aspen Plus. Aspen Plus is a commercial software to simulate chemical and industrial processes. It is based on process flowsheets where material, heat, and work streams along with different types of blocks (e.g. reactors, pressure changers, heaters, mixers, splitters, etc.) allow for designing and running simulations. Calculation tools such as calculators, design specs, and sensitivity analysis are used to manipulate variables and introduce mathematical equations and relationships to perform comprehensive studies of the analysed systems. The extensive and comprehensive chemical database allows the simulation of a variety of processes and reactions.

4.2 Solid oxide cells

4.2.1 SOEC and SOFC electrochemical models

An electrochemical model based on equations proposed by Ni et al. [148–150] for planar cells was developed to describe the RSOC operation. The electrochemical equations were adapted and implemented in a Fortran routine in Aspen Plus. Two separate models were developed to simulate SOEC and SOFC processes. The two SOEC and SOFC models are mostly identical and differ just for the concentration overpotential equations. Consequently, switching from one to another equation is simply achieved by exchanging the "anode" with the "cathode" subscription. The electrochemical characteristic and parameters are associated to the typical Ni-YSZ-LSM electrode/electrolyte material. The models were validated, for both SOEC and SOFC mode, in a temperature range typical of high temperature solid oxide cell systems [115,151], following experimental data reported by the same authors [148–150]. The main phenomena occurring in a cell during electrolysis (or fuel oxidation during SOFC operation) are described through special equations and theories: Nernst equation, reversible potential equation, Butler-Volmer equations, concentration overpotential theories, Bosanquet and Chapman-Enskog theories of gas diffusion. The electrochemical model was developed and implemented after carrying out a comprehensive analysis of a significant number of models found in literature. Many of these, as reported in the works in which they were found, were not complete or some of the parameters were missing, making it impossible to correctly simulate the processes. The equations and models used in the present work were the most complete.

In the electrochemical SOEC/SOFC model, the equilibrium voltage E_{eq} is expressed by Nernst equation (Eq. (4.1)). Nernst equation, linked to the standard change in the Gibbs free energy of an electrochemical reaction, binds the reduction potential of a reaction to the standard electrode potential, the influence of the temperature, the activities of the species involved, often approximated using their concentrations (partial pressures).

$$E_{eq} = E_0 + \frac{RT_c}{2F} ln\left(\frac{p_{H_2} p_{O_2}^{\frac{1}{2}}}{p_{H_2O}}\right) \tag{4.1}$$

In Eq. (4.1), E_0 is the reversible potential [V], R is the universal gas constant [J/(mol K)], T_c is the operating temperature of the cell [K], F is the Faraday constant [C/mol], and p_i is the partial pressure of the generic chemical species. Partial pressures at electrodes surface are calculated as mean values of the cathode and anode inlet and outlet [152].
The reversible potential E_0 is calculated as a function of cell temperature by Eq. (4.2), which is used to simulate the reversible potential of solid oxide cells [115]:

$$E_0 = 1.253 - 2.4516 \times 10^{-4}\, T_c \tag{4.2}$$

The reversible potential is the maximum electromotive force provided by the cell in SOFC mode and the minimum voltage to apply to the cell in SOEC mode.
The net voltage of the cell (E_{SOEC} and E_{SOFC}) is expressed by Eq. (4.3) by adding or subtracting the overpotentials (also known as polarisations) η_i to the equilibrium voltage E_{eq}:

$$E_{SOEC/SOFC} = E_{eq} \pm [\eta_{ohm} + (\eta_{act} + \eta_{conc})_{an} + (\eta_{act} + \eta_{conc})_{cat}] \tag{4.3}$$

where η_{ohm} represents the ohmic overpotential and η_{act} and η_{conc} represent the activation and concentration overpotentials for both the anode and cathode, respectively.
Ohmic overpotential is estimated using Eq. (4.4) [153]. Ohmic overpotential is given by the resistance that the electrolyte and electrodes oppose to the flow of ions and electrons, respectively. Typically, the ohmic overpotential can be defined using Ohm's law where the total resistance of the cell is given by the sum of the electronic, ionic, and contact resistance.

$$\eta_{ohm} = J t_{el} \rho \tag{4.4}$$

In Eq. (4.4), t_{el} is the electrolyte thickness [m], J is the current density [A/m^2] and ρ is the electrical resistivity [Ωm] defined by Eq. (4.5):

$$\rho = 2.99 \times 10^{-5}\, exp\left(\frac{10300}{T_c}\right) \tag{4.5}$$

Usually, the resistance offered by the electrolyte is several orders of magnitude larger than that of the electrodes, thus it is common to consider only t_{el}.
Activation overpotentials are derived from the Butler-Volmer equation [154] and are defined by Eq. (4.6). This type of overpotentials is given by sluggish electrode kinetics owing to different electrochemical steps occurring on the surface of the electrodes.

$$\eta_{act,i} = \frac{RT_c}{F} sinh^{-1}\left(\frac{J}{2J_{0,i}}\right) = \frac{RT_c}{F} ln\left(\frac{J}{2J_{0,i}} + \sqrt{\left(\frac{J}{2J_{0,i}}\right)^2 + 1}\right) \tag{4.6}$$

Exchange current densities $J_{0,i}$ are defined by Eq. (4.7) and (4.8):

$$J_{0,an} = \gamma_{an}\, exp\left(-\frac{E_{act,an}}{RT_c}\right) \tag{4.7}$$

$$J_{0,cat} = \gamma_{cat}\, exp\left(-\frac{E_{act,cat}}{RT_c}\right) \tag{4.8}$$

where γ_{an} and γ_{cat} are the pre-exponential factors [A/m^2], and $E_{act,an}$ and $E_{act,cat}$ are the activation energy levels (at zero overpotential) for the anode and cathode [J/mol], respectively. In a SOFC, typical values of the activation energies at 1073 K are 1.0 × 10^5 J/mol and 1.2 × 10^5 J/mol for the anode and cathode, respectively. Since at zero overpotential the forward and backward reaction rate is the same, the values of the activation energies of a SOFC can be used as an approximation of those of a SOEC, with the proper change in the anode and cathode notation. These parameters are found in the literature for the Ni-YSZ/YSZ/LSM

electrode [149,150,155]. Considering the recommended values of $J_{0,an} = 5300\ \mathrm{A/m^2}$ and $J_{0,cat} = 2000\ \mathrm{A/m^2}$ at 1073 K [149] and the activation energy levels reported above, the pre-exponential factors at 1073 K can be evaluated. Using the calculated pre-exponential factors and the activation energy levels, that depend on the materials constituting the cell, the exchange current densities can be calculated for temperatures of the cell, T_c, different from 1073 K.

As previously specified, the concentration overpotential equations differ from SOEC to SOFC. SOEC concentration overpotentials are calculated by Eq. (4.9) and (4.10) [149]:

$$\eta_{conc,an} = \frac{RT}{2F} ln\left(\left(1 + \frac{JRT_c d_{an}}{4FD_{O_2}^{eff} p_{O_2}^0}\right)^{\frac{1}{2}}\right) \tag{4.9}$$

$$\eta_{conc,cat} = \frac{RT_c}{2F} ln\left[\frac{1 + JRT_c d_{cat}/(2FD_{H_2O}^{eff} p_{H_2}^0)}{1 - JRT_c d_{cat}/(2FD_{H_2O}^{eff} p_{H_2O}^0)}\right] \tag{4.10}$$

where p_i^0 are the anode and cathode mean pressures [Pa], d_{an} and d_{cat} are the anode and cathode thicknesses [m], respectively, and $D_{O_2}^{eff}$ and $D_{H_2O}^{eff}$ are the effective diffusion coefficients for oxygen and steam [$\mathrm{m/s^2}$], respectively. The concentration overpotentials are related to the mass transport losses due to the dilution of the reactants in the products (i.e. the diffusion of species within each other). Indeed, a limited mass transport rate reduces the supply of the reactants and the evacuation of products causing a concentration gradient that influences the mass transport process. At high current densities, concentration losses bring about a significant loss of cell potential.

The diffusion is related to both the interaction between molecules and that between molecules and pores. Effective diffusion coefficients are calculated using Bosanquet equations (4.11), (4.12):

$$\frac{1}{D_{O_2}^{eff}} = \frac{\xi}{\eta}\left(\frac{1}{D_{O_2-N_2}} + \frac{1}{D_{O_2,K}}\right) \tag{4.11}$$

$$\frac{1}{D_{H_2O}^{eff}} = \frac{\xi}{\eta}\left(\frac{1}{D_{H_2-H_2O}} + \frac{1}{D_{H_2,K}}\right) \tag{4.12}$$

where ξ/η is the tortuosity versus porosity ratio, $D_{O_2-N_2}$ and $D_{H_2-H_2O}$ are the molecular diffusion coefficients of oxygen in air (actually, nitrogen) and of hydrogen in water vapour, and $D_{O_2,K}$ and $D_{H_2,K}$ are the Knudsen diffusion coefficients of oxygen and hydrogen, respectively. The molecular diffusion coefficients and the Knudsen diffusion coefficients are evaluated referring to the Chapman–Enskog theory of ideal gases [156].

In general, Eq. (4.11) and (4.12) can be written as the Bosanquet formula (4.13) (interpolation formula supported by the kinetic theory of gases [157]) to evaluate the diffusion coefficient in the transition region [158]:

$$\frac{1}{D_{electrode}^{eff}} = \frac{\xi}{\eta}\left(\frac{1}{D_{i-j}} + \frac{1}{D_{i,K}}\right) \tag{4.13}$$

where D_{i-j}, the molecular diffusion of the species i in the species j, can be expressed using the equations from (4.14) to (4.19), as proposed in [156], referring to the Chapman-Enskog theory of ideal gases, while $D_{i,k}$ (Knudsen diffusion coefficient for the species i related to the self-diffusion coefficient derived from the kinetic theory of gases [159]) is calculated by Eq. (4.20):

$$D_{i-j} = \frac{0.0000266 T_c^{\frac{3}{2}}}{p M_{i,j}^{\frac{1}{2}} \sigma_{i,j}^2 \Omega_D} \tag{4.14}$$

where p [bar], T_c [K], D_{i-j} [m^2/s], while the molecular weight $M_{i,j}$ [g/mol] is expressed by Eq. (4.15):

$$M_{i,j} = 2\left(\frac{1}{M_i} + \frac{1}{M_j}\right)^{-1} \tag{4.15}$$

$\sigma_{i,j}$ [Å] is the mean characteristic length of species i and j:

$$\sigma_{i,j} = \frac{\sigma_i + \sigma_j}{2} \tag{4.16}$$

Ω_D is the diffusion collision integral (which is dimensionless) given by Eq. (4.17):

$$\Omega_D = \frac{1.06036}{\Gamma^{0.15610}} + \frac{0.19300}{exp(0.47635\Gamma)} + \frac{1.03587}{exp(1.52996\Gamma)} + \frac{1.76474}{exp(3.89411\Gamma)} \tag{4.17}$$

where Γ is a dimensionless temperature coefficient expressed by Eq. (4.18):

$$\Gamma = \frac{T_c}{\varepsilon_{i,j}} \tag{4.18}$$

where $\varepsilon_{i,j}$ is the Lennard-Jones energy [K]:

$$\varepsilon_{i,j} = \sqrt{\frac{\varepsilon_i}{k_B}\frac{\varepsilon_j}{k_B}} \tag{4.19}$$

being k_B the Boltzmann's constant.
Table 4.1 reports the main parameters to calculate the effective diffusion coefficient [156]:

Table 4.1 – Parameters for diffusion calculation

	H_2O	H_2	O_2	N_2	CO	CO_2
σ_i [Å]	2.641	2.827	3.467	3.798	3.690	3.941
ε_i/k_B [K]	809.1	59.7	106.7	71.4	91.7	195.2

Finally, the Knudsen diffusion is expressed as [160,161]:

$$D_{i,K} = \frac{d_p}{3}\sqrt{\frac{8000 R T_c}{\pi M_i}} \tag{4.20}$$

In Eq. (4.20), R is the universal gas constant [J/(mol K)], d_p the average pore size [m] and M_i the molecular weight [g/mol], so that $D_{i,K}$ results in m^2/s.
In the case of the SOFC, the concentration overpotentials are different from the corresponding overpotentials of the SOEC. In particular, in the SOFC model, Eq. (4.21) and (4.22) are used [150,162]:

$$\eta_{conc,an} = \frac{RT_c}{2F} ln\left[\frac{1 + JRT_c d_{an}/(2FD_{H_2O}^{eff} p_{H_2O}^0)}{1 - JRT_c d_{an}/(2FD_{H_2O}^{eff} p_{H_2}^0)}\right] \tag{4.21}$$

$$\eta_{conc,cat} = \frac{RT_c}{4F} ln\left[\frac{p_{O_2}^0}{\frac{p_c}{\delta_{O_2}} - \left(\frac{p_c}{\delta_{O_2}} - p_{O_2}^0\right) exp\left(\frac{JRT_c d_{cat}\delta_{O_2}}{4FD_{O_2}^{eff} p_c}\right)}\right] \quad (4.22)$$

where p_c is the cell operating pressure [Pa]. The dimensionless coefficient δ_{O_2} is defined by Eq. (4.23):

$$\delta_{O_2} = \frac{D_{O_2,K}^{eff}}{D_{O_2,K}^{eff} + D_{O_2}^{eff}} \quad (4.23)$$

where $D_{O_2,K}^{eff}$ is the effective Knudsen diffusion of oxygen, defined as the oxygen Knudsen diffusion coefficient, multiplied by η/ξ.

4.2.2 SOEC Aspen Plus model

A simplified functional scheme of the model of the SOEC as it was implemented in Aspen Plus is reported in Fig. 4.1. The main component of the SOEC system is the electrochemical cell. To correctly simulate the process, the SOEC system developed in Aspen Plus includes blocks such as reactors, heat exchangers, mixers and separators. In a SOEC the electrolysis of steam is carried out following the three reactions typical of the water splitting process (3.8)-(3.10).

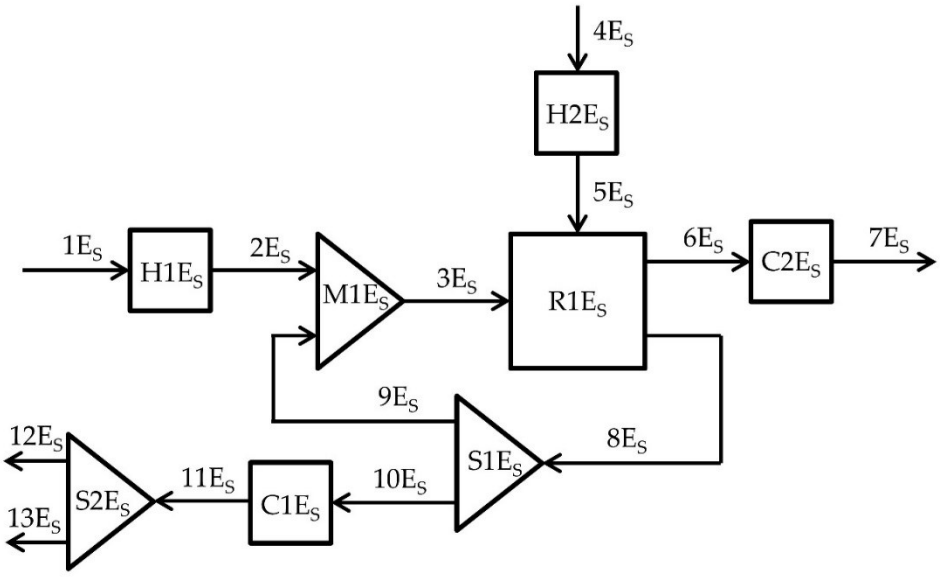

Fig. 4.1 – Simplified functional scheme of the solid oxide electrolyser section (C = Cooler; H = Heater; M = Mixer; R = Reactor; S = Splitter)

Water (1E$_S$ in the scheme of Fig. 4.1) enters the SOEC at ambient temperature (25 °C) and is preheated, vaporised and superheated (H1E$_S$) up to the SOEC operating temperature. Afterwards, it is mixed with a fraction (9E$_S$) of the cathode exhaust (8E$_S$) in the mixer M1E$_S$. Typically, this is done to obtain a molar composition of the cell inlet equal to 90% water and 10% hydrogen to prevent electrode oxidation [163–165]. Inside the reactor (R1E$_S$), water electrolysis is accomplished following reactions (3.8)-(3.10). Both a cathode and an anode exhaust exit the cell: the former (8E$_S$) is composed of hydrogen and water vapour, while the latter (6E$_S$) by air rich in oxygen. Indeed, air (4E$_S$) is fed to the SOEC as a sweep gas to clean the anode side from the produced oxygen and to guarantee a sufficient transportation rate on the surface of the anode. The air rich in oxygen is then cooled down (C2E$_S$) to the established SOEC outlet temperature (7E$_S$), allowing the recovery of thermal energy. The water/hydrogen mixture (8E$_S$) is split (S1E$_S$) to ensure the

required water/hydrogen ratio at the reactor inlet. The remaining flow ($10E_S$) is cooled down ($C1E_S$) to condense the water vapour contained in the mixture. Gaseous hydrogen ($12E_S$) is then separated ($S2E_S$) by the liquid water ($13E_S$) and sent to the MSS.

4.2.3 SOEC model validation

The electrochemical model described in Par. 4.2.1 and the Aspen Plus flowsheet described in Par. 4.2.2 were validated using the experimental data reported in Ni et al. [149]. While the electrochemical model had already been validated by the same authors [149] in their work, the model developed within Aspen Plus, as it is in this thesis, required to be verified in order to guarantee its effectiveness. Table 4.2 shows the parameters used in the validation. The reported parameters are found in Ni et al. [149]. The pre-exponential factors are calculated as described in Par. 4.2.1 for Eq. (4.7) and (4.8).

Table 4.2 – Parameters used in SOEC model validation [149]

Parameter	Value
Temperature [K]	1173, 1223, 1273
Operating pressure [bar]	1
Pre-exponential factor (cathode) γ_{cat} [A/m^2]	3.91084×10^8
Activation energy (cathode) $E_{act,cat}$ [J/mol]	1.0×10^5
Pre-exponential factor (anode) γ_{an} [A/m^2]	1.38875×10^8
Activation energy (anode) $E_{act,an}$ [J/mol]	1.2×10^5
Electrode porosity η	0.48
Electrode tortuosity ξ	5.4
Average pore size d_p [µm]	2.14
Electrode thickness t_{el} [µm]	1000
Cathode thickness d_{cat} [µm]	100
Anode thickness d_{an} [µm]	100

Figure 4.2 shows the results of the validation carried out considering the model results and the experimental data of the SOEC. The curves reported in Fig. 4.2 are also known as one of various characteristic curves that can be obtained for an electrolyser. Other characteristic curves are, for instance, the power density – current density curve or the efficiency – current density curve. The validation was carried out at ambient pressure (1 bar) and at a temperature of 1173, 1223, 1273 K.

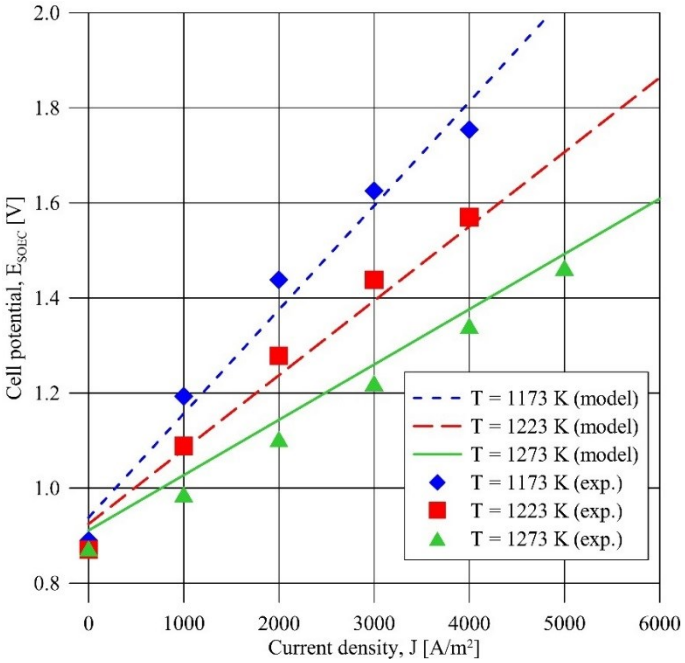

Fig. 4.2 – Comparison between model results and experimental data (SOEC)

On the y-axis is reported the cell potential, evaluated with Eq. (4.3), whilst on the x-axis is the current density. The lines represent the results of the Aspen Plus model, while the symbols represent the experimental data used for the validation. The curves shown in Fig. 4.2 were obtained by varying the water flow rate while keeping constant the utilisation factor. For each curve the values of the current density and the SOEC voltage were calculated by the model. Even though the results of the model do not perfectly follow the trend of the experimental data points, given the objectives of this thesis (i.e. the macro scale analysis of a complex energy storage system from the energy and mass balance point of view rather than the study of the exact electrochemical behaviour of the cell), the voltage – current density characteristic curve obtained and the validation carried out were considered accurate enough to guarantee a correct simulation of the SOEC. Furthermore, if a comparison with the curves of the model reported in [149] is carried out, a similar trend between the model defined in this thesis and the model defined by the authors can be observed.

4.2.4 SOFC Aspen Plus model

A simplified functional scheme of the model of the SOFC as it was implemented in Aspen Plus is reported in Fig. 4.3. The stored methanol feeds an RSOC to produce electrical energy in SOFC mode. Even though the same RSOC is used for both the SOEC-mode and the SOFC-mode, the SOFC flowsheet differs from the SOEC one due to the different operating modes, and different artifices employed to simulate the process.

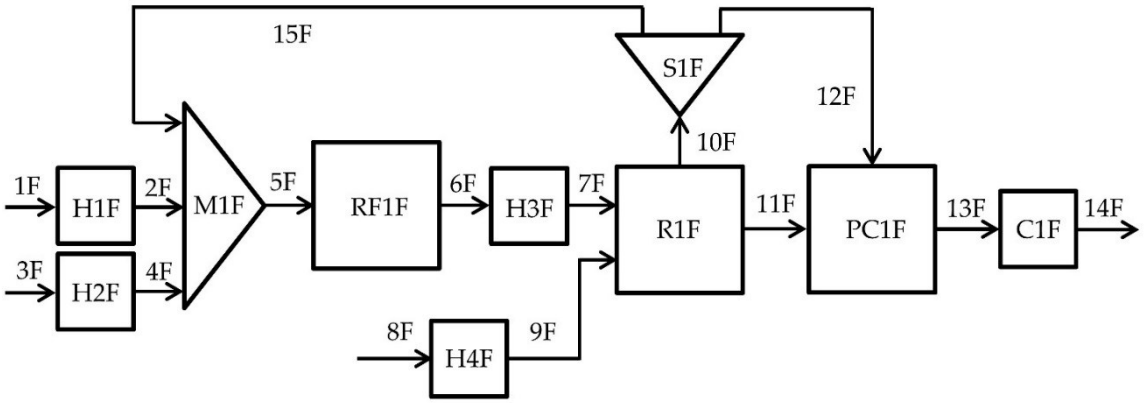

Fig. 4.3 – Simplified functional scheme of the solid oxide fuel cell section (C = Cooler; H = Heater; M = Mixer; PC = Post combustor; R = Reactor; RF = Reformer; S = Splitter)

The cell is fed with methanol (1F), water (3F) and air (8F). Fuel and water are preheated and vaporised in H1F and H2F (at 64.6 °C and 100 °C, respectively) and then mixed with the anode recycle (15F) in M1F. Through the recycling of high-temperature anode exhausts, the mixture of methanol and water vapour (5F) reaches a set temperature and enters the reformer (RF1F) (typical pre-reforming temperature is 300 °C). Reforming reactions allow the hydrogen content to be increased and the carbon monoxide content to be reduced in the cell feeding (6F/7F). Equilibrium reactions at a constant temperature of 300 °C were considered for the simulation of the reforming process. These reactions are: methanol decomposition (4.24), water gas shift reaction (4.25) and methanol steam reforming reaction (4.26).

$$CH_3OH \rightarrow 2H_2 + CO \tag{4.24}$$

$$CO + H_2O \rightarrow H_2 + CO_2 \tag{4.25}$$

$$CH_3OH + H_2O \rightarrow 3H_2 + CO_2 \tag{4.26}$$

Hydrogen from the reforming process is oxidised and electricity is produced following the reactions (4.27) and (4.28) that take place at the SOFC anode and cathode, respectively:

$$2H_2 + 2O^{2-} \rightarrow 2H_2O + 4e^- \tag{4.27}$$

$$2O_2 + 4e^- \rightarrow 2O^{2-} \tag{4.28}$$

Inside the reactor (R1F), hydrogen reacts with air (9F), previously heated in H4F, producing electricity and hot steam. The solid oxide fuel cell is simulated as an electrochemical reactor, operating at high temperature as in the SOEC mode. Cathode exhaust (11F) together with a portion of the anode exhaust (12F) feed a post-combustor (PC1F), where residual fuel (mainly hydrogen and carbon monoxide, with traces of unreacted methanol) is burnt, producing heat to support fuel cell operation. Combustion products (13F) are cooled (C1F) by heat recovery. A portion of the heat produced by the SOFC is used for supporting cell operation, while residual heat can be recovered and stored in the TES for later use in the SOEC section.

4.2.5 SOFC model validation

The electrochemical model and the Aspen Plus flowsheet used to model the SOFC (described in Par. 4.2.1 and Par. 4.2.4) were validated using the experimental data reported in Ni et al. [150]. As already explained in Par. 4.2.3, the electrochemical model had been validated by the same authors in their work [150]. Table 4.3

shows the parameters used to validate the model. The validation was carried out considering hydrogen as the fuel feeding the SOFC.

Table 4.3 – Parameters used in SOFC model validation [150]

Parameter	Value
Temperature [K]	873, 973, 1073
Operating pressure [bar]	1
Pre-exponential factor (cathode) γ_{cat} [A/m^2]	1.38875×10^8
Activation energy (cathode) $E_{act,cat}$ [J/mol]	1.2×10^5
Pre-exponential factor (anode) γ_{an} [A/m^2]	3.91084×10^8
Activation energy (anode) $E_{act,an}$ [J/mol]	1.0×10^5
Electrode porosity η	0.48
Electrode tortuosity ξ	5.4
Average pore size d_p [µm]	3.0
Electrode thickness t_{el} [µm]	8
Cathode thickness d_{cat} [µm]	20
Anode thickness d_{an} [µm]	1000

Figure 4.4 shows the results of the validation carried out considering the Aspen Plus model and the experimental data of the SOFC, as it was reported by Ni et al. [150]. The validation was carried out at ambient pressure (1 bar) and at a temperature of 873, 973, 1073 K.

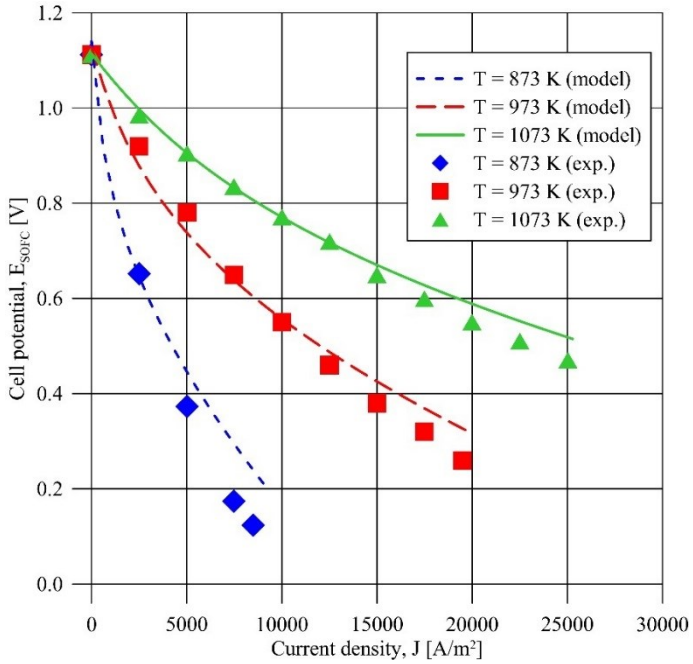

Fig. 4.4 – Comparison between model results and experimental data (SOFC)

On the y-axis is the cell potential evaluated as Eq. (4.3) while on the x-axis the current density. The lines represent the results of the Aspen Plus model whilst the symbols represent the experimental data used for the validation. As with what has already been described in Par. 4.2.3, the characteristic curves of the SOFC were obtained varying the fuel (hydrogen) mass flow.

The trend of the model is consistent with the available experimental data points at low current densities but tends to diverge when the current density increases over 5000 A/m^2 (873 K curve) and 10000 A/m^2 (973 and 1073 K curves). Even though the curves do not perfectly follow the experimental data, the Aspen Plus model was considered accurate enough to be used for the calculation of the voltage – current density characteristic of the cell and consequently for the power and efficiency calculation of the section. Indeed, as reported in Par. 3.3, typical operating voltage of solid oxide cells are in a range from 3000 to 20000 A/m^2. In this range, especially for higher temperatures, the divergence is still acceptable for the macroscale analysis considered in this study. Nevertheless, the divergence might be associated to some of the modelling parameters that were not explicitly reported in the original model (e.g. some parameters used to calculate the diffusion coefficients of the concentration overpotentials) and that were gathered via a further literature analysis.

4.3 Alkaline electrolysis

4.3.1 AEL electrochemical model

An electrochemical model proposed by Ursúa and Sanchis [166] was adapted to simulate the alkaline electrolyser behaviour. The original model was developed from the static-dynamic experimental analysis of an AEL made up of 22 round cells of 300 cm^2 each connected in series, characterised by a production of 1 Nm^3/h of hydrogen at a nominal current of 120 A. The operating pressure can be varied between 5 and 25 bar.

The equilibrium voltage of the stack, function of its temperature and pressure, is expressed as Eq. (4.29):

$$E_{eq} = N_S \left[E_0 + \frac{RT_c}{2F} ln\left(\frac{(p - p_{v,KOH})(p - p_{v,KOH})^{\frac{1}{2}}}{a_{H_2O,KOH}} \right) \right] \tag{4.29}$$

where E_0 is the reversible potential of one cell; the logarithm term takes into account the stack operating pressure p [bar] and the vapor pressure $p_{v,KOH}$ [bar] while $a_{H_2O,KOH}$ represents the water activity in the KOH solution. The term N_S is the number of cells of a stack. Considering the parallel and series theory of electrical engineering, when an electrolyser module is composed of various stacks in series and parallel, N_S is the total number of cells in series within one of the parallel constituting the module. Indeed, voltage drop is the same between parallels and is added up along a series.

The reversible potential E_0 is calculated as Eq. (4.30):

$$E_0 = 1.5184 - 1.5421 \times 10^{-3}\, T_c + 9.526 \times 10^{-5}\, T_c\ ln(T_c) + 9.84 \times 10^{-8}\, T_c^2 \tag{4.30}$$

The vapor pressure in the KOH solution $p_{v,KOH}$ is obtained as Eq. (4.31):

$$p_{v,KOH} = exp\left(2.302a + b\ ln\left(p_{v,H_2O}\right)\right) \tag{4.31}$$

where a and b are expressed as Eq. (4.32) and (4.33):

$$a = -0.0151m - 1.6788 \times 10^{-3}m^2 + 2.2588 \times 10^{-5}m^3 \tag{4.32}$$

$$b = 1 - 1.206 \times 10^{-3}m + 5.6024 \times 10^{-4}m^2 - 7.8228 \times 10^{-6}m^3 \tag{4.33}$$

where m is the molar concentration of the KOH solution supposed equal to 7.64 mol/kg.

The term p_{v,H_2O} is defined by Eq. (4.34):

$$p_{v,H_2O} = exp\left(81.6179 - \frac{7699.68}{T_c} - 10.9\, ln(T_c) + 9.5891 \times 10^{-3}\, T_c\right) \tag{4.34}$$

Finally, $a_{H_2O,KOH}$ is defined as Eq. (4.35):

$$a_{H_2O,KOH} = exp\left(-0.05192m + 0.003302m^2 + \frac{3.177m - 2.131m^2}{T_c}\right) \quad (4.35)$$

The model reported considering Eq. (4.29)-(4.35) is applicable in a range from 0 to 250 °C, from 1 to 200 bar and for a KOH concentration from 2 to 18 mol/kg.
The AEL net voltage is evaluated adding to the equilibrium potential the overvoltage caused by the ohmic and activation resistances as shown in Eq. (4.36):

$$E_{AEL} = E_{eq} + \left[V_{ohm} + V_{act,an} + V_{act,cat}\right] \quad (4.36)$$

As opposed to the SOC, mass transfer phenomena (i.e. concentration overpotentials) in alkaline electrolysis are negligible.
The total ohmic overvoltage, V_{ohm}, is evaluated using Eq. (4.37):

$$V_{ohm} = N_s \frac{r}{A} \quad (4.37)$$

where N_s is the number of cells in series inside a single stack, r is the area-specific resistance of each cell [Ωm^2], A is the area of the cell [m^2]. The equation for the area-specific resistance was obtained by the authors [166] with Eq. (4.38):

$$r = r_1 + r_2 T_c + \frac{r_3}{T_c} + \frac{r_4}{T_c^2} \quad (4.38)$$

that defines the ohmic dependence on temperature.
The activation overpotentials are based on a modified expression of the Tafel equation as reported in Eq. (4.39) and (4.40):

$$V_{act,an} = N_s V_{act,an} = N_s\, s\, ln\left(\frac{1}{t} i_{act,an} + 1\right) \quad (4.39)$$

$$V_{act,cat} = N_s V_{act,cat} = N_s\, v\, ln\left(\frac{1}{w} i_{act,cat} + 1\right) \quad (4.40)$$

where $i_{act,an}$ and $i_{act,cat}$ are the activation currents [A] for of the anode and cathode, respectively, while s, t, v, and w are obtained from Eq. (4.41)-(4.44) using correlation parameters estimated by the experimental characterisation of the stack:

$$s = s_1 + s_2 T_c + s_3 T_c^2 \quad (4.41)$$

$$t = t_1 + t_2 T_c + t_3 T_c^2 \quad (4.42)$$

$$v = v_1 + v_2 T_c + v_3 T_c^2 \quad (4.43)$$

$$w = w_1 + w_2 T_c + w_3 T_c^2 \quad (4.44)$$

The correlation coefficients obtained by the authors are reported in Table 4.4 [166].

Table 4.4 – Correlation parameters for activation overpotentials [166]

i	1	2	3	4
r_i	59.5482 × 10^{-6} Ωm^2	-340.8224 × 10^{-9} $\Omega m^2 °C^{-1}$	-106.9708 × 10^{-6} $\Omega m^2 °C$	2.7075 × 10^{-3} $\Omega m^2 °C^2$
s_i	25.2300 × 10^{-3} V	-234.0338 × 10^{-6} $V °C^{-1}$	3.1832 × 10^{-6} $V °C^{-2}$	/
t_i	54.6185 × 10^{-3} A	-2.4601 × 10^{-3} $A °C^{-1}$	52.1217 × 10^{-6} $A °C^{-2}$	/
v_i	110.3623 × 10^{-3} V	-1.6466 × 10^{-3} $V °C^{-1}$	22.8382 × 10^{-6} $V °C^{-2}$	/
w_i	45.7027 A	0.7781 $A °C^{-1}$	-10.5743 × 10^{-3} $A °C^{-2}$	/

To make the original system scalable, the model was improved in the Fortran routines of Aspen Plus. Stacks arranged in series and parallel allow producing the desired hydrogen quantity while guaranteeing the designed current density in each cell. In the modified model, depending on the desired hydrogen production and on the voltage and current values, different arrangements in series and parallel can be chosen. The water flow rate expressed in mol/s, which is the same as the hydrogen flow rate that each cell can produce, was calculated from Eq. (4.45):

$$n_{H_2} = \frac{I}{2\,F} \tag{4.45}$$

where n_{H_2} are the moles of produced hydrogen, and I is the electric current. Considering the nominal current of 120 A of the stack analysed by Ursúa and Sanchis [166], a production of approximately 6.22·10^{-4} $mol_{H_2}/s/cell$ is achieved. Inside the Aspen environment, this value was considered as the starting point for the evaluation of the AEL system performance. Since this value corresponds to both the water split and the hydrogen produced by a single cell, multiplying it for the total number of cells allows the calculation of the total hydrogen production of the system. To define inside the Aspen Plus flowsheet the desired quantity of water to be electrolysed, 6.22·10^{-4} $mol_{H_2O}/s/cell$ is multiplied for the total number of cells (obtained dividing the desired hydrogen production for the production of a single cell) and set as the input for the inlet water stream. Considering the initial stack composed of 22 cells as the building block of the studied electrolysis modules, the number of stacks to be arranged in series and parallel, depending on the desired total voltage and current output, is selected. Moreover, to allow further scalability and diversification the model was modified to simulate cells characterised by different dimensions (i.e. active area). Under the same current density, the larger the active area, the larger the hydrogen produced by the cell and the lower the number of cells to produce the same quantity of hydrogen. Keeping the current constant but changing the active area of the single cell would bring about a variation in the cell current density (J). To maintain this value constant at the nominal one (4000 A/m^2, found dividing the nominal current of 120 A for the area of a cell 300 cm^2), a multiplier factor was implemented both in the flowsheet and in the sensitivity analysis. The multiplier factor allows keeping a constant current density even when the area is varied. Hence, it is possible to apply a further variation in the stack/module composition by varying the cell area while keeping the optimal current density.

Since the electrolyser is not an ideal device and it is characterised by parasitic current loss, a Faraday efficiency defined as the ratio between the actual hydrogen production rate and the theoretical production should be considered. This efficiency is bound to the characteristic of the electrolyser and depends on the operating temperature. Ulleberg [167] developed an empirical relation to calculate the Faraday efficiency of the electrolyser studied in his research. Since Ursúa and Sanchis [166] did not mention the Faraday efficiency of the electrolyser which their model was based on, in this thesis the Faraday efficiency model developed by Ulleberg [167] and reported by Eq. (4.46), was applied.

$$\eta_F = a_1\, exp\left(\frac{a_2 + a_3 T_c + a_4 T_c^2}{I/A} + \frac{a_5 + a_6 T_c + a_7 T_c^2}{(I/A)^2}\right) \tag{4.46}$$

Table 4.5 reports the parameters used in Eq. (4.46).

Table 4.5 – Parameters for the Faraday efficiency calculation [167]						
a_1	a_2 [m^2A^{-1}]	a_3 [$m^2A^{-1}°C^{-1}$]	a_4	a_5 [m^2A^{-1}]	a_6 [$m^2A^{-1}°C^{-1}$]	a_7
0.995	-9.5788	-0.0555	0	1502.7083	-70.8005	0

4.3.2 AEL Aspen Plus model

A simplified functional scheme of the model of the AEL as it was implemented in Aspen Plus is reported in Fig. 4.5.

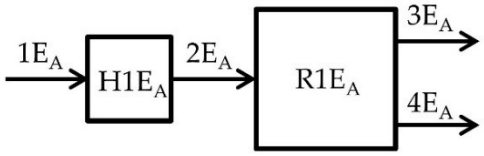

Fig. 4.5 – Simplified functional scheme of the alkaline electrolyser section (H = Heater, R = Reactor)

In the simplified functional scheme, water ($1E_A$) is heated to the cell operating temperature in a heater ($H1E_A$) and enters the reactor ($R1E_A$) where the water splitting reactions are carried out (reactions (3.3) and (3.4)). The reactor is modelled as a stoichiometric reactor using the block RStoic in Aspen Plus, where the water splitting reaction is carried out and a complete conversion of water is considered. While in the actual flowsheet the stream (composed of hydrogen and oxygen) exiting the reactor is split using a separator block, in Fig. 4.5 the hydrogen ($3E_A$) and the oxygen ($4E_A$) are depicted as already separated, as it happens at the cathode and anode side in the real system. Even though the flowsheet developed in Aspen Plus is simple, the electrochemical behaviour and the characteristic of the electrolyser are defined by the comprehensive model described in Par. 4.3.1 and implemented in the Fortran routine.

4.3.3 AEL model validation

The electrochemical model presented in Par. 4.3.1 and defined in the Aspen Plus routines was validated via a comparison with the experimental results reported in Ursúa and Sanchis [166]. The validation was carried out at 25 bar for a temperature of 15, 35 and 65 °C (as the experimental tests carried out in [166]). Table 4.6 reports the values of the main parameters considered for the validation. The other parameters necessary to run the model are those reported in Par. 4.3.1

Table 4.6 – Parameters used in AEL model validation	
Parameter	Value
Temperature [°C]	15, 35, 65 °C
Operating pressure [bar]	25
Number of cells	22
Cell area [cm^2]	300

Figure 4.6 shows the comparison between the model developed in Aspen Plus and the experimental curves that the authors [166] obtained from the experimental testing of the considered commercial stack.

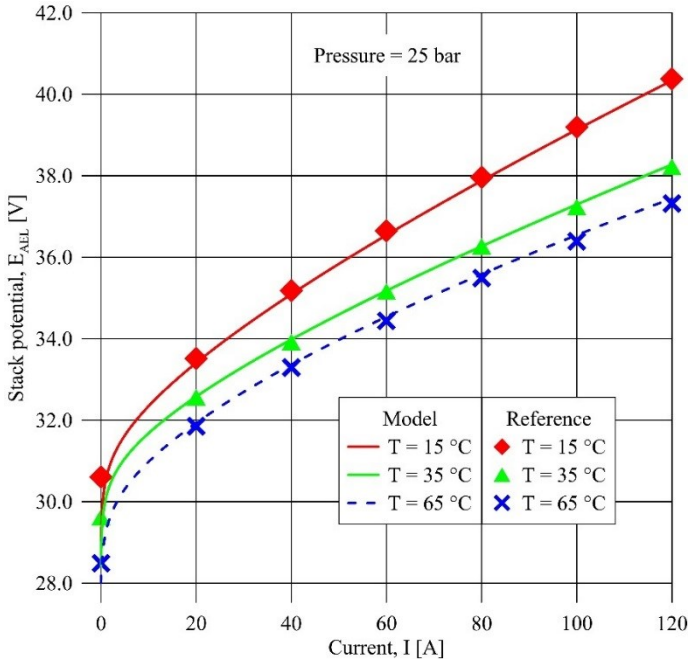

Fig. 4.6 – Comparison between model results and experimental data (AEL)

The Aspen Plus model follows the reference experimental curves closely, demonstrating the accuracy of the Aspen Plus simulation and of the model developed by Ursúa and Sanchis. Hence, the model can be used to simulate the alkaline electrolysis stack, or modules (composed of several stacks in series and parallel), with an accurate evaluation of the system voltage and consequently of its power consumption and efficiency.

4.4 Methanol reactor model

The methanol synthesis process is carried out following the carbon monoxide hydrogenation (4.47), the carbon dioxide hydrogenation (4.48), and the reverse water gas shift reaction (4.49) occurring in a kinetic reactor:

$$CO + 2H_2 \leftrightarrows CH_3OH \tag{4.47}$$

$$CO_2 + 3H_2 \leftrightarrows CH_3OH + H_2O \tag{4.48}$$

$$CO_2 + H_2 \leftrightarrows CO + H_2O \tag{4.49}$$

As these reactions are linearly dependent, only Eq. (4.48) and (4.49) were considered in the model developed in Aspen Plus.

The catalytic reaction over the commercial catalyst $Cu/ZnO/Al_2O_3$ was simulated by a kinetic Langmuir-Hinshelwood Hougen-Watson (LHHW) model, as proposed by Van-Dal and Bouallou [168], and rearranged to be compatible with the Aspen Plus input as comprehensively reported by Al-Malah [169]. The kinetic model was developed by Van-Dal and Bouallou [168] starting from the original Vanden Bussche and Froment [170] model that was subsequently modified by Mignard and Pritchard [171].

The reaction rates of reactions (4.48) and (4.49) are given by Eq. (4.50) and (4.51):

$$r_{CH_3OH} = \frac{k_1 P_{CO_2} P_{H_2} - k_6 P_{H_2O} P_{CH_3OH} P_{H_2}^{-2}}{\left(1 + k_2 P_{H_2O} P_{H_2}^{-1} + k_3 P_{H_2}^{0.5} + k_4 P_{H_2O}\right)^3} \tag{4.50}$$

$$r_{CO} = \frac{k_5 P_{CO_2} - k_7 P_{H_2O} P_{CO} P_{H_2}^{-1}}{1 + k_2 P_{H_2O} P_{H_2}^{-1} + k_3 P_{H_2}^{0.5} + k_4 P_{H_2O}} \quad (4.51)$$

where the kinetic constant values, k_i, were calculated by Eq. (4.52):

$$ln(k_i) = A_i + \frac{B_i}{T} \quad (4.52)$$

Table 4.7 reports the kinetic parameters used in the LHHW model [168].

Table 4.7 – Kinetic parameters for the LHHW model

Kinetic parameters	A_i	B_i
k_1	-29.87	4811.2
k_2	8.147	0
k_3	-6.452	2068.4
k_4	-34.95	14928.9
k_5	4.804	-11797.5
k_6	17.55	-2249.8
k_7	0.131	-7023.5

4.4.1 Methanol reactor model validation

To verify that the reactor and the kinetic model defined in Aspen Plus worked as expected, a validation was carried out. To validate the model, information provided by Van-Dal and Bouallou [168] was considered. The Aspen Plus flowsheet used to validate the kinetic model was simply composed of an inlet and an outlet stream connected to an adiabatic reactor supposed to be a stainless-steel tube filled with the catalyst, defined as an RPlug block in Aspen Plus environment. The main parameters defined within the reactor environment are the reactor length and diameter, the catalyst loading and the particles density. The inlet stream is composed of carbon monoxide, carbon dioxide, hydrogen and argon used as an inert. Inlet pressure and temperature are 50 bar and 220 °C, respectively, while the mass flow is equal to 2.8×10^{-5} kg/s. Table 4.8 summarises the main parameters used to validate the methanol kinetic model [168].

Table 4.8 – Parameters for the methanol kinetic model validation (i)

Parameter	Value
Reactor	RPlug adiabatic
Reactor length [m]	0.15
Reactor diameter [m]	0.016
Reactor catalyst loading [g]	34.8
Particle density [kg/m^3]	1775

Table 4.8 - Parameters for the methanol kinetic model validation (ii)	
Inlet stream	
Pressure	50 bar
Temperature	220 °C
Mass flow	2.8×10^{-5} kg/s
Composition (vol.)	
Ar	0.11
CH_3OH	0.00
CO	0.04
CO_2	0.03
H_2	0.82
H_2O	0.00

Among other charts and data visualisation options, Aspen Plus provides the molar composition of the stream along the reactor length. Table 4.9 summarises the results obtained with the Aspen Plus simulation of the kinetic reactor model.

Table 4.9 – Aspen Plus molar fraction along the reactor					
Length [m]	CH_3OH	CO	CO_2	H_2O	H_2
0.000	0.0000	0.0000	0.0300	0.0400	0.8200
0.015	0.0165	0.0113	0.0197	0.0361	0.8028
0.030	0.0222	0.0107	0.0207	0.0303	0.8014
0.045	0.0225	0.0106	0.0207	0.0300	0.8013
0.060	0.0225	0.0106	0.0207	0.0300	0.8013
0.075	0.0225	0.0106	0.0207	0.0300	0.8013
0.090	0.0225	0.0106	0.0207	0.0300	0.8013
0.105	0.0225	0.0106	0.0207	0.0300	0.8013
0.120	0.0225	0.0106	0.0207	0.0300	0.8013
0.135	0.0225	0.0106	0.0207	0.0300	0.8013
0.150	0.0225	0.0106	0.0207	0.0300	0.8013

In Fig. 4.7, the results reported in Table 4.9 are compared to the reference data from Van-Dal and Bouallou [168]. The molar fraction of the main chemical species, namely carbon monoxide, methanol, carbon dioxide, and water, is reported in the y-axis as a function of the reactor length. The results of the model, represented by the symbols, are consistent with the reference data without noticeable errors. Therefore, the kinetic model as it was developed and implemented in Aspen Plus is accurate and can be used to simulate the kinetic conversion of the reactants into methanol.

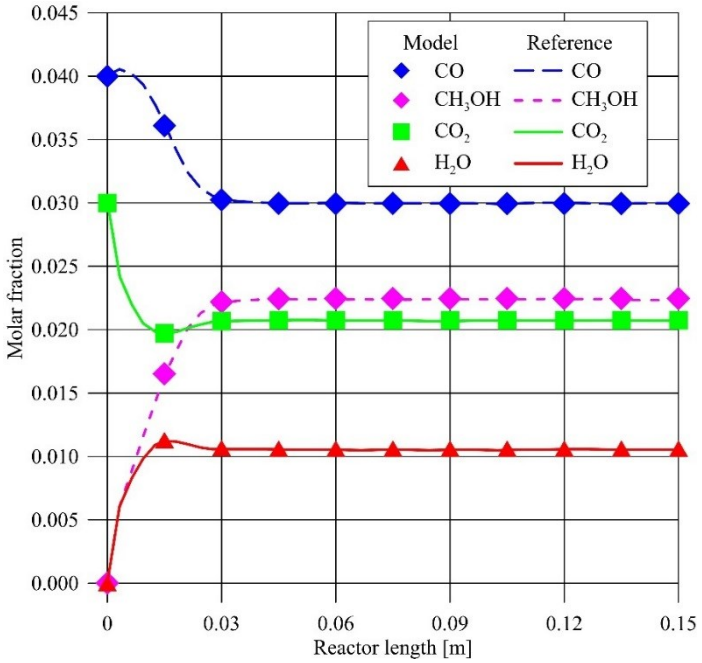

Fig. 4.7 – Comparison between model results and reference data (methanol reactor)

4.4.2 Methanol synthesis section Aspen Plus model

A simplified functional scheme of the model of the MSS as it was implemented in Aspen Plus is reported in Fig. 4.8. The MSS allows the production of methanol through the catalytic hydrogenation of CO_2 [65,168,172]. The core of the system is the synthesis reactor, where pressurised H_2 and CO_2 react to produce methanol. The catalytic conversion process occurs on the commercial catalyst $Cu/ZnO/Al_2O_3$.

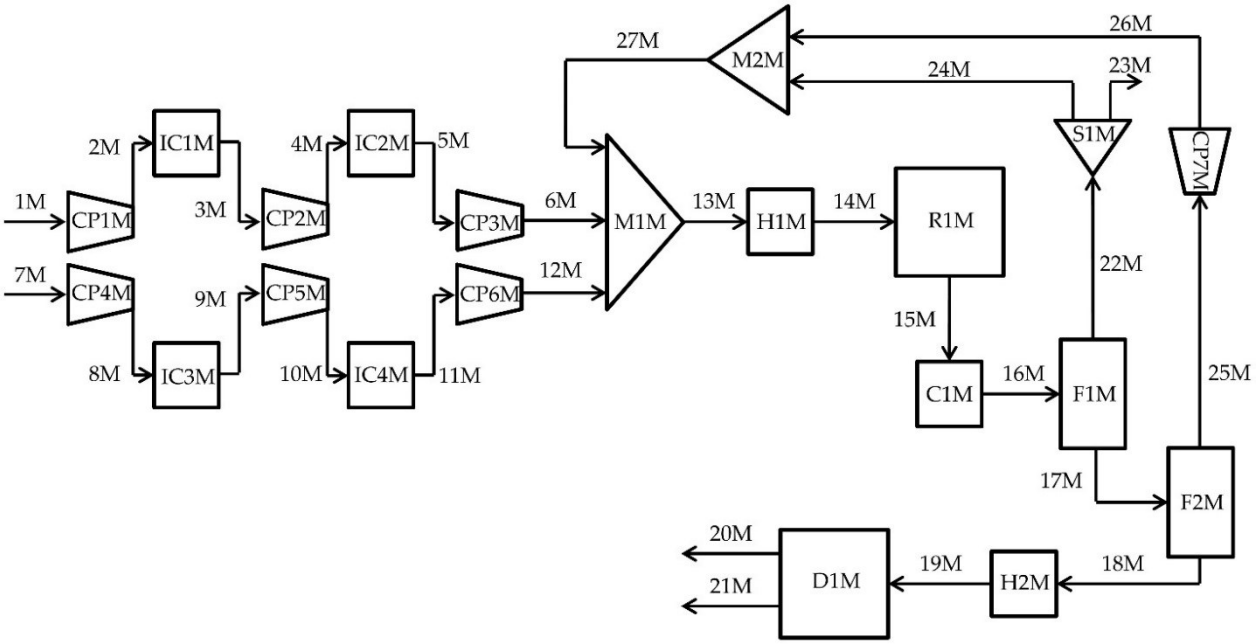

Fig. 4.8 – Simplified functional scheme of the methanol synthesis and purification section (C = Cooler; CP = Compressor; D = Distillation column; F = Flash; H = Heater; IC = Intercooler; M = Mixer; R = Reactor; S = Splitter)

The hydrogen (1M) produced during SOEC operation and the previously captured CO_2 are first compressed in two intercooled compression trains up to a suitable pressure for the methanol synthesis process (in this case assumed equal to 65 bar) and then mixed (M1M) with compressed recycle gas (27M), obtaining a hydrogen-rich mixture (13M). Both compressor trains are each composed of 3 compressors (CP1M-CP2M-

CP3M and CP4M-CP5M-CP6M) and two intercoolers (IC1M-IC2M and IC3M-IC4M). The compressors were supposed isentropic with an efficiency of 0.75. The pressure ratio of each compressor was set to a value slightly higher than 4, whereas the intercooling temperature was set to 38 °C. The hydrogen-rich stream (13M) is heated up (H1M) to 210 °C (14M), which is a typical inlet temperature of such reactors. Inside the reactor (R1M), assumed adiabatic, the temperature increases due to exothermic reactions. Downstream of the reactor, hot products (15M) are cooled down (C1M) to 50 °C. At this temperature a first flash process occurs (F1M), separating the unreacted gas (22M), largely composed of hydrogen, from the liquid water/methanol mixture (17M). A further flash (F2M) is performed at a lower pressure (1.2 bar) and temperature (22 °C) to separate the residual gases, mainly composed of CO_2. Incondensable gases (25M) from F2M are compressed up to 65 bar (CP7M), mixed in M2M with 24M and then in the mixer M1M with the reactor feedings (6M and 12M). To avoid the accumulation of by-products, 1% by volume of the recycled gas is extracted as purge gas (23M). The liquid stream (18M) is then heated up to 80 °C (H2M) before entering the distillation column (D1M). From the bottom of the distillation column, water (21M) is recuperated in the liquid phase and can be recycled back to the SOEC. From the top of the distillation column, almost pure methanol (20M) with a small content of carbon dioxide is gathered and methanol and CO_2 are subsequently separated through methanol condensation. Then, methanol is sent to the storage tank, ready to feed the RSOC in SOFC mode. Table 4.10 reports the main operating parameters of the MSS [65,168,172].

Table 4.10 – MSS main operating parameters

	Value
Reactor type	Adiabatic
Reactor pressure [bar]	65
Reactor inlet temperature [°C]	210
Number of compressors for each compression train	3
Pressure ratio of each compressor	4.02
Intercooling temperature [°C]	38
F1M pressure [bar]	65
F1M temperature [°C]	50.5
F2M pressure [bar]	1.2
F2M temperature [°C]	22
Methanol storage pressure [bar]	1
Methanol storage temperature [°C]	25

The main blocks of the MSS are the reactor and the distillation column, which were implemented in Aspen Plus through an RPlug reactor and a RadFrac column, respectively. Table 4.11 and Table 4.12 report the main parameters of the reactor and distillation column, respectively.

Table 4.11 – Main parameters of the methanol synthesis reactor

Parameter	Value
Reactor	RPlug adiabatic
Bed voidage	0.4
Catalyst density [kg/m^3]	1775
Pressure [bar]	65
Feeding temperature [°C]	210

Table 4.12 – Main parameters of the distillation column	
Parameter	Value
Column	RadFrac
Number of trays	57
Reflux ratio	1.2
Feeding temperature [°C]	80
Operating pressure [bar]	1.01

4.5 Thermal energy storage model

A preliminary design of the LHTES system was carried out using a numerical simulation model specifically developed in MATLAB-Simulink environment based on a transient one-dimensional (1-D) two-equation model (LTNE). With this model it is possible to study the behaviour of the storage unit and find the optimal size configuration by calculating the temperature trend of the thermal fluid and the PCM during the heat transfer process. The TES system consists of a single tank based on a packed bed configuration filled with PCM held in capsules 0.05 m in diameter. The porous bed is considered homogeneous and isotropic, the energy losses are supposed negligible, while the shape of the thermocline generated within the bed along the axis of the tank is calculated by considering a constant radial temperature profile. A detailed description of the model, developed by some colleagues the author's thesis worked with in Cagliari and adopted here, is reported in their works [173,174], where the apparent heat capacity method was used to model the PCM melting process.

4.6 Organic Rankine cycle Aspen Plus model

A simplified functional scheme of the model of the ORC as it was developed in Aspen Plus is reported in Fig. 4.9. While in the case of the SOEC, SOFC, and AEL models, special mathematical and electrochemical equations implemented in Fortran routines were necessary to obtain the desired results from the simulation (i.e. the voltage, the current, the power consumed or produced etc.), in the case of the ORC the Aspen Plus flowsheet based on blocks and streams was sufficient to gather the desired results of heat transferred between streams and power produced by the turbine. Indeed, the built-in blocks used in the ORC model (i.e. the turbine, pump, heat exchanger, etc.) as well as the fluid properties contained in the Aspen Plus database are sufficient to simulate this type of process without further implementation of user-defined models. On the contrary, Aspen Plus does not have special blocks to simulate the electrochemical processes, so user-defined models were necessary for that specific simulation.

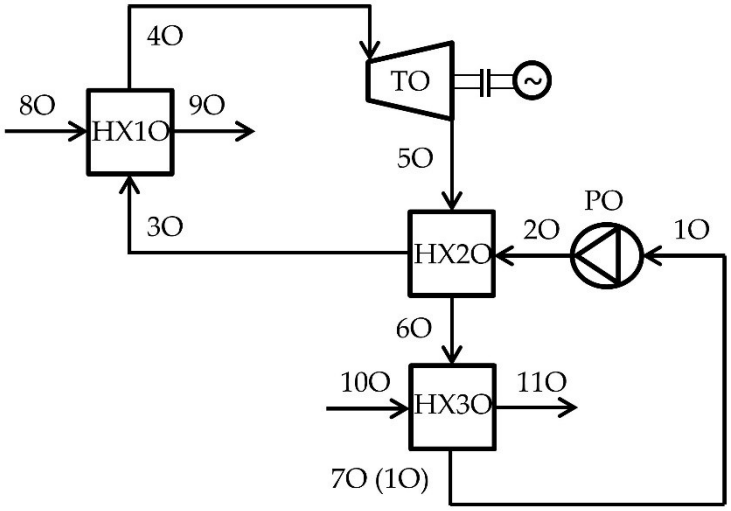

Fig. 4.9 – Simplified functional scheme of the ORC (HX = Heat exchanger, P = Pump, T = Turbine)

As with what is reported in Fig. 3.6, a heat source (8O) is cooled (9O) by releasing heat to the working fluid in the heat exchanger HX1O (typically called evaporator). During this heat transfer process, the working fluid is heated up to the maximum temperature of the cycle (3O to 4O) and sent to the turbine. The working fluid expansion from 4O to 5O produces work and, through an electric generator, electricity. The residual heat in the turbine exhaust is used to preheat the working fluid (2O) in the regenerator (HX2O). Finally, exploiting cold water or air (10O), the working fluid (6O) is cooled to the initial temperature (7O = 1O) in the condenser (HX3O). Then, the cycle begins again with the working fluid (1O) pumped (PO) to the maximum pressure of the cycle. Benzene, butylbenzene, and toluene were considered as potential working fluids, as extensively described in Par. 5.4. Finally, the configuration employed in this study was chosen because of its simplicity and because of the low temperature and mass flow of the available heat source (i.e. the hot gases coming from the SOFC section).

Chapter 5

Performance of the analysed systems

5.1 Introduction

The models described in Chapter 4 were used to simulate and analyse the various complex systems based on different technologies and arranged in different layouts, as they were shown in the same chapter. The general layout depicted in Fig. 3.1, as already described extensively in Par. 3.1, is characterised by an electrolyser, a chemical synthesis section, a fuel cell, an ORC (optional) and a heat recovery/storage section. The technologies adopted in some of these subsections are unvaried between each layout, namely the fuel cell section based on solid oxide technology and the methanol synthesis section, composed of the kinetic reactor and the distillation column. Hence, to guarantee a coherent comparison between the different layouts, the main parameters of these two subsections were considered as fixed between each layout. Especially, the power of the solid oxide fuel cell was defined as the main design parameter for the overall system. Given the design power of the SOFC, the methanol flow rate coming from the storage is fixed. If this value is fixed, then the amount of hydrogen and CO_2 that produces the desired methanol in the MSS is fixed. However, since the electrolysis technology varies from one configuration to the other, the water flow rate and the power requested by the electrolyser is different from one layout to the other. One of the configurations analysed in this study is based on the RSOC technology (a solid oxide cell that can be operated as an electrolyser and as a fuel cell). Typically, SOFC technology is available in a range from 10 kW to 1 MW [114]. Moreover, even though RSOC are based on SOFC technology, state of the art RSOC systems are characterised by a power production in fuel cell mode of 30-50 kW and a power consumed in electrolysis mode of 150 kW [175]. Therefore, in a future perspective, an RSOC with a power production of 1 MW in SOFC mode was considered. For the sake of comparison, also in the system based on alkaline electrolysis a SOFC power of 1 MW was considered. Thus, the overall systems were all sized to produce 1 MW of electric power in SOFC mode. Such a power requires a renewable methanol production of approximately 370 kg/h, in the order of magnitude of the capacity of the only existing commercial renewable methanol plant [18]. The flow rates of the streams feeding the electrolyser and the methanol synthesis sections were calculated to guarantee such a methanol production.

The innovative technology of RSOCs was taken into consideration first, while the commercially mature technology (i.e. alkaline water electrolysis) was analysed and studied subsequently.

5.2 System based on reversible solid oxide cells

The system to produce and use renewable methanol studied in this paragraph is composed of three main sections: a) an RSOC section capable of working as an SOEC or as an SOFC, depending on RES availability, b) a methanol synthesis and purification section, and c) a TES section to recover waste heat. Figure 5.1 shows a simplified scheme of the overall system and the interconnections between the subsections composing the plant. Water, air, and renewable electricity feed the RSOC in SOEC mode to produce hydrogen, and air rich in oxygen as a by-product. Hydrogen and previously captured CO_2 (process not accounted in this study) are compressed to the operating pressure of the methanol reactor, where catalytic CO_2 hydrogenation takes place. Unreacted gases are recycled, and crude methanol is purified in a distillation column and stored at ambient conditions. Then, during discharge mode, methanol is reformed to hydrogen

that is oxidised in the RSOC in SOFC mode. The heat integration block appearing in the functional scheme of Fig. 5.1 represents the heat transfer processes required to allow the system to reach operating conditions. For instance, heat exchangers and heaters are contained in the heat integration block. A detail of the heat recovery (TES) section is reported in the lower-right corner of Fig. 5.1. The magnification shows the TES (based on PCM), a gas-water heat exchanger (GWHX), and the interactions between the SOFC gases, the TES, the air, and the water. During charge mode, the SOFC gases heat the TES. During discharge mode, air circulates in a closed loop gaining heat from the TES and releasing it inside the GWHX to the water feeding the SOEC.
The models of each section were developed in Aspen Plus to simulate water splitting (and fuel oxidation), as well as the other processes. The models and the parameters that were used to simulate the system depicted in Fig. 5.1 are found within Chapter 4.

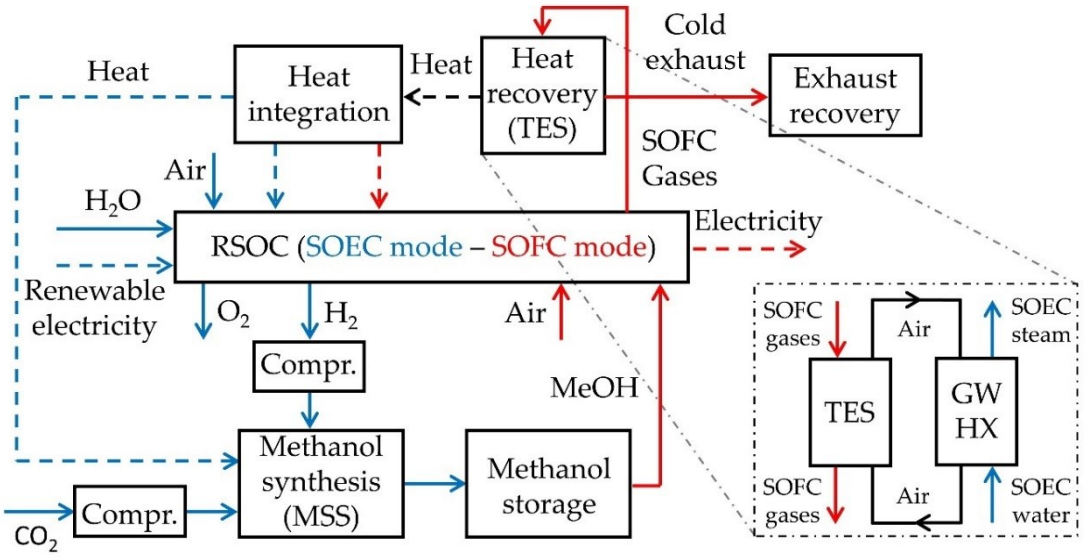

Fig. 5.1 – Simplified functional scheme of the overall system based on RSOC

As already stated, the system was sized considering a design SOFC power of 1 MW_{el} that requires a methanol flow rate of approximately 370 kg/h. The flow rates of the main flows (namely air, water and CO_2) feeding the other main sections were calculated to guarantee the desired methanol production.
The RSOC was supposed to work at 850 °C in both modes, a typical temperature used in these devices to avoid too high temperatures (the higher the operating temperature, the more difficult the thermal management and the lower the material duration over time) and to operate the SOEC in thermo-neutral state. The operating pressure was set equal to the that of the ambient. This is because working at high pressure brings about problems in the cells materials, causes earlier faults, and increases the complexity of the overall system while reducing its reliability [176]. Moreover, working at high pressure can bring about pressure gradients within the cell, causing premature break [124]. The SOEC and the SOFC are operated considering a utilisation factor of 0.85 for water and fuel, respectively.

5.2.1 SOEC (RSOC)

The SOEC is fed with approximately 780 kg/h of water to produce the hydrogen flow rate necessary in the MSS section. In the SOEC, water electrolysis is performed at ambient pressure and at 850 °C. At the selected operating conditions, thermo-neutral operation is performed, so no external heat is required, and all the heat needed by the electrolysis (Fig. 3.3) is provided by the Joule effect within the SOEC. Figure 5.2 recalls the simplified functional scheme of the SOEC section reported previously in Fig. 4.1. Water ($1E_S$) and sweep air ($4E_S$) are heated to the SOEC operating temperature ($H1E_S$ and $H2E_S$, respectively). Water is mixed ($M1E_S$)

with a portion of the produced hydrogen ($9E_S$), the mixture is electrolysed in the reactor/cell ($R1E_S$) and hydrogen and oxygen are produced. Both the hydrogen-water mixture ($10E_S$) and the air ($6E_S$) are cooled to ambient temperature while the released heat can be recovered to reduce the overall thermal energy requirement of the SOEC.

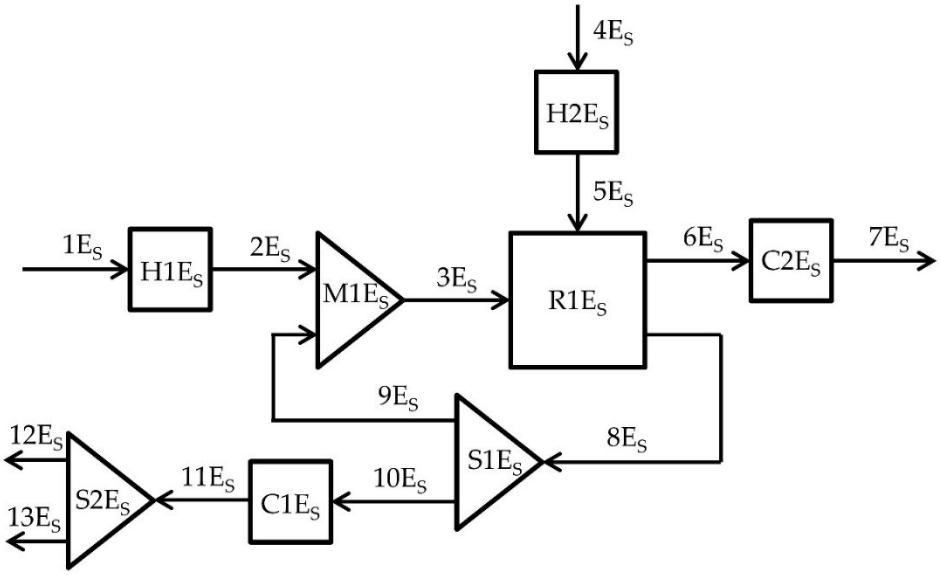

Fig. 5.2 – Simplified functional scheme of the solid oxide electrolyser section (C = Cooler; H = Heater; M = Mixer; R = Reactor; S = Splitter)

Table 5.1 summarises the mass flow rate, temperature, and molar fraction of the main streams depicted in the simplified scheme of Fig. 5.2.

Table 5.1 – Composition (by vol.) of the main streams in the SOEC

	$1E_S/2E_S$	$3E_S$	$4E_S/5E_S$	$6E_S/7E_S$	$8E_S$	$9E_S$	$10E_S/11E_S$	$12E_S$	$13E_S$
Mass flow [kg/s]	0.217	0.224	0.236	0.403	0.057	0.0066	0.0503	0.021	0.0293
Temp [°C]	25/850	850	25/850	850/25	850	850	850/25	25	25
H_2	0.0000	0.1000	0.0000	0.0000	0.8650	0.8650	0.8650	1.0000	0.0000
N_2	0.0000	0.0000	0.7728	0.4724	0.0000	0.0000	0.0000	0.0000	0.0000
O_2	0.0000	0.0000	0.2073	0.5155	0.0000	0.0000	0.0000	0.0000	0.0000
Ar	0.0000	0.0000	0.0092	0.0056	0.0000	0.0000	0.0000	0.0000	0.0000
H_2O	1.0000	0.9000	0.0103	0.0063	0.1350	0.1350	0.1350	0.0000	1.0000
CO_2	0.0000	0.0000	0.0003	0.0002	0.0000	0.0000	0.0000	0.0000	0.0000

Figure 5.3 shows a variation of the scheme reported in Fig. 4.1 and Fig. 5.2. In this figure, the thermal integrations and interactions between the different streams are highlighted.

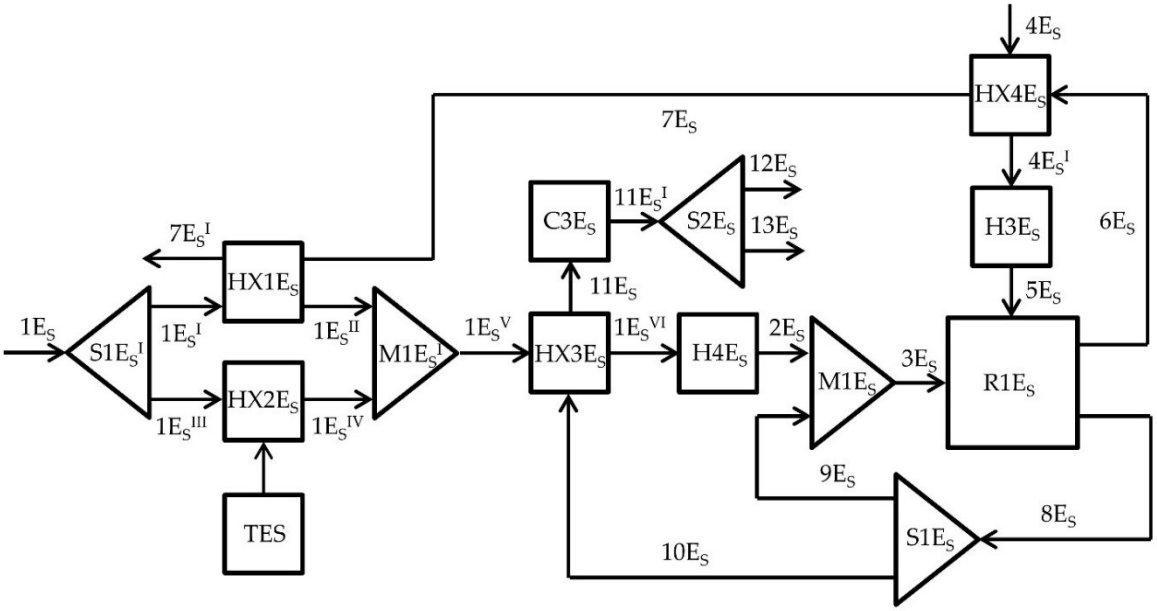

Fig. 5.3 – Simplified functional scheme of the SOEC section with thermal integrations (C = Cooler; H = Heater; HX = Heat exchanger; M = Mixer; R = Reactor; S = Splitter)

On the anode side, hot (850 °C) exhausts ($6E_S$) are used to preheat the cold sweep air ($4E_S$) up to 800 °C in $HX4E_S$ (assuming a minimum temperature difference between the hot inlet and the cold outlet of 50 °C). Globally, the energy that can be recovered by coupling the cold sweep air to the anode exhaust is approximately 200 kW. About 15 kW of thermal power must still be supplied by an additional heater ($H3E_S$) to complete the air sweep heating process from 800 to 850 °C. Since the anode exhaust ($6E_S$) is composed of both the sweep air and the oxygen produced in the SOEC, heating the sweep air from ambient temperature to 800 °C cools the anode exhaust to about 405 °C ($7E_S$), allowing further heat recovery from the hot exhaust. On the cathode side water is preheated, vaporized and superheated through two different sources to reach the operating temperature before entering the cell. A fraction of the water flow rate ($1E_S^I$, about 185 out of the total 780 kg/h) is preheated and vaporized in $HX1E_S$ exploiting the residual heat of the hot anode exhaust ($7E_S$). The remainder ($1E_S^{III}$) is preheated and vaporized in $HX2E_S$ by an external source or harvesting the heat from the SOFC exhaust gases stored in the TES system during discharge mode operation. Approximately 425 kW are recovered and saved by this integration. Then, saturated steam is superheated to about 680 °C exploiting the hot cathode exhaust ($10E_S$ composed of hydrogen and water) in $HX3E_S$, saving approximately 260 kW. An external heater (H4E) is required to reach the SOEC operating temperature (850 °C), absorbing a power of 85 kW. In addition, a portion of the cathode exhaust ($9E_S$) is recycled to the reactor ($R1E_S$) inlet to reach a suitable feed composition (90% water, 10% hydrogen) to avoid electrode oxidation [164]. Given the 76 kg/h of hydrogen required in the subsequent MSS and assuming a water utilisation factor of 0.85, a water flow rate of 780 kg/h is needed. The SOEC requires an electric power of approximately 2.6 MW_{el}.

Table 5.2 summarises the exact energy balances of the heating and cooling processes within the SOEC system. The available heat in the cooling process, reported in the columns on the right, can be used to reduce the total thermal energy requirements of the SOEC, reported in the heating process column on the left.

Table 5.2 – Main heat transfers in the SOEC

Heating process	Heat [kW]	Cooling process	Heat [kW]
Sweep air PH by heat recovery ($HX4E_S$)	197.8	Anode exhaust 1st cooling ($HX4E_S$)	-197.8
Sweep air PH by external source ($H3E_S$)	13.8	Anode exhaust 2nd cooling ($HX1E_S$)	-133.9
Water PH and VAP by heat recovery ($HX1E_S$)	133.9	Cathode exhaust 1st cooling ($HX3E_S$)	-260.8
Water PH and VAP by external source or TES ($HX2E_S$)	426.6	Cathode exhaust 2nd cooling ($C3E_S$)	-101.2
Steam SH by heat recovery ($HX3E_S$)	260.8		
Steam SH by external source ($H4E_S$)	84.5		

PH: preheating; VAP: vaporisation; SH: superheating

The sweep air preheating ($H3E_S$), the water preheating and vaporisation ($HX2E_S$), and the steam superheating ($H4E_S$) are carried out exploiting some type of external sources. Whilst the water preheating and vaporisation ($HX2E_S$) is carried out exploiting the heat stored in the TES, the other two processes are supposed to be performed using two external electrical heaters.

5.2.2 MSS (RSOC)

The methanol synthesis section allows the production of the liquid fuel used to store electricity. By assuming a duration of 6 hours for both the charging and discharging processes, the methanol flow rate produced in the MSS was set equal to that consumed in the SOFC (≈ 370 kg/h). By assuming a molar ratio equal to the stoichiometric one in reaction (4.48), such a methanol production requires a flow rate of H_2 and CO_2 equal to approximately 76 kg/h (≈ 840 Nm^3/h) and 550 kg/h (≈ 280 Nm^3/h), respectively. The feeding streams (H_2 and CO_2) are compressed to the operating pressure (65 bar) through two trains of three intercooled compressors each, characterised by an intercooling temperature of 38 °C. The total power absorbed by the compressors is roughly 240 kW. Of these, 183 kW are required for the hydrogen compression while 56 kW are required to compress the CO_2. Then, the compressed reactants are preheated to 210 °C before entering the reactor. Since the global CO_2 hydrogenation process is exothermic and the reactor is supposed adiabatic, the temperature increases to approximately 290 °C. The reactor exhaust (mainly H_2, and only about 4% by volume of methanol, see Table 5.3) is purified from unreacted species and incondensable gases via two flash processes. The flashed gases are recycled back to the reactor inlet to boost the production of methanol. The first flash occurs at a temperature of 50 °C and a pressure of 65 bar. Then, the pressure and temperature of the liquid stream are reduced to about 1.2 bar and 22 °C, respectively, and the flow is subjected to the second flash process. The crude methanol exiting the second flash is sent to a distillation column, where the separation of water and methanol takes place. The distillate at the top of the column is a mixture of methanol and CO_2, with a methanol purity of 96.4% (by volume). The unreacted CO_2 is separated from methanol by simply condensing the latter. A comprehensive description of this process and the model used is reported in Par. 4.4. Figure 5.4 recalls the simplified functional scheme of the MSS previously reported in Fig. 4.8.

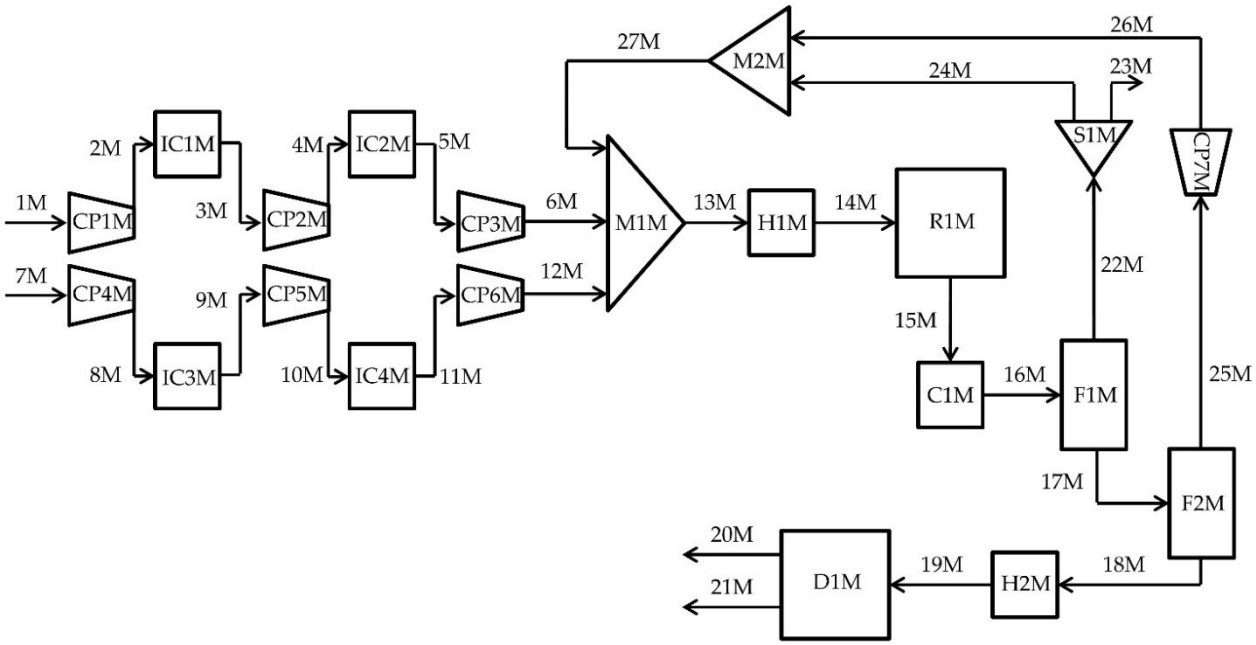

Fig. 5.4 – Simplified functional scheme of the methanol synthesis and purification section (C = Cooler; CP = Compressor; D = Distillation column; F = Flash; H = Heater; IC = Intercooler; M = Mixer; R = Reactor; S = Splitter)

Tables 5.3 and 5.4 summarise the main parameters (i.e. mass flow, temperature, and molar fraction) of the main streams in the MSS. The stream names correspond to those depicted in Fig. 5.4.

Table 5.3 – Composition (by vol.) of the main streams in the MSS (i)

	1M/2M	3M/4M	5M/6M	7M/8M	9M/10M	11M/12M	13M/14M	15M/16M
Mass flow [kg/s]	0.021	0.021	0.021	0.153	0.153	0.153	0.860	0.860
Temp [°C]	25/219	38/240	38/240	25/159	38/176	38/179	75/210	291/50
CH_3OH	0.0000	0.0000	0.0000	0.0000	0.0000	0.0000	0.0031	0.0384
H_2O	0.0000	0.0000	0.0000	0.0000	0.0000	0.0000	0.0012	0.0369
CO_2	0.0000	0.0000	0.0000	1.0000	1.0000	1.0000	0.1297	0.1032
H_2	1.0000	1.0000	1.0000	0.0000	0.0000	0.0000	0.8210	0.7729
CO	0.0000	0.0000	0.0000	0.0000	0.0000	0.0000	0.0450	0.0486

Table 5.4 – Composition (by vol.) of the main streams in the MSS (ii)

	17M	18M/19M	20M	21M	22M	24M	25M/26M	27M
Mass flow [kg/s]	0.214	0.167	0.109	0.059	0.646	0.639	0.047	0.686
Temp [°C]	50	22/80	63	100	50	50	22/485	57
CH_3OH	0.4260	0.4874	0.9640	0.0000	0.0030	0.0030	0.0535	0.0036
H_2O	0.4259	0.4944	0.0000	1.0000	0.0013	0.0013	0.0098	0.0014
CO_2	0.1459	0.0182	0.0360	0.0000	0.0993	0.0993	0.9209	0.1099
H_2	0.0000	0.0000	0.0000	0.0000	0.8435	0.8435	0.0003	0.8327
CO	0.0022	0.0000	0.0000	0.0000	0.0529	0.0529	0.0155	0.0524

Since the reactor outlet is at high temperature (≈ 290 °C), it can be employed to heat some streams within the MSS, reducing the thermal energy that otherwise would be provided by an external source. Thus, to reduce

the heat requirements in the MSS a heat integration between the hot streams, cold streams, and other processes was performed. Figure 5.5, which is a variation of the scheme reported in Fig. 4.8 and Fig. 5.4, shows the interactions between the hot streams and the other entities in the flowsheet. The preheating of the reactants (≈ 350 kW) is carried out by exploiting the heat of the reactor exhaust, reducing its temperature from 290 (15M) to 175 °C ($15M^{I}$) in the block HX1M. During this process, the cold stream (13M) is heated from 75 to 210 °C. Since the reboiling process in the distillation column occurs at 100 °C and requires 180 kW, heat is provided by the same reactor exhaust, that is cooled from 175 to 124 °C ($15M^{II}$) while releasing heat in the distillation column. Finally, the reactor exhaust heats the crude methanol (18 M) up to the inlet temperature of the distillation column (80 °C) in the block HX2M, allowing a further recovery of roughly 135 kW and a reduction in the temperature of the exhaust gases to 106 °C ($15M^{III}$). To reach the first flash condition (50 °C), roughly 235 kW should be further removed from the reactor outlet gases in the cooler C2M. Globally, a total of approximately 665 kW is recovered and exploited within the MSS, reaching the thermal self-sustainability of the section.

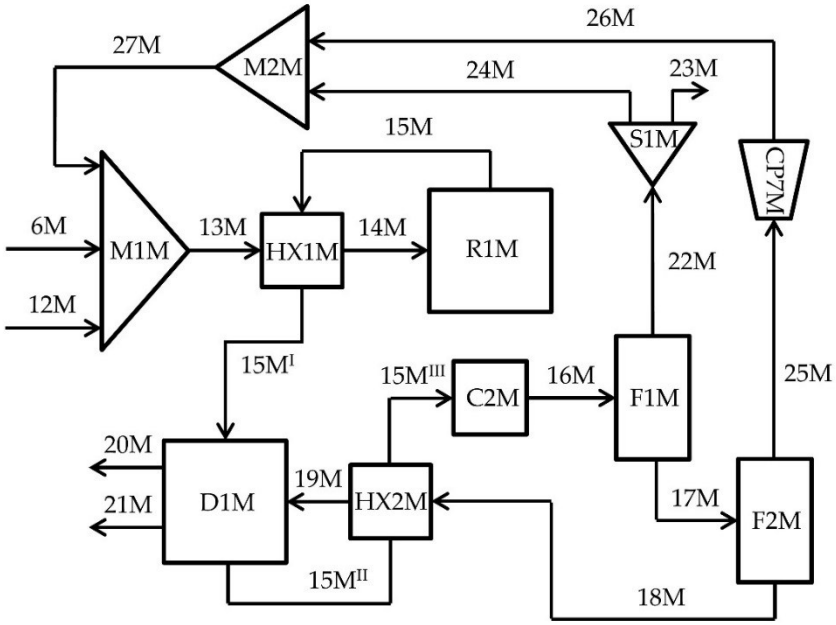

Fig. 5.5 – Simplified functional scheme of the methanol synthesis and purification section with thermal integrations (C = Cooler; CP = Compressor; D = Distillation column; F = Flash; HX = Heat exchanger; M = Mixer; R = Reactor; S = Splitter)

In Table 5.5 the exact energy balances of the heating and cooling processes within the MSS are reported.

Table 5.5 – Main heat transfers in the MSS

Heating process	Heat [kW]	Cooling process	Heat [kW]
Reactor inlet by heat recovery (HX1M)	350.3	Reactor outlet 1st cooling (HX1M)	-350.3
Distillation reboiling by heat recovery (D1M)	180.0	Reactor outlet 2nd cooling (D1M)	-180.0
Crude methanol by heat recovery (HX2M)	135.2	Reactor outlet 3rd cooling (HX2M)	-135.2
		Reactor outlet 4th cooling (C2M)	-233.7

Apart from the reactor outlet 4th cooling (C2M), that is at a low temperature and cannot be easily recovered, the cooling heat of the reactor outlet (15M) can be harvested integrally by the heating processes within the MSS.

5.2.3 SOFC (RSOC)

As previously specified, the SOFC was designed and sized to produce a power of 1 MW. The SOFC section is fed with methanol, along with water and air. Methanol and water (that are mixed to achieve an optimal steam-to-carbon-ratio) are vaporised separately and then mixed together with a portion of the SOFC outlet to reach a temperature of 300 °C. Then, methanol is reformed (following reactions (4.24)-(4.26)) to a mixture rich in hydrogen (H_2 content about 64% by vol.) to produce electricity in the cell. Water flow rate is obtained setting a suitable steam to carbon ratio in the reformer (equal to 1.25 [177]). As in SOEC mode, the SOFC operates at a temperature of 850 °C with a fuel utilisation factor of 0.85. Residual gases from the SOFC, mainly composed of H_2 and CO, are burnt in a post combustor to increase the exhaust temperature. The exhaust gases are used to preheat the inlet air, causing a reduction in their temperature. The other streams are heated to the operating temperature by exploiting the heat produced by the exothermal reactions in the cell (closing the thermal balance). Finally, the residual heat contained in the exhaust gases can be stored in a TES system to provide energy for water preheating and vaporisation in the SOEC during charge mode, substituting the external heater.

Figure 5.6 recalls the simplified functional scheme of the SOFC previously reported in Fig. 4.3. The exothermic reactions taking place inside the SOFC produce a large amount of thermal energy that is used: a) to preheat and vaporise methanol (H1F) and water (H2F), b) to sustain the endothermic reforming reactions (RF1F), c) to increase the temperature of the reformed gas up to that of the cell operation (850°C) (H3F), and d) to complete the air heating process to the cell operating temperature (H4F). Due to the exothermic reactions taking place in the post-combustor, the hot gases leaving the SOFC are characterised by a temperature slightly lower than 990 °C. The thermal energy carried by the hot gases is firstly used to close the heat balance of the SOFC and then stored in the TES.

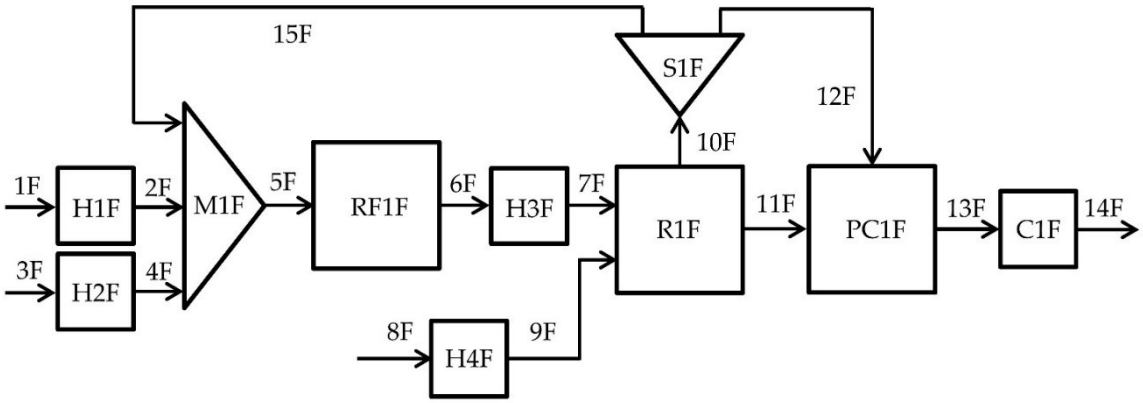

Fig. 5.6 – Simplified functional scheme of the solid oxide fuel cell section (C = Cooler; H = Heater; M = Mixer; PC = Post combustor; R = Reactor; RF = Reformer; S = Splitter)

Table 5.6 summarises the main parameters of the streams flowing through the SOFC depicted in Fig. 5.6. The mass flow rate, temperature, and molar fraction are reported in the table.

Table 5.6 – Composition (by vol.) of the main streams in the SOFC										
	1F/2F	3F/4F	5F	6F/7F	8F/9F	10F	11F	12F	13F/14F	15F
Mass flow [kg/s]	0.103	0.044	0.208	0.208	2.234	0.337	2.106	0.276	2.382	0.061
Temp [°C]	25/64	25/100	300	300/850	25/850	850	850	850	987/25	850
H*2*	0.0000	0.0000	0.0306	0.6401	0.0000	0.0960	0.0000	0.0960	0.0000	0.0960
N_2	0.0000	0.0000	0.0000	0.0000	0.7728	0.0000	0.8152	0.0000	0.7063	0.0000
O_2	0.0000	0.0000	0.0000	0.0000	0.2074	0.0000	0.1639	0.0000	0.1325	0.0000
Ar	0.0000	0.0000	0.0000	0.0000	0.0092	0.0000	0.0097	0.0000	0.0084	0.0000
H_2O	0.0000	1.0000	0.4987	0.0943	0.0103	0.6384	0.0109	0.6384	0.1145	0.6384
CO	0.0000	0.0000	0.0119	0.0375	0.0000	0.0375	0.0000	0.0375	0.0001	0.0375
CO_2	0.0000	0.0000	0.0727	0.2281	0.0003	0.2281	0.0003	0.2281	0.0382	0.2281
CH_3OH	1.0000	0.0000	0.3861	0.0000	0.0000	0.0000	0.0000	0.0000	0.0000	0.0000

Figure 5.7 shows a variation of the SOFC scheme of Fig. 4.3 and Fig. 5.6, where the thermal integrations and interactions between the different streams are reported. According to the SOFC heat balance, the cold air (8F) must be heated from 25 °C to approximately 760 °C ($8F^{I}$) before entering the cell, requiring 1766 kW. Such a thermal power can be obtained by cooling the hot post-combustor exhaust gases (13F) to 380 °C (HX1F). The heating process from 760 °C to the operating temperature of the cell requires approximately 235 kW, provided by the heat produced within the SOFC (H4F). The residual thermal energy of the exhaust gases ($13F^{I}$) can be released (HX2F) and stored in the TES system. A total thermal power of at least 425 kW must be stored by the TES system during SOFC operation to complete the water vaporisation process during SOEC operation. The specific analysis of the thermal storage process is described in the following Par. 5.2.4.

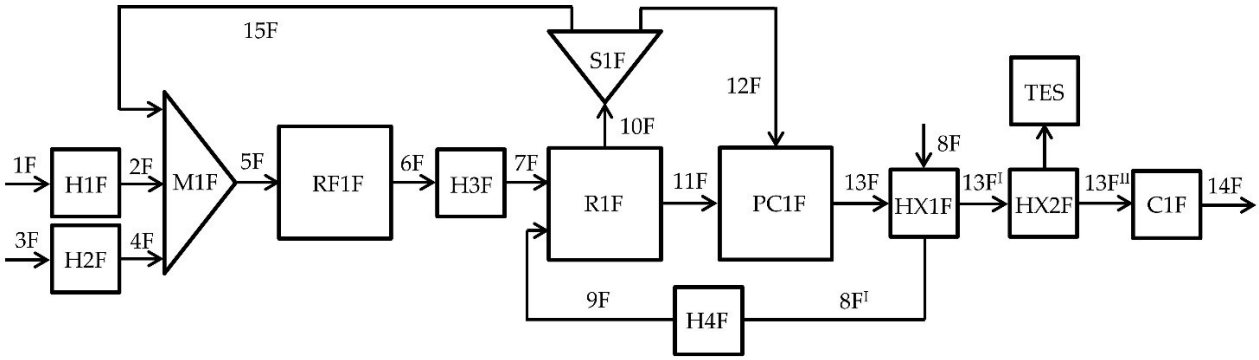

Fig. 5.7 – Simplified functional scheme of the SOFC section with thermal integrations (C = Cooler; H = Heater; HX = Heat exchanger; M = Mixer; PC = Post combustor; R = Reactor; RF = Reformer; S = Splitter)

A summary of the heating and cooling processes within the SOFC is reported in the left and right column of Table 5.7, respectively. The post-combustor exhaust 3rd cooling (C1F) refers to heat at low temperature that cannot be conveniently recovered and used.

Table 5.7 – Main heat transfers in the SOFC

Heating process	Heat [kW]	Cooling process	Heat [kW]
Inlet fuel by thermal balance (H1F)	126.4	Post-combustor exhaust 1st cooling (HX1F)	-1765.6
Inlet water by thermal balance (H2F)	114.6	Post-combustor exhaust 2nd cooling (HX2F)	-426.6
Reformer by thermal balance (RF1F)	212.6	Post-combustor exhaust 3rd cooling (C1F)	-819.0
Reformed gases by thermal balance (H3F)	291.0	Thermal balance (H1F, H2F, RF1F, H3F, H4F)	-979.0
Inlet air by heat recovery (HX1F)	1765.6		
Inlet air by thermal balance (H4F)	234.4		
Thermal energy storage (HX2F)	426.6		

5.2.4 Thermal energy storage results

To store the energy contained in the SOFC hot gases, a latent heat thermal energy storage system (LHTES) was analysed. Given the operating conditions and the temperature range of the considered application, sodium hydroxide (NaOH) was identified as a suitable PCM. Table 5.8 reports the main characteristics of the chosen PCM [178].

Table 5.8 – Main characteristics of the PCM

Parameter	Value
Phase change temperature [°C]	318
Latent heat of fusion [kJ/kg]	165
Mean density [kg/m^3]	2100
Specific heat [J/(kgK)]	2080

Figure 5.8 shows the magnification already reported in Fig. 5.1. SOFC gases flow from the top (0 m) to the bottom (3 m) of the TES during the charging process, whilst air flows from the bottom (3 m) to the top (0 m) during the discharging process. The reference system along the bed height (z) follows the discretisation of the MATLAB-Simulink model.

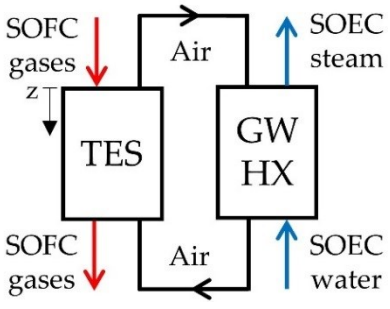

Fig. 5.8 – Detail of the TES section

The temperature profile (thermocline) in the TES system during the charging and discharging processes are shown in Figures 5.9 and 5.10 for a 6-hour long period. The two figures represent regime conditions obtained after a transition period to warm-up the system. The TES system is sized for releasing the thermal power required by the SOEC during the system charge mode (approximately 425 kW), allowing the bed to store 2.5 MWh for the 6-hour operation. Assuming a bed porosity of 0.4 and an aspect ratio of 1, both a bed diameter and height equal to 3 m were calculated with the special MATLAB-Simulink script. The script allowed the optimisation of the TES to match the requirements of power and energy stored for the 6-hour

operation in charge and discharge mode. The TES system is considered adiabatic, so the heat losses are neglected.

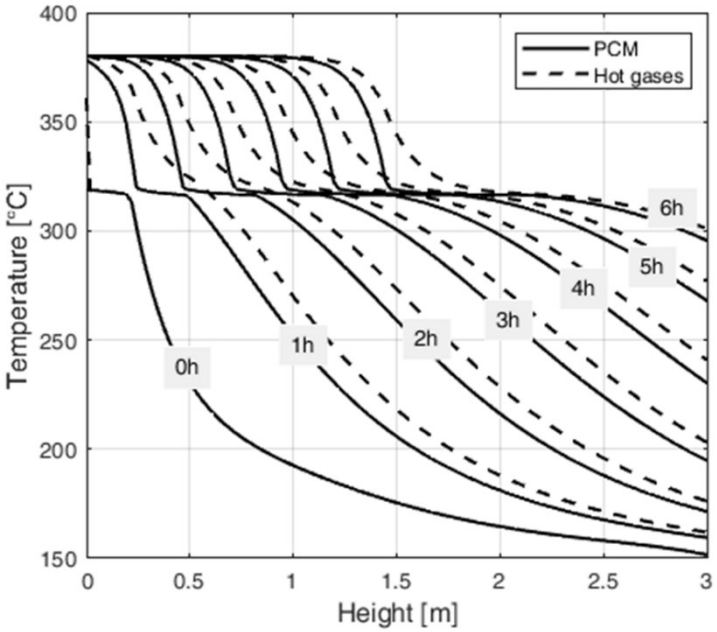

Fig. 5.9 – Thermocline profile during the charge phase

In Figures 5.9 and 5.10 solid lines represent the temperature evolution of the PCM, while dotted lines represent the evolution of the hot gases (Fig. 5.9) or cold air (Fig. 5.10). During the charge phase (Fig. 5.9) hot gases coming from the SOFC at 380 °C flow from the top (0 m) to the bottom (3 m) of the bed (cf. Fig. 5.8). Since Figures 5.9 and 5.10 represent regime conditions, the temperature profile inside the bed at the beginning of the charge phase (0h, Fig. 5.9) overlaps the temperature profile at the end of the previous discharge phase (6h, Fig. 5.10) since no thermal losses were considered. Initially, the heat exchange takes place in form of sensible heat between the hot gases and the PCM in solid phase. Then, at approximately 320 °C the transition process occurs, and the heat is stored as latent. Finally, the heat transfer takes place again in form of sensible heat between the hot gases and the PCM in liquid phase. At the end of the charge phase (6h, Fig. 5.9), roughly half of the PCM is in the liquid phase, while the remaining part is in transition or solid phase. It is clear how the energy contained in the bed increases with time, since the temperature at a fixed height of the bed grows from the 0h to the 6h curve.

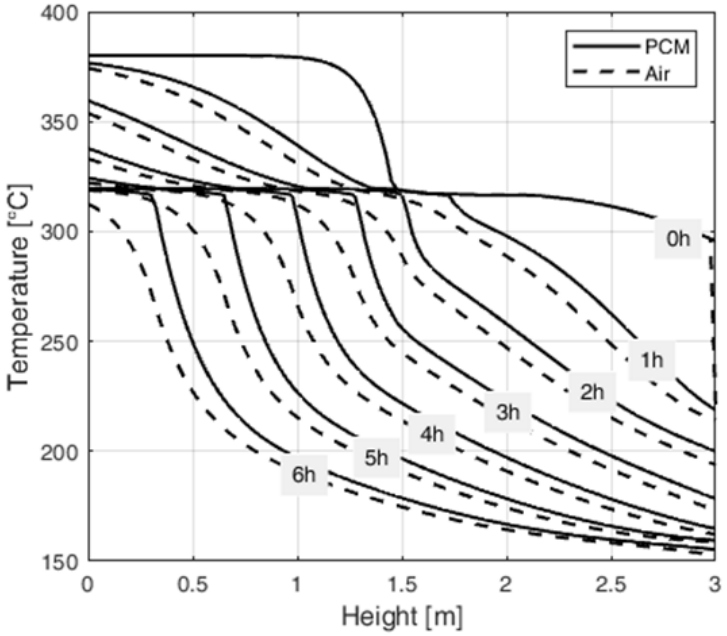

Fig. 5.10 – Thermocline profile during the discharge phase

Figure 5.10 shows the discharging process during which air (2.4 kg/s) circulates in a closed-circuit recovering the heat stored in the PCM and releasing it to the water feeding the SOEC. During the discharge phase, the flow direction is reversed, so the air flows from the bottom (3 m) to the top (0 m) of the tank. The beginning of the discharge phase (0h, Fig. 5.10) coincides with the ending of the charge phase (6h, Fig. 5.9). As Fig. 5.10 shows, at the end of the discharge phase almost 80% of the thermal energy stored in the PCM bed is released mainly in form of latent heat. Indeed, at the end of the discharging process only the upper layers of the bed (from 0 to 0.25 m) are in liquid or transition phase.

With the chosen TES configuration and size, the thermal power released by the TES system allows the preheating and vaporisation of the desired rate of water feeding the SOEC (0.17 kg/s). Globally, a total thermal energy of approximately 2.5 MWh is exchanged within the TES system and the GWHX during each of the 6-hour operation cycle.

5.2.5 Performance indexes (RSOC-based system)

The definition of a global performance index of an overall energy system such as the one proposed in this thesis can be ambiguous, due to its complexity and the management of different forms of energy. In fact, the performance of the SOEC, MSS and SOFC can be evaluated through suitable efficiency indexes, but several performance indexes defined differently can be found in literature. The indexes reported here were firstly defined in Lonis et al. [179].

The efficiency of the SOEC η_{SOEC} can be expressed, similarly to [180], by Eq. (5.1):

$$\eta_{SOEC} = \frac{\dot{m}_{H_2} \cdot H_{i,H_2}}{P_{SOEC} + P_{BOP,SOEC}} \tag{5.1}$$

where $\dot{m}_{H_2}$ and H_{i,H_2} are the mass flow and the lower heating value of the hydrogen, respectively, P_{SOEC} and $P_{BOP,SOEC}$ are the electric power of the SOEC and of the SOEC auxiliaries, respectively.

The efficiency of the SOFC η_{SOFC} can be defined, similarly to that of the SOEC, by Eq. (5.2):

$$\eta_{SOFC} = \frac{P_{SOFC} - P_{BOP,SOFC}}{\dot{m}_{MeOH} \cdot H_{i,MeOH}} \tag{5.2}$$

where P_{SOFC} and $P_{BOP,SOFC}$ are the electric power of the SOFC and of the SOFC auxiliaries, respectively, and $\dot{m}_{MeOH}$ and $H_{i,MeOH}$ are the mass flow and the lower heating value of methanol, respectively.
For the RSOC, an overall round trip efficiency can be defined ignoring (gross efficiency, $\eta_{RSOC,G}$) or including (net efficiency, η_{RSOC}) the parasitic power consumption caused by the balance of the plant, as shown by Eqs. (5.3) and (5.4), respectively [141,181]:

$$\eta_{RSOC,G} = \frac{P_{SOFC}}{P_{SOEC}} \tag{5.3}$$

$$\eta_{RSOC} = \frac{P_{SOFC} - P_{BOP,SOFC}}{P_{SOEC} + P_{BOP,SOEC}} \tag{5.4}$$

Referring to the net efficiency, η_{RSOC}, by combining Eqs. (5.1), (5.2) and (5.4), the following Eq. (5.5) is obtained:

$$\eta_{RSOC} = \eta_{SOEC} \cdot \eta_{SOFC} \frac{\dot{m}_{MeOH} \cdot H_{i,MeOH}}{\dot{m}_{H_2} \cdot H_{i,H_2}} = \eta_{SOEC} \cdot \eta_{SOFC} \cdot \eta_{MSS,C} \tag{5.5}$$

where $\eta_{MSS,C}$ is the chemical energy conversion efficiency of the MSS, defined analogously to a gasifier "cold gas" efficiency.
The actual MSS overall efficiency can be defined by Eq. (5.6) similarly to [182]:

$$\eta_{MSS} = \frac{\dot{m}_{MeOH} \cdot H_{i,MeOH}}{\dot{m}_{H_2} \cdot H_{i,H_2} + \dot{E}_{MSS} + P_{BOP,MSS}} \tag{5.6}$$

The term $\dot{E}_{MSS}$ is the external power supplied to the MSS to preheat the reactants. In Eq. (5.6), $\dot{E}_{MSS}$ is assumed to be introduced in the form of chemical potential power like the methanol and hydrogen chemical power in the same Eq. (5.6), and in Eqs. (5.1) and (5.2), which is then converted into thermal power inside the MSS. For this reason, Eqs. (5.1), (5.2) and (5.6) are thermodynamically consistent. Finally, $P_{BOP,MSS}$ is the power requirement of the MSS auxiliaries, mainly due to the compression of the reactants.
A global efficiency can be defined for the overall system considering Eq. (5.7):

$$\eta_G = \frac{P_{SOFC} - P_{BOP,SOFC}}{P_{SOEC} + P_{BOP,SOEC} + \dot{E}_{MSS} + P_{BOP,MSS}} \tag{5.7}$$

By combining Eq. (5.7) with Eqs. (5.1), (5.2) and (5.5) and rearranging the various terms, the following Eq. (5.8) is obtained:

$$\eta_G = \eta_{SOEC} \cdot \eta_{SOFC} \cdot \eta_{MSS,C} \cdot \varphi_{SOEC} = \eta_{RSOC} \cdot \varphi_{SOEC} \tag{5.8}$$

being:

$$\varphi_{SOEC} = \frac{P_{SOEC} + P_{BOP,SOEC}}{P_{SOEC} + P_{BOP,SOEC} + \dot{E}_{MSS} + P_{BOP,MSS}} \tag{5.9}$$

The term φ_{SOEC}, expressed by Eq. (5.9), represents the fraction of power entering the SOEC with respect to the total power entering the overall system. It is ideally equal to 1 in case the MSS does not require an external power supply ($\dot{E}_{MSS} = 0$, $P_{BOP,MSS} = 0$).
Moreover, by combining Eq. (5.8) with Eq. (5.6), the following alternative expression of the global efficiency (Eq. (5.10)) is obtained:

$$\eta_G = \eta_{SOEC,R} \cdot \eta_{SOFC} \cdot \eta_{MSS} \tag{5.10}$$

where $\eta_{SOEC,R}$ is a rectified efficiency of the SOEC given by Eq. (5.11):

$$\eta_{SOEC,R} = \frac{\dot{m}_{H_2} \cdot H_{i,H_2} + (\dot{E}_{MSS} + P_{BOP,MSS})}{P_{SOEC} + P_{BOP,SOEC} + (\dot{E}_{MSS} + P_{BOP,MSS})} \tag{5.11}$$

The term $\eta_{SOEC,R}$ coincides with η_{SOEC} when the MSS does not require an external power supply ($\dot{E}_{MSS} = 0$, $P_{BOP,MSS} = 0$). In this case, it is also $\eta_{MSS} = \eta_{MSS,C}$. From a physical point of view, the rectified efficiency $\eta_{SOEC,R}$ represents the efficiency that the SOEC would have if it was also powered with the power ($\dot{E}_{MSS} + P_{BOP,MSS}$) entering the MSS, returning this power in full to the MSS together with the hydrogen produced. This would mean to consider the SOEC and the MSS as a single overall block.
Also, by combining Eqs. (5.8) and (5.10), the following Eq. (5.12) is obtained:

$$\eta_{RSOC} = \frac{\eta_{SOEC,R}}{\varphi_{SOEC}} \cdot \eta_{SOFC} \cdot \eta_{MSS} \tag{5.12}$$

as well as Eq. (5.13):

$$\eta_{SOEC} \cdot \varphi_{SOEC} \cdot \eta_{MSS,C} = \eta_{SOEC,R} \cdot \eta_{MSS} \tag{5.13}$$

Equation (5.13) synthesises the correlation between the relevant efficiency parameters of the comprehensive SOEC-MSS system. Finally, these parameters are used to define the efficiency of the power to liquid process η_{PtL} as Eq. (5.14):

$$\eta_{PtL} = \frac{\dot{m}_{MeOH} \cdot H_{i,MeOH}}{P_{SOEC} + P_{BOP,SOEC} + \dot{E}_{MSS} + P_{BOP,MSS}} = \eta_{SOEC} \cdot \varphi_{SOEC} \cdot \eta_{MSS,C} \tag{5.14}$$

The above-mentioned performance indexes were applied to two different system configurations: a) with a simple thermal integration without TES and b) with the introduction of the TES system to improve the thermal integration between sections and operating modes.
To calculate the performance indexes, the values of the power and heat produced and required by each section were collected from the Aspen Plus models. Table 5.9 summarises the terms needed for the calculation of the efficiencies. The system was analysed with (case A) and without (case B) the presence of the TES system to recover heat.

Table 5.9 – Main results of the SOEC, methanol synthesis, and SOFC sections

Section	Process	Case	Power [kW]
SOEC	P_{SOEC}	A, B	2528
	$\dot{m}_{H_2} \cdot H_{i,H_2}$	A, B	2520
	$P_{BOP,SOEC}$	A	525
		B	98.3
Methanol synthesis	$\dot{m}_{MeOH} \cdot H_{i,MeOH}$	A, B	2033
	$\dot{m}_{H_2} \cdot H_{i,H_2}$	A, B	2520
	$P_{BOP,MSS}$	A, B	239
	$\dot{E}_{MSS}$	A, B	0
SOFC	P_{SOFC}	A, B	1000
	$\dot{m}_{\mathrm{MeOH}} \cdot H_{i,\mathrm{MeOH}}$	A, B	2033
	$P_{BOP,SOFC}$	A, B	0

The specific power consumption of the SOEC is 33.41 kWh/kg (2.98 kWh/Nm^3). If also the BOP power is considered, then the specific power increases to 40.34 kWh/kg (3.60 kWh/Nm^3) without the TES system

and to 34.71 kWh/kg (3.10 kWh/Nm^3) with the TES system. These values are consistent with those reported in the literature [183].
As previously specified, the introduction of the TES allows saving approximately 425 kW in the SOEC, substituting the external heat supply for water vaporisation with recovered heat. Since the reboiling heat (that would be considered within the term $\dot{E}_{MSS}$) is recovered from the hot exhaust of the reactor with a proper thermal integration, the value reported in Table 5.9 is equal to 0. In the same way, since the SOFC auxiliaries absorb a negligible power, $P_{BOP,SOFC}$ is set equal to 0.
Table 5.10 shows the performance indexes calculated for both case A and case B. While in both cases the integration within each section was performed by recirculating the outlet streams to preheat the inlet streams, water vaporisation heat was recovered via the TES system only in case B. Thus, case A is characterised by lower efficiencies due to higher energy requirements to be provided from external sources (for instance, electric heaters).

Table 5.10 – Performance indexes results of the RSOC-based system

Efficiency	A	B
η_{SOEC}	0.825	0.960
$\eta_{SOEC,R}$	0.838	0.963
φ_{SOEC}	0.927	0.917
$\eta_{MSS,C}$	0.807	0.807
η_{MSS}	0.737	0.737
η_{PtL}	0.618	0.710
η_{SOFC}	0.492	0.492
η_{RSOC}	0.328	0.381
η_G	0.304	0.349

The efficiency of the SOEC η_{SOEC} is considerably higher (≈ 0.83) than that of conventional low temperature electrolysers, since the process is carried out at high temperature reducing the electricity input. The thermal energy recovery using a TES system allows a further increase in the SOEC efficiency up to 0.96. Since the methanol synthesis process is characterised by an efficiency η_{MSS} slightly lower than 0.74 for both cases, the PtL efficiency η_{PtL} is equal to 0.62 and 0.71 for case A and case B, respectively. Both the SOEC and PtL efficiency values are consistent with literature data. The SOFC shows an efficiency η_{SOFC} slightly lower than 0.50, also consistent with literature values but slightly low mainly because of the methanol conversion process in the reformer. Globally, the efficiency of the RSOC is as low as 0.33-0.38. Finally, in the base case without the TES system, an efficiency of the overall system η_G equal to 0.30 is obtained. The integration with the TES allows for a better recovery of the heat released by the SOFC, boosting the global efficiency to almost 0.35.
Due to the presence of the SOFC that produces excess heat during the discharge mode, such a system can be operated as a standalone plant capable of behaving as an energy storage system and as a fuels and chemicals production facility.

5.3 System based on alkaline water electrolysis (without ORC)

Following the analysis of the system based on an innovative technology (i.e. reversible solid oxide cells), a study of a configuration based on a commercially mature technology, namely the alkaline water electrolysis, was carried out. Since it is premature to consider an effective deployment of a system based on RSOC, it was chosen to analyse a different solution that would be already available and usable in the immediate. Figure

5.11 recalls the simplified functional scheme of the overall system based on AEL and SOFC, already shown in Fig. 3.7. Using the parameters defined and described in Par. 4.3, the alkaline water electrolysis is performed at 65 °C, nominal temperature for the electrolyser described in Par. 4.3.1. The minimum operating pressure of the chosen electrolyser is 5 bar while the maximum is 25 bar. The SOFC is operated at 850 °C and produces electricity with the methanol synthesised in the synthesis section. As with the RSOC-based system, water and renewable electricity feed the electrolyser module.

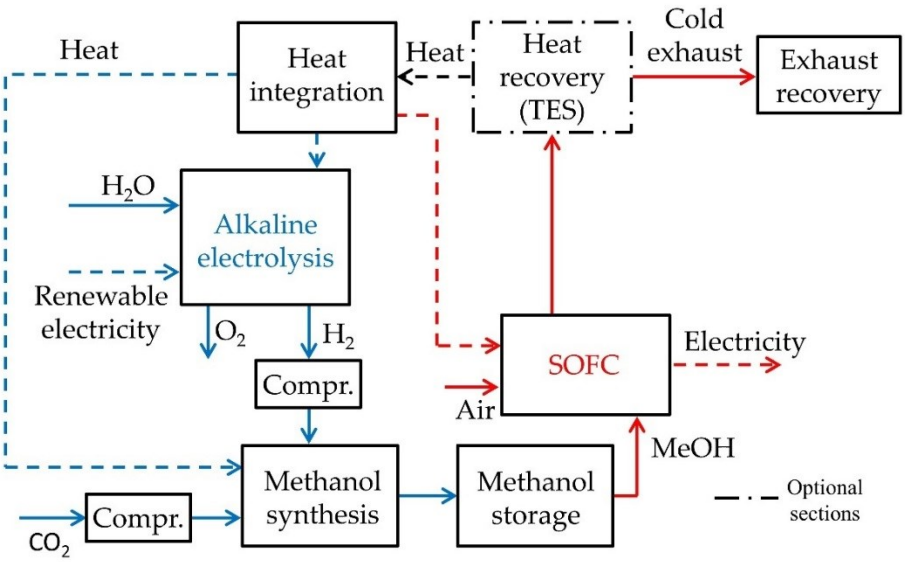

Fig. 5.11 – Simplified functional scheme of the overall system based on alkaline electrolysis without ORC

Since the AEL is operated at low temperature, differently from the RSOC-based system, the presence of a heat recovery to improve the performance of the system is not necessary. Indeed, the energy to preheat the water to the operating temperature of the cell comes from the electrolysis process. Since the operating voltage of one cell (1.70 V at 65 °C and 25 bar) is above the thermoneutral voltage (at which the heat generated by the Joule effect into the cell is equal to the heat demand of the electrolysis reaction, and so no waste heat is produced) at the same conditions (1.47 V), the heat produced in the cell is used to preheat the inlet water. Hence, the heat released during SOFC operation might be used or stored for different applications, such as the introduction of an ORC or to produce hot district water. Nevertheless, the heat recovery section was kept in the scheme of Fig. 5.11 to show the opportunity to recover the heat released by the SOFC exhaust gases. As what has been done in the RSOC, the size and characteristics of the AEL-based system were defined considering a SOFC power of 1 MW_{el}. Hence, the methanol synthesis section and the SOFC are practically identical to those analysed previously in Par. 5.2. Since the AEL must be operated between 5 and 25 bar, to consider the inlet pressure of the hydrogen a slight modification in the MSS is necessary. Indeed, hydrogen is sent to the MSS at a higher pressure than the case of the RSOC-based system. A further study of the hydrogen compression section is necessary to analyse what solution allows the lowest power consumption.

5.3.1 AEL

The description for the AEL is simple compared to the SOEC of the RSOC-based system. Given the simplicity of the scheme (Fig. 4.5) and the fact that water, hydrogen and oxygen are the only chemical species present during this process, it is not necessary to provide a table that summarises the composition and the conditions of each stream. Indeed, water is pressurised by a pump, is heated exploiting the heat produced by the AEL (heat released because of the operating voltage larger than the thermoneutral voltage) and finally it is electrolysed in hydrogen and oxygen. Since there is no utilisation factor (all the supplied water is

supposed to be electrolysed), and the water is ideally completely electrolysed in the system, a lower flow rate than the RSOC case is necessary, namely approximately 675 kg/h, to produce the 76 kg/h of hydrogen required by the MSS.

Figure 5.12 represents the characteristic curves of the power consumption (left) and efficiency (right) of the AEL as a function of the pressure, parametrised with the temperature. Figure 5.13 represents the consumed power (left) and efficiency (right) as a function of temperature, parametrised with the pressure. From the power and efficiency point of view, the model shows an increase in the former and a decrease in the latter when, given a fixed temperature, the pressure increases. Nevertheless, when the pressure is fixed, an increase in the temperature causes a decrease in the power and an increase in the efficiency, as it is reported in Fig. 3.3.

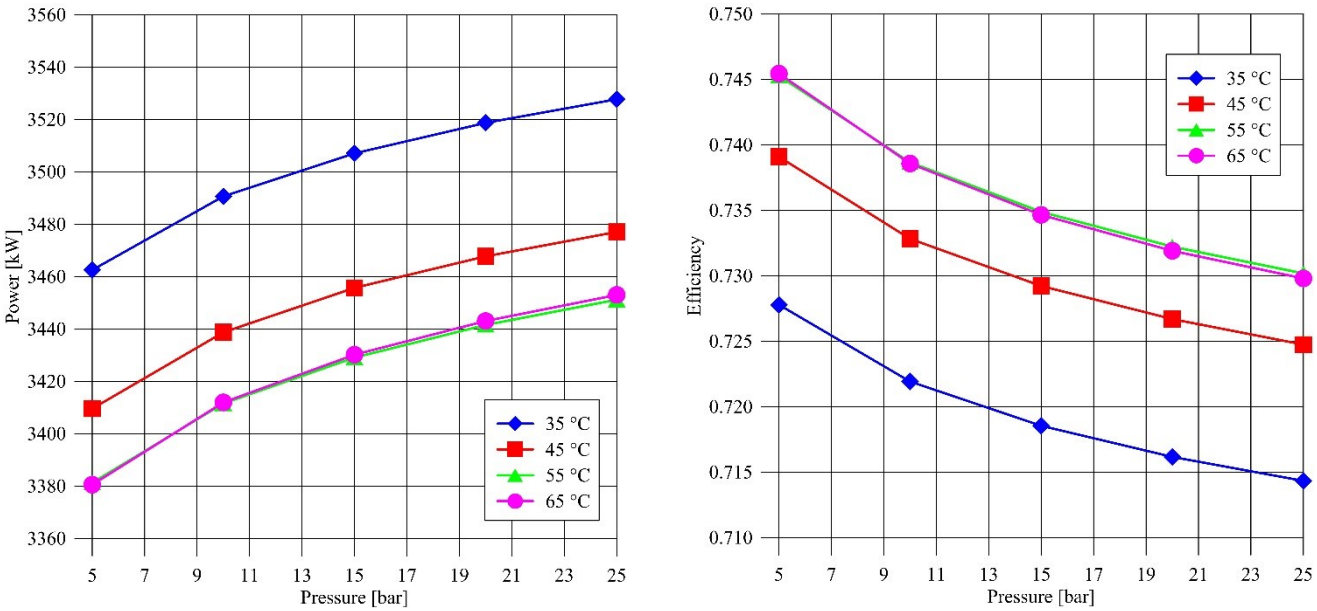

Fig. 5.12 – Power-pressure (left) and efficiency-pressure (right) characteristics

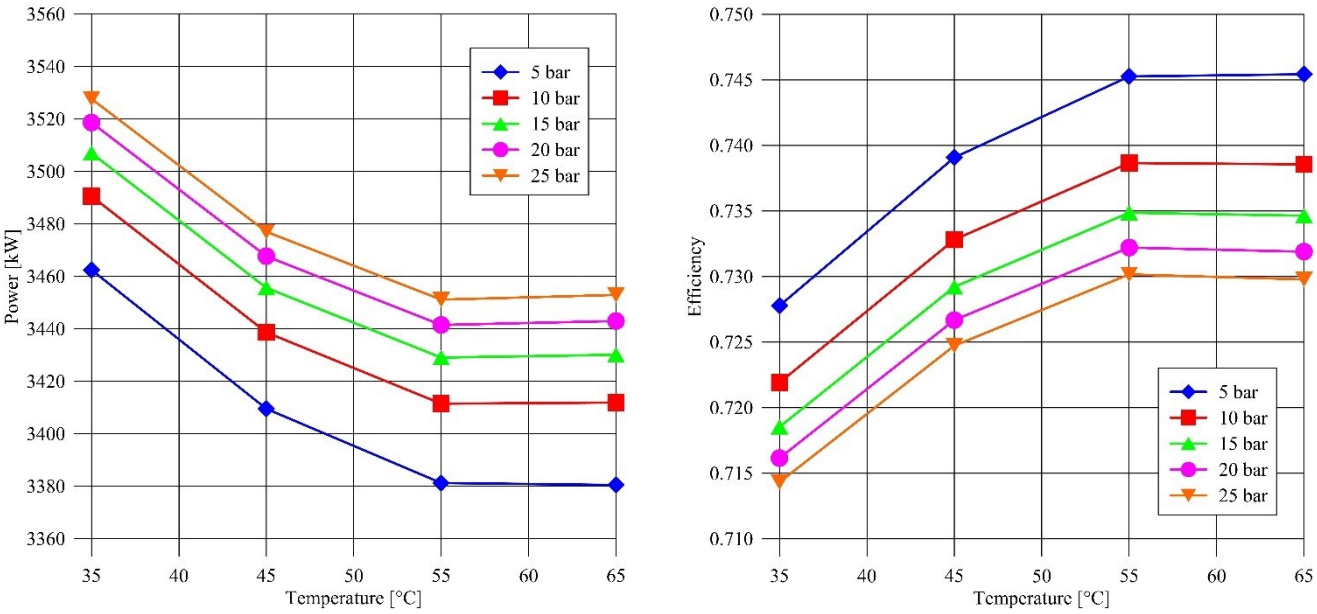

Fig. 5.13 – Power-temperature (left) and efficiency-temperature (right) characteristics

Even though a higher electrolysis pressure causes an increase in the consumed power and a decrease in the efficiency (Fig. 5.13), it is worth analysing the two cases of lowest and highest pressure allowable by the

AEL and studying the influence on the power absorbed by the compressors in the MSS. Indeed, the chosen pressure in the AEL section has an influence in the configuration of the compressors in the MSS. Table 5.11 summarises the findings regarding this analysis for a fixed temperature of 65 °C.

Table 5.11 – Comparison operating pressure AEL (65 °C)

	5 bar	25 bar	Power difference
Pump work [kW]	0.09	0.51	0.42
AEL power [kW]	3380.5	3453.0	72.5

The absolute difference between the values of power at 5 and 25 bar is 73 kW (also considering the pump work).
The description and operation of the AEL are the same with and without the ORC.

5.3.2 MSS (AEL)

The MSS general scheme remains the same as the one presented in Fig. 5.4. The main difference is due to the higher-pressure operation of the alkaline electrolyser module that produces high pressure hydrogen. Hence, the compression work required in the MSS is lower than in the case of ambient pressure operation. Three different configurations were considered: a) AEL operating pressure of 5 bar and two intercooled compressors in the MSS, b) AEL operating pressure of 5 bar and three intercooled compressors in the MSS, and c) AEL operating pressure of 25 bar and one compressor in the MSS. As the previous case based on the RSOC, the intercooling temperature is set to 38 °C. The compression ratios are 3.6 and 2.35 in the case of two and three compressors, respectively, and 2.6 in the case of one compressor (i.e. initial hydrogen pressure of 25 bar). Table 5.12 summarises the results obtained for the different configurations.

Table 5.12 – Methanol synthesis: hydrogen compression power

AEL pressure	1st compr. [kW]	2nd compr. [kW]	3rd compr. [kW]	Total [kW]
5 bar (2 compr.)	53.6	63.6	/	117.2
5 bar (3 compr.)	33.5	38.5	38.9	110.9
25 bar	37.9	/	/	37.9 (110.4*)
*Total power considering the higher consumption of the AEL at 25 bar				

Since the power consumed by the AEL at 25 bar is 72.5 kW larger than that at 5 bar (Table 5.11), this value must be summed to the compressor power in the MSS at 25 bar (Table 5.12), obtaining a total of 110.4 kW. Hence, the total power to perform the electrolysis in the AEL and the hydrogen compression in the MSS in the three cases is approximately the same. Therefore, to reduce the complexity of the layout, the 25-bar operating pressure was chosen, allowing the use of only one compressor in the MSS instead of two or three as in the case with an AEL operating pressure of 5 bar.
The MSS is the same between the two alternatives with and without ORC.

5.3.3 SOFC (AEL)

The SOFC section is almost identical to that of the RSOC layout, so no further information is necessary. The only difference is that the heat contained in the SOFC exhaust is not stored to vaporise the water in the electrolyser section, but it is used to run the ORC.
When the ORC is introduced in the system, the heat of the hot exhaust gases is used to produce electricity by heating up the ORC working fluid.

5.3.4 Performance indexes (AEL-based system without ORC)

The performance of the system was studied considering a series of performance indexes following what had been done with those of the RSOC (Par. 5.2.5). The equations used to describe the performance of the AEL are slightly different because in this case, it is not possible to define a proper reversible efficiency since the AEL and the SOFC are two different systems. Nevertheless, many terms had been already explained and are not recalled in the following.

The efficiency of the AEL η_{AEL} is defined by Eq. (5.15):

$$\eta_{AEL} = \frac{\dot{m}_{H_2} \cdot H_{i,H_2}}{P_{AEL} + P_{BOP,AEL}} \tag{5.15}$$

where P_{AEL} and $P_{BOP,AEL}$ are the electric power of the AEL and of the AEL auxiliaries, respectively.

The efficiency of the SOFC η_{SOFC} can be defined similarly to that of the AEL by Eq. (5.16):

$$\eta_{SOFC} = \frac{P_{SOFC} - P_{BOP,SOFC}}{\dot{m}_{MeOH} \cdot H_{i,MeOH}} \tag{5.16}$$

The MSS overall efficiency can be defined by Eq. (5.17):

$$\eta_{MSS} = \frac{\dot{m}_{MeOH} \cdot H_{i,MeOH}}{\dot{m}_{H_2} \cdot H_{i,H_2} + \dot{E}_{MSS} + P_{BOP,MSS}} \tag{5.17}$$

The term $\dot{E}_{MSS}$ is the external power supplied to the MSS to preheat the reactants and is considered as it was in the case of the RSOC-based system. The same chemical energy conversion efficiency of the MSS defined previously, is reported in Eq. (5.18):

$$\eta_{MSS,C} = \frac{\dot{m}_{MeOH} \cdot H_{i,MeOH}}{\dot{m}_{H_2} \cdot H_{i,H_2}} \tag{5.18}$$

A global efficiency can be defined for the overall system using Eq. (5.19):

$$\eta_G = \frac{P_{SOFC} - P_{BOP,SOFC}}{P_{AEL} + P_{BOP,AEL} + \dot{E}_{MSS} + P_{BOP,MSS}} \tag{5.19}$$

By combining Eq. (5.19) with Eqs. (5.15), (5.16) and (5.18) and rearranging the various terms, the following Eq. (5.20) is obtained:

$$\eta_G = \eta_{AEL} \cdot \eta_{SOFC} \cdot \eta_{MSS,C} \cdot \varphi_{AEL} \tag{5.20}$$

being:

$$\varphi_{AEL} = \frac{P_{AEL} + P_{BOP,AEL}}{P_{AEL} + P_{BOP,AEL} + \dot{E}_{MSS} + P_{BOP,MSS}} \tag{5.21}$$

The term φ_{AEL}, given by Eq. (5.21), recalls what was explained for Eq. (5.9). It is the fraction of power entering the AEL with respect to the total power entering the overall system.

By combining Eq. (5.20) with Eq. (5.17), the following alternative expression (Eq. (5.22)) of the global efficiency is obtained:

$$\eta_G = \eta_{AEL,R} \cdot \eta_{SOFC} \cdot \eta_{MSS} \tag{5.22}$$

where $\eta_{AEL,R}$ is a rectified efficiency of the AEL given by Eq. (5.23):

$$\eta_{AEL,R} = \frac{\dot{m}_{H_2} \cdot H_{i,H_2} + (\dot{E}_{MSS} + P_{BOP,MSS})}{P_{AEL} + P_{BOP,AEL} + (\dot{E}_{MSS} + P_{BOP,MSS})} \tag{5.23}$$

The term $\eta_{AEL,R}$ coincides with η_{AEL} when the MSS does not require an external power supply. The rectified efficiency $\eta_{AEL,R}$ corresponds to the one obtained for the SOEC in Eq. (5.11). It is the efficiency that the alkaline electrolysis would have if it was also powered with the power entering the MSS, returning this power in full to the MSS together with the hydrogen produced.
Also, by combining Eqs. (5.20) and (5.22), the following Eq. (5.24) is obtained:

$$\eta_{AEL} \cdot \varphi_{AEL} \cdot \eta_{MSS,C} = \eta_{AEL,R} \cdot \eta_{MSS} \tag{5.24}$$

In this way, the correlation between the relevant efficiency parameters of the comprehensive AEL-MSS system is highlighted. Finally, a power-to-liquids efficiency η_{PtL} is defined as Eq. (5.25):

$$\eta_{PtL} = \frac{\dot{m}_{MeOH} \cdot H_{i,MeOH}}{P_{AEL} + P_{BOP,AEL} + \dot{E}_{MSS} + P_{BOP,MSS}} \tag{5.25}$$

The values of power required to calculate the performance indexes of the AEL-based system are reported in Table 5.13. These results are obtained for an AEL operating temperature and pressure of 65 °C and 25 bar, respectively, without the presence of the ORC.

Table 5.13 – Main results of the AEL, methanol synthesis, and SOFC sections without ORC

Section	Process	Power [kW]
AEL	P_{AEL}	3453
	$\dot{m}_{H_2} \cdot H_{i,H_2}$	2520
	$P_{BOP,AEL}$	0.5
Methanol synthesis	$\dot{m}_{MeOH} \cdot H_{i,MeOH}$	2033
	$\dot{m}_{H_2} \cdot H_{i,H_2}$	2520
	$P_{BOP,MSS}$	93.5
	$\dot{E}_{MSS}$	0
SOFC	P_{SOFC}	1000
	$\dot{m}_{MeOH} \cdot H_{i,MeOH}$	2033
	$P_{BOP,SOFC}$	0

The specific power consumption of the AEL is 45.64 kWh/kg (4.07 kWh/Nm^3), consistent with the values reported in the literature for comparable alkaline electrolysers [166].
Table 5.14 summarises the results obtained for each of the performance indexes defined previously.

Table 5.14 – Performance indexes results of the AEL-based system without ORC

Efficiency		Efficiency		Efficiency	
η_{AEL}	0.730	$\eta_{AEL,R}$	0.737	φ_{AEL}	0.974
$\eta_{MSS,C}$	0.807	η_{MSS}	0.778	η_{SOFC}	0.492
η_{PtL}	0.573	η_G	0.282		

The efficiency of the alkaline electrolyser is lower than that of the SOEC by 9.5-23 percentage points, depending on the RSOC configuration (i.e. without and with the TES system). The efficiency of the methanol synthesis section (0.778) is higher than that of the RSOC-based system (0.737) because of the lower power consumed by the hydrogen compressors. Indeed, since the alkaline electrolyser is operated at high pressure, the hydrogen enters the MSS at a higher pressure and the compression work is lower. Since

the efficiency of the AEL (0.730) is significantly lower than that of the SOEC (0.960), and the efficiency of the MSS is only slightly larger (≈ 6 percentage points), the PtL efficiency (0.573) is lower than that of the RSOC-based case (0.710). Finally, the global efficiency, obtained as the chain of the performance indexes of each subsection, is 28.2%.

5.4 System based on alkaline water electrolysis (with ORC)

Figure 5.14 recalls Fig. 3.8 and represents the simplified functional scheme of the system based on alkaline water electrolysis with the introduction of the ORC engine. The ORC is in series with the SOFC, it is fed with hot exhaust gases of the latter and it allows an enhanced production of electricity by exploiting the thermal energy that otherwise would be wasted. With this solution, it is possible to increase the overall system efficiency.

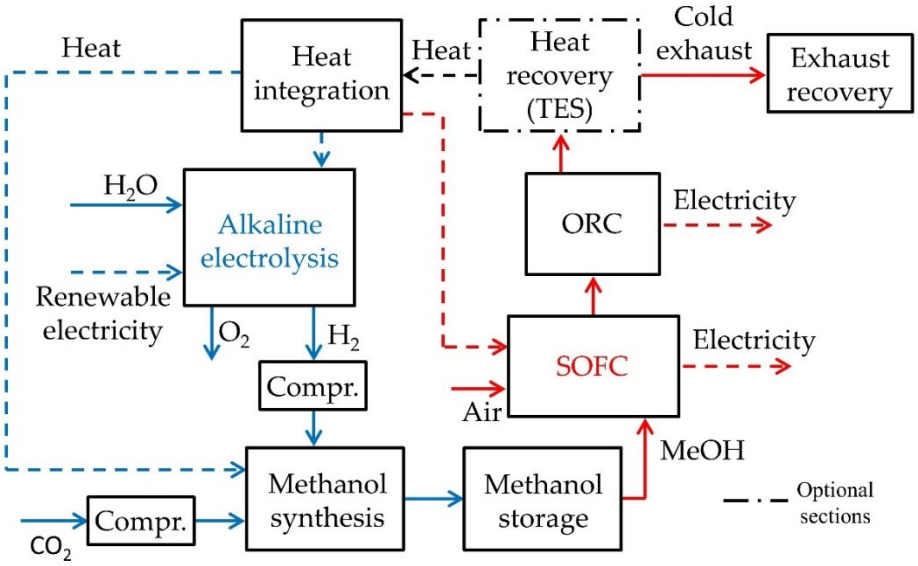

Fig. 5.14 – Simplified functional scheme of the overall system based on alkaline electrolysis with ORC

An ORC engine is a relatively simple and low-cost power system that exploits low grade thermal heat (usually below 350 °C). Typically, it is composed of an evaporator, a turbine, a condenser, a pump, and a regenerator [133]. In this study, since the hot circuit is at atmospheric pressure, a separate thermal oil circuit is not necessary. Hence, the ORC working fluid is directly heated up by the SOFC hot gases. Figure 5.15 represents the simplified functional scheme of the ORC as it was developed in Aspen Plus and as it was already shown in Fig. 4.9. The working fluid at ambient conditions (1O) is pumped to the maximum pressure of the cycle (PO) and is preheated in the regenerator (HX2O) prior to be heated to the maximum temperature of the cycle in the evaporator (HX1O). Subsequently, the vaporised working fluid (4O) enters the turbine (TO) where it expands before entering the regenerator. Finally, the working fluid is cooled to the initial conditions using a cooling media, namely water or air (10O and 11O). The working fluid is then pumped to the maximum pressure and the cycle begins again.

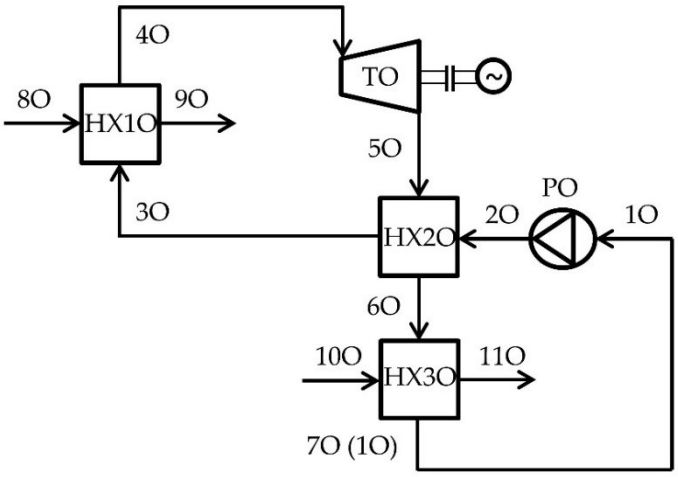

Fig. 5.15 – Simplified functional scheme of the ORC (HX = Heat exchanger, P = Pump, T = Turbine)

Regarding the ORC, given the temperature of the hot source (≈ 380 °C), three potential working fluids were analysed, namely benzene, toluene, and butylbenzene [184,185]. These three fluids are characterised by different properties reported in Table 5.15. While the critical temperature and pressure are reported in the NIST Chemistry WebBook Database [186], the operating temperature and pressure were defined as the maximum values obtainable by the exploitation of the heat source used in this system. These values represented also the maximum limits to avoid working with a supercritical liquid and guarantee the evaporation of the working fluid in the circuit.

Table 5.15 – ORC working fluids properties

Working fluid	T_{crit}	P_{crit}	T_{op}	P_{op}
Benzene	289 °C	48.9 bar	289 °C	48.5 bar
Toluene	320 °C	41.0 bar	315 °C	40.5 bar
Butylbenzene	387 °C	28.9 bar	370 °C	28.5bar

A comparison between these working fluids was carried out. Benzene was found to be the most convenient (consistently with the findings of Viktor et al. [185]) providing the highest efficiency, due to both its high critical pressure (48.9 bar) and low critical temperature (289 °C) [186].
In the proposed configuration, the ORC system was designed to reach a hot outlet – cold inlet temperature difference of 30 °C in the evaporator, that led to an outlet temperature of the hot source (9O) of 115 °C. The ORC turbine produces 210 kW harvesting approximately 700 kW from the available hot source. An operating temperature of 289 °C, a pressure of 48.5 bar, and a condenser pressure slightly higher than 0.2 bar were assumed. The regenerator (HX2O) allows an internal recovery of waste heat equal to 110 kW, increasing the working fluid temperature to 84 °C before the evaporator (3O).

5.4.1 Performance indexes (AEL-based system with ORC)

Compared to the equations used in Par. 5.3.4 to define the performance of the AEL-based system, the introduction of the ORC brings about a variation in the efficiency of the SOFC section and of the global efficiency. The modified equations are (5.26) and (5.27):

$$\eta_{SOFC+ORC} = \frac{P_{SOFC} - P_{BOP,SOFC} + P_{ORC} - P_{BOP,ORC}}{\dot{m}_{MeOH} \cdot H_{i,MeOH}} \quad (5.26)$$

$$\eta_{G,ORC} = \frac{P_{SOFC} - P_{BOP,SOFC} + P_{ORC} - P_{BOP,ORC}}{P_{AEL} + P_{BOP,AEL} + \dot{E}_{MSS} + P_{BOP,MSS}} \quad (5.27)$$

The terms P_{ORC} and $P_{BOP,ORC}$ are the electric power produced by the turbine of the ORC and the balance of plant of the system, respectively, mainly consisting of the power absorbed by the pump to bring the working fluid to the maximum pressure of the process. The other equations do not change compared to those defined and described in the case of the AEL without ORC in Par. 5.3.4.
Table 5.16 reports the values of the terms used to calculate the performance indexes described previously.

Table 5.16 – Main results of the AEL, methanol synthesis, and SOFC sections with ORC

Section	Process	Power [kW]
AEL	P_{AEL}	3453
	$\dot{m}_{H_2} \cdot H_{i,H_2}$	2520
	$P_{BOP,AEL}$	0.5
Methanol synthesis	$\dot{m}_{MeOH} \cdot H_{i,MeOH}$	2033
	$\dot{m}_{H_2} \cdot H_{i,H_2}$	2520
	$P_{BOP,MSS}$	93.5
	$\dot{E}_{MSS}$	0
SOFC	P_{SOFC}	1000
	$\dot{m}_{MeOH} \cdot H_{i,MeOH}$	2033
	$P_{BOP,SOFC}$	0
ORC	P_{ORC}	210.4
	$P_{BOP,ORC}$	7.2

Table 5.17 summarises the results obtained for each of the performance indexes of the AEL-based system with the introduction of the ORC, using the data reported in Table 5.16.

Table 5.17 – Performance indexes results of the AEL-based system with ORC

Efficiency		Efficiency		Efficiency	
η_{AEL}	0.730	$\eta_{AEL,R}$	0.737	φ_{AEL}	0.974
$\eta_{MSS,C}$	0.807	η_{MSS}	0.778	η_{PtL}	0.573
$\eta_{SOFC+ORC}$	0.592	$\eta_{G,ORC}$	0.339		

The introduction of the ORC led to an increase in the global efficiency of more than 5 percentage points compared to the case without the recovery in the ORC. In particular, the efficiency increased from 28.2% to 33.9%.

5.5 Comparison of the results

Table 5.18 summarises the main results obtained from the analysis of the performance indexes of each studied layout and their subsystems.

Table 5.18 – Comparison of the performance indexes of the studied layouts

Efficiency	RSOC (w/o TES)	RSOC (w/ TES)	AEL (w/o ORC)	AEL (w/ ORC)
$\eta_{electrolysis}$	0.825	0.960	0.730	0.730
η_{MSS}	0.737	0.737	0.778	0.778
η_{PtL}	0.618	0.710	0.573	0.573
$\eta_{SOFC}/\eta_{SOFC+ORC}$	0.492	0.492	0.492	0.592
$\eta_G/\eta_{G,ORC}$	0.304	0.349	0.282	0.339

As it was expected, the system based on solid oxide cells showed the highest efficiency both without and with the TES system, because of the high operating temperature that allows for lower electricity consumption. The efficiency of the methanol synthesis section resulted larger in the AEL-based system because the electrolyser was operated at high pressure (25 bar), reducing the number of compressors in the MSS and the total power consumption, saving more than 70 kW. Nevertheless, at higher pressures the AEL showed a lower efficiency and in the end, the overall power consumption of the overall block composed of the AEL and the MSS remained the same (Table 5.12). Since the power-to-liquids efficiency is directly related to the efficiencies of the electrolyser and the methanol sections, the value is higher for the RSOC-based system, because of the electrolysis efficiency that is significantly larger (0.960) than that of the AEL (0.730). The efficiency of the SOFC is the same in the first three cases (0.492) and it is boosted by 10 percentage points with the introduction of the ORC in the AEL configuration (0.592), that allows the production of approximately 210 kW in the turbine by the exploitation of the residual heat of the hot gases. The SOFC efficiency might be further improved by considering an optimisation of the methanol reforming process, to reduce the energy losses related to methanol reforming. Finally, the global efficiency, that can be obtained by Eqs. (5.7) and (5.19) or as a chain of efficiencies by Eqs. (5.8) and (5.20), is higher in the system based on RSOC, reaching a value of 0.349. This result is related to the high efficiency of the electrolysis brought about by the high temperature operation. Nevertheless, if the RSOC system without TES, and the AEL system with the ORC are compared, then the latter has a higher efficiency than the former owing to the introduction of the ORC engine and the absence of the TES system. Indeed, the RSOC-based system achieves an efficiency of 0.304 while the AEL-based system with the ORC achieves an efficiency of 0.339. The two optimised configurations, namely the RSOC with the TES system and the AEL with the ORC engine, are characterised by similar efficiencies with a difference of only 1 percentage point in favour of the RSOC-based system. As shown in Table 5.18, the optimised RSOC-based system achieves a global efficiency of 0.349 while the AEL-based system attains 0.339.

Since the difference between the two optimised configurations is negligible, other aspects should be taken into account. The solid oxide cells (SOEC/SOFC) and the alkaline cells are not at the same technology readiness level. While the former is still not commercially mature with a TRL of 6-7, and is expected to reach a TRL of 9 by the 2030 [187], the latter is already largely diffused and commercially available. However, since also the power-to-methanol process employing captured CO_2 and renewable energy is at a TRL of 6-7 [63], a binary technological improvement of the solid oxide cells and renewable power-to-methanol technologies might be expected, leading to a harmonised progress of both the single technologies and the overall system.

The main drawback of such systems consists of their high cost, related to the electricity production from RES and the production costs of the electrolysers. For instance, SOEC methanol production processes are approximately 15 times more expensive than conventional production from fossil fuels [147]. In addition, even though RES is becoming economically convenient and cheaper than conventional electricity production (cf. Par 2.2.1), the costs related to the electrolysers, both considering the AEL or SOEC technology, remains remarkably large. Schimdt et al [77] provided a capital cost of 1000-1200 EUR/kW for the AEL and higher than 2000 EUR/kW for the SOEC technology. Nonetheless, in a future perspective these costs are expected

to drop sensibly [77,145–147]. Furthermore, owing to an increase in SOC installed capacity as well as R&D on cell materials and assembly, a large reduction in SOC costs is foreseen in the next decades leading to expected costs and lifetime comparable to those of alkaline and PEM cells by 2030 [77,147], leading this technology to be competitive in the future market. Pérez-Fortes et al. [188] analysed a methanol production facility that recycles CO_2 from a conventional power plant using conventional CCU technology. The system resulted economically unfeasible owing to the high costs of H_2 production and CO_2 capture with the available technology. Hence, the feasibility of the production of methanol from these raw materials is directly related to the development of the technologies used to gather them. Clearly, if a serious R&D effort is put into the technological progress on this field, the costs might be lowered enough to guarantee the economic feasibility of this methanol production approach.

Even though nowadays the costs of renewable methanol production are still too high to represent a competitive and feasible solution to the climate change, the author of this thesis believes that such a technology would play a fundamental role in the decarbonisation of society. Indeed, it is difficult to imagine a complete desertion of the conventional fuel technologies in a short period. Indeed, the use of liquid and gaseous fuels should still be expected for many years from now. For instance, renewable methanol might be used, as already happens in Iceland, to fuel vehicles with a net CO_2 emission equal to zero while using existing technologies (internal combustion engines or fuel cells). This solution, in the long term, could be more sustainable than substituting all vehicles with electric alternatives. Indeed, electric vehicles technology relies on the use of electrochemical batteries, manufactured exploiting rare materials that are collected at the cost of heavy pollution of soil and water.

Finally, the CCU application analysed in this thesis and in numerous other works, should be used side by side with CCS technologies, to both create a closed carbon cycle (avoiding the emission of new carbon in the atmosphere) and reduce the overall amount of CO_2 in the atmosphere. Indeed, CCU alone would not be enough to stop and reverse the climate change.

5.5.1 Comparison with other energy storage technologies

The energy storage efficiency evaluated for the systems analysed in this work can be compared to the efficiency of other energy storage technologies commonly adopted, or in development, worldwide. Already in Par. 2.1 some of the main energy storage technologies were illustrated. In this paragraph, a comparison between the energy storage efficiency of the most common technologies and the efficiency of the systems studied in this work is presented. Table 5.19 summarises the typical efficiency of the energy storage systems [189] as they were presented in Fig. 2.1.

Table 5.19 – Comparison of the efficiency of different energy storage technologies

Technology	Efficiency [%]		Technology	Efficiency [%]	
	Min	Max		Min	Max
Hydrogen	20	65	NiCd batteries	65	86
CAES	10	71	PHS	71	86
SMES	40	100	NaS batteries	70	86
Redox flow batteries	55	86	Flywheel	70	91
Lead-acid batteries	66	81	Lithium batteries	81	100
Zinc-bromine batteries	65	81	Double-layer capacitor	86	100

The systems analysed in this work showed an energy storage efficiency, considered as the power-to-liquids efficiency, higher than 55%. Specifically, the power-to-methanol system based on AEL showed a PtL efficiency of 57% while the system based on RSOC was characterised by an efficiency between 62 and 71% depending on the chosen thermal energy storage strategy. The system showed a good efficiency value, in agreement with commonly employed technology. Compared to the energy storage technologies reported in Table 5.19, power-to-liquids is a technology with many advantages that can determine its success in future time. The storage capacity is not limited by the size of the system since the produced fuel can be readily stored as a liquid at ambient conditions in simple plastic tanks. Hence, even a small facility can store and pile up a high amount of energy by simply providing a large enough number of tanks and containers. The amount of stored energy would not depend on the size of the conversion and production sections. In addition, since the energy is stored in a stable chemical compound kept in sealed containers, there are no energy losses related to electrical, mechanical, or thermal dissipation. This kind of losses is common in the other energy storage technologies and are responsible for self-discharge phenomena over time. While energy storage facilities such as CAES and PHS requires great civil works, namely large reservoirs (that are often manmade) or natural caverns that must be adapted for the purpose, power-to-liquids system are not particularly larger or more complex than other similar renewable energy storage systems. It is clear how, regarding PHS and CAES, the dimension of the civil works strongly influences the overall storable energy. Hydrogen production and storage are carried at extremely low temperature and high pressure, and a significant attention must be paid to safely perform such tasks. In addition, this process is extremely energy demanding reducing the overall efficiency of the storage process (Table 2.4). Nevertheless, similarly to other power-to-X technologies, the amount of stored energy depends only on the dimension of the containers and not on the dimension of the conversion system. Flywheels, SMES, and double-layer capacitors are usually capable of high powers while the main drawback is related to the limited amount of storable energy, directly related to the physical dimensions of the system. Finally, considering other forms of electrochemical storage, power-to-methanol does not require rare, expensive, and highly pollutant materials that are commonly adopted in the electrochemical batteries. The extraction and refining of these materials are related to soil and water pollution that has already arisen nearby the mines where the raw materials are extracted. Nonetheless, power-to-methanol systems as they were studied in this work are characterised by other problems, such as remarkably high costs for the electrolysis of water or for the fuel cell, as well as complex layout design with several heat exchangers and connections among and within each section. However, considering a future development of this kind of technology, the costs are foreseen to decrease significantly leading to a competitive energy storage system, easily scalable and deployable anywhere, almost without the need for rare materials or special construction conditions. In addition, power-to-liquids system are not affected by self-discharge problems and the energy and power density can be adapted and varied depending on the final user and chosen application.

Chapter 6

Conclusion and future research

Climate change is one of the most challenging and daunting problems of this time. To stop and reverse the process, efforts in every existing field must be carried out. In this context, power-to-X technologies powered by renewable energy and fed with captured CO_2 might be part of the solution. Indeed, in future RES will be more diffused than ever and storage systems with large capacities will be necessary to provide a continuous flow of energy even when the local production from RES is low or insufficient. Power-to-X, and especially power-to-liquids, exploiting RES and captured CO_2 represents an interesting approach to boost RES penetration, limit the injection of new CO_2 in atmosphere, and a way to achieve the complete independence from fossil fuels. Ideally, a widespread power-to-liquids and power-to-methanol society/economy would allow the creation of a closed carbon cycle where RES are boosted by a continue production of long-term stability chemicals, storable at ambient conditions, while the atmospheric CO_2 is used an indefinite number of times in almost all the possible applications where the fossil fuels are exploited nowadays. Nevertheless, such an approach should be coupled to proper CCS technologies to rebalance the CO_2 levels in the atmosphere.

This thesis concerns the conceptual design and performance analysis of a few integrated energy systems for the production and use of methanol from renewable hydrogen and captured CO_2. Methanol is treated as a renewable energy storage medium and a hydrogen carrier. In this thesis, two different main solutions, that can be considered in a short-term and long-term perspective, are analysed: a power-to-methanol system based on alkaline water electrolysis and a power-to-methanol system based on solid oxide cells. While the former is based on mature technology that can be readily deployed, the latter still needs further R&D to be competitive in the present market. Hence, the two systems might be considered as complementary in a long-term perspective, with an initial deployment of the mature technology that will be slowly substituted by the more innovative one on the long term. The system is composed of an electrolyser, simulated considering the two different technologies (namely RSOC and AEL), that produces hydrogen exploiting renewable energy, a methanol synthesis and purification section where recycled CO_2 and the produced hydrogen react to produce methanol, a fuel cell section and a few different solutions to recover and use the heat in excess. Methanol is fed to a fuel cell (a SOFC or an RSOC in SOFC mode) to produce electricity when necessary. To produce electricity, the methanol feeding the SOFC is reformed and turned into a hydrogen rich gas. The heat contained in the hot exhaust gases are recovered and stored in a TES system or used in an ORC. Depending on the considered electrolysis technology, by recovering heat and providing it during the electrolysis or by producing electricity directly in the turbine of the ORC, it is possible to boost the efficiency of the overall systems.

To comprehensively analyse the sections constituting the systems, special models were developed using the software Aspen Plus and MATLAB. The adopted electrochemical, kinetic, and mathematical models, along with the Aspen Plus flowsheets and process simulations, allowed a thoroughly analysis of the main subsections of each system, such as the electrolysis section, the methanol synthesis and purification section, the electricity production section (fuel cell and organic Rankine cycle), and the thermal energy storage system. The models were validated considering experimental data gathered from literature. A good agreement between the results of the models and the existing data was found. The performance of the

systems was evaluated using these models. The main design parameter was defined as the power of the fuel cell section, imposed equal to 1 MW_{el}, that was not varied from one system configuration to the others. From this design value, consistent with state of the art SOFC (but still too large compared to state of the art RSOC), all the main parameters (such as methanol, hydrogen, and CO_2 flow rate, as well as the water for the electrolysis and the power consumption) of the other sections were evaluated. For instance, a methanol consumption of 370 kg/h is required in the SOFC. To produce such a methanol quantity, 76 kg/h of hydrogen and 550 kg/h of CO_2 are needed. Water consumption in the electrolysis process is equal to 780 kg/h and 675 kg/h in the RSOC in charge mode and in the AEL, respectively, due to different water utilisation factors in the two cases.
A preliminary design of the TES system was carried out along with the dynamic analysis of the charging and discharging processes, resulting in a bed of encapsulated PCM of 3 m in diameter and height. A survey on potential PCMs led to the choice of NaOH capsules as the most suitable for the considered temperature range.

Both systems showed a good power-to-liquids efficiency as high as 70%, consistent or even slightly larger than the values reported in literature for comparable systems employed for electricity conversion to chemicals. The energy storage efficiencies obtained for the PtL systems studied in this work were compared to other energy storage technologies commonly used nowadays. The results obtained are consistent with the values of the most common energy storage technologies, lying between 57 and 71%. Nevertheless, the round-trip efficiency of the overall system (i.e. the power-to-power efficiency, from the conversion of the inlet renewable electricity to the conversion of methanol into electricity), is not particularly high (around 35%) because of the low conversion efficiency in the reforming process in SOFC mode.

Given the promising preliminary results in terms of the efficiency of the systems analysed in this work, future research should focus on the further optimisation of each section and on the dynamic analysis of the system to verify its effectiveness when a real RES load is applied. Scarce works regarding the dynamic characterisation of such complex systems are found in literature, so it might be worth exploring and analysing the overall plants from this point of view. An integration with other energy sources, such as biomass, might be considered as well in order to provide a more constant and steady power supply to the system. Indeed, electrolysers typically operate better with a constant electricity input. Nevertheless, solutions such as system partitioning, and partial load operation might be considered and studied to provide different operating solutions in terms of renewable load following.
Even though the economic aspect is not favourable yet due to high technology costs and low TRL, a preliminary economic analysis would be interesting. Economic analyses of complex systems are not so common. Indeed, typical economic analyses found in literature are more focused on the single subsections, whilst the complex overall systems are rarely considered in specific economic analyses.
Finally, an on-field study exploiting small scale reversible solid oxide cells and methanol synthesis reactors within a microgrid might be considered to study real-world operating conditions of such complex systems. The synergy with a microgrid would be fundamental to improve and optimise the efficiency of the system, harmonising all the subsystems to pursue an optimal renewable energy utilisation.

Bibliography

[1] European Climate Change Programme | Climate Action n.d. https://ec.europa.eu/clima/policies/eccp_en (accessed April 5, 2019).

[2] UNFCCC. United Nations Framework Convention on Climate Change 1992;20481.

[3] First European Climate Change Programme | Climate Action n.d. https://ec.europa.eu/clima/policies/eccp/first_en (accessed April 5, 2019).

[4] Second European Climate Change Programme | Climate Action n.d. https://ec.europa.eu/clima/policies/eccp/second_en (accessed April 5, 2019).

[5] US Department of Commerce, NOAA ESRL. ESRL Global Monitoring Division - Global Greenhouse Gas Reference Network n.d. https://www.esrl.noaa.gov/gmd/ccgg/trends/monthly.html (accessed September 9, 2019).

[6] Gao Y, Gao X, Zhang X. The 2 °C Global Temperature Target and the Evolution of the Long-Term Goal of Addressing Climate Change—From the United Nations Framework Convention on Climate Change to the Paris Agreement. Engineering 2017;3:272–8. doi:10.1016/J.ENG.2017.01.022.

[7] Paris Agreement | Climate Action n.d. https://ec.europa.eu/clima/policies/international/negotiations/paris_en (accessed April 5, 2019).

[8] European Commission. A Roadmap for moving to a competitive low carbon economy in 2050 - Communication from the Commission to the European Parliament, the Council, the European and Social Committee and the Committee of the Regions. 2011.

[9] Low Carbon Technologies n.d. https://ec.europa.eu/clima/policies/innovation-fund_en (accessed April 5, 2019).

[10] World Health Organization | Air pollution. WHO 2019. https://www.who.int/airpollution/en/ (accessed July 16, 2019).

[11] European Commission. A Clean Planet for all. A European strategic long-term vision for a prosperous, modern, competitive and climate neutral economy - Communication from the Commission to the European Parliament, the Council, the European and Social Committee and the Committe. 2018.

[12] 2050 Energy Strategy - European Commission n.d. https://ec.europa.eu/energy/en/topics/energy-strategy-and-energy-union/2050-energy-strategy (accessed April 5, 2019).

[13] European Commision. Energy Roadmap 2050 - Impact assessment and scenario analysis - Communication from the Commission to the European Parliament, the Council, the European and Social Committee and the Committee of the Regions. 2012.

[14] Hoegh-Guldberg O, Jacob D, Taylor M, Bindi M, Brown S, Camilloni I, et al. Impacts of 1.5°C of Global Warming on Natural and Human Systems. Glob. Warm. 1.5 ºC, 2018.

[15] Intergovernmental Panel on Climate Change. Climate Change 2014: Mitigation of Climate Change: Working Group III Contribution to the IPCC Fifth Assessment Report. 2014. doi:10.1017/CBO9781107415416.

[16] da Silva Veras T, Mozer TS, da Costa Rubim Messeder dos Santos D, da Silva César A. Hydrogen: Trends, production and characterization of the main process worldwide. Int J Hydrogen Energy 2017;42:2018–33. doi:10.1016/j.ijhydene.2016.08.219.

[17] MefCO2 (Methanol fuel from CO2) - Synthesis of methanol from captured carbon dioxide using surplus electricity. | SPIRE n.d. https://www.spire2030.eu/mefco2 (accessed February 13, 2019).

[18] George Olah Plant — CRI - Carbon Recycling International n.d. http://carbonrecycling.is/george-olah/ (accessed July 19, 2018).

[19] Wuebben P. Renewable methanol: A Tera-Watt-Hour Scale Renewable Power and Energy Strategy. Oppor Challenges Methanol as a Glob Energy Carr - Stanford Univ 2017. https://ngi.stanford.edu/sites/default/files/Wuebben_Standford_Aug_Paul_Wuebben.pdf.

[20] Ganesh I. Conversion of carbon dioxide into methanol - A potential liquid fuel: Fundamental challenges and opportunities (a review). Renew Sustain Energy Rev 2014;31:221–57. doi:10.1016/j.rser.2013.11.045.

[21] Huggins RA. Energy Storage - Fundamentals, Materials and Applications. Second. Springer US;

2015. doi:10.1007/978-3-319-21239-5.
[22] Luo X, Wang J, Dooner M, Clarke J. Overview of current development in electrical energy storage technologies and the application potential in power system operation. Appl Energy 2015;137:511–36. doi:10.1016/j.apenergy.2014.09.081.
[23] Hameer S, Niekerk JL Van. A review of large-scale electrical energy storage 2015:1179–95. doi:10.1002/er.
[24] Ibrahim H, Ilinca A. Techno-Economic Analysis of Different Energy Storage Technologies. In: Zobaa FA, editor. Energy Storage Technol. Appl. 1st ed., IntechOpen; 2013, p. 1–40. doi:10.5772/52220.
[25] Felderhoff M, Urbanczyk R, Peil S. Thermochemical heat storage for high temperature applications-A review. Green 2013;3:113–23. doi:10.1515/green-2013-0011.
[26] Abedin AH, Rosen MA. A Critical Review of Thermochemical Energy Storage Systems. Open Renew Energy J 2011;4:42–6. doi:10.2174/1876387101004010042.
[27] Cot-Gores J, Castell A, Cabeza LF. Thermochemical energy storage and conversion: A-state-of-the-art review of the experimental research under practical conditions. Renew Sustain Energy Rev 2012;16:5207–24. doi:10.1016/j.rser.2012.04.007.
[28] de Valladares M-R. Global Trends and Outlook for Hydrogen. 2017.
[29] Wernicke H-J, Plass L, Schmidt F. Methanol Generation. In: Bertau M, Offermanns H, Plass L, Schmidt F, Wernicke H-J, editors. Methanol Basic Chem. Energy Feed. Futur. Asinger's Vis. Today, Berlin, Heidelberg: Springer Berlin Heidelberg; 2014, p. 51–301. doi:10.1007/978-3-642-39709-7_4.
[30] Ethanol - Biofuels Association of Australia n.d. http://biofuelsassociation.com.au/biofuels/ethanol/ (accessed March 8, 2019).
[31] IRENA. Renewable Power Generation Costs in 2017. IRENA - International Renewable Energy Agency. 2018.
[32] Milani D, Khalilpour R, Zahedi G, Abbas A. A model-based analysis of CO2 utilization in methanol synthesis plant. J CO2 Util 2015;10:12–22. doi:10.1016/j.jcou.2015.02.003.
[33] Mignard D, Pritchard C. Processes for the Synthesis of Liquid Fuels from CO2 and Marine Energy. Chem Eng Res Des 2006;84:828–36. doi:10.1205/cherd.05204.
[34] O'Brien JE, McKellar MG, Stoots CM, Herring JS, Hawkes GL. Parametric study of large-scale production of syngas via high-temperature co-electrolysis. Int J Hydrogen Energy 2009;34:4216–26. doi:10.1016/j.ijhydene.2008.12.021.
[35] Graves C, Ebbesen SD, Mogensen M, Lackner KS. Sustainable hydrocarbon fuels by recycling CO2 and H2O with renewable or nuclear energy. Renew Sustain Energy Rev 2011;15:1–23. doi:10.1016/j.rser.2010.07.014.
[36] Albrecht FG, Konig DH, Dietrich RU. The potential of using power-to-liquid plants for power storage purposes. Int Conf Eur Energy Mark EEM 2016;2016-July. doi:10.1109/EEM.2016.7521203.
[37] Albrecht F, Estelmann S, Dietrich R. Technical Economic Evaluation of Renewable Jet Fuel from Power, Biomass and/or Carbon Dioxide. 4th Eur Refin Technol Conf 2017.
[38] Albrecht FG, König DH, Baucks N, Dietrich R. A standardized methodology for the techno-economic evaluation of alternative fuels – A case study. Fuel 2017;194:511–26. doi:10.1016/j.fuel.2016.12.003.
[39] Albrecht F, Estelmann S, Dietrich R. Synthetic jet fuel from renewable energy sources for sustainable aviation 2017.
[40] Fasihi M, Bogdanov D, Breyer C. Techno-Economic Assessment of Power-to-Liquids (PtL) Fuels Production and Global Trading Based on Hybrid PV-Wind Power Plants. Energy Procedia 2016;99:243–68. doi:10.1016/j.egypro.2016.10.115.
[41] Schmidt P, Weindorf W, Roth A, Batteiger V, Riegel F. Power-to-Liquids Potentials and Perspectives for the Future Supply of Renewable Aviation Fuel 2016:32.
[42] Schmidt P, Batteiger V, Roth A, Weindorf W. Power-to-Liquids as Renewable Fuel Option for Aviation : A Review 2018:127–40. doi:10.1002/cite.201700129.
[43] Keim W. Fossil Feedstocks--What Comes After? In: Bertau M, Offermanns H, Plass L, Schmidt F, Wernicke H-J, editors. Methanol Basic Chem. Energy Feed. Futur. Asinger's Vis. Today, Berlin, Heidelberg: Springer Berlin Heidelberg; 2014, p. 23–37. doi:10.1007/978-3-642-39709-7_2.
[44] American Methanol Institute, Malcolm Pirnie Inc. Evaluation of the fate and transport of methanol in the environment. 1999.
[45] Biedermann P, Grube T, Hrsg BH, editors. Methanol as an Energy Carrier. vol. 55.

Forschungszentrum Jülich GmbH; 2006.
[46] Offermanns H, Schulz K, Brandes E, Schendler T. Substance Properties of Methanol. In: Bertau M, Offermanns H, Plass L, Schmidt F, Wernicke H-J, editors. Methanol Basic Chem. Energy Feed. Futur. Asinger's Vis. Today, Berlin, Heidelberg: Springer Berlin Heidelberg; 2014, p. 303–25. doi:10.1007/978-3-642-39709-7_5.
[47] Institute for Occupational Safety and Health of the German Social Accident Insurance. Methanol - IFA GESTIS Substance database n.d.
[48] Bergins C, Fox EL, Tran KC, Wuebben P. Commercialization of Low Carbon Methanol. Fuels Lubr Futur 2016:22–5. doi:10.1007/s40111-015-0517-0.
[49] Fuels - Higher and Lower Calorific Values n.d. https://www.engineeringtoolbox.com/fuels-higher-calorific-values-d_169.html (accessed October 29, 2019).
[50] Offermanns H, Plass L, Bertau M. Introduction. In: Bertau M, Offermanns H, Plass L, Schmidt F, Wernicke H-J, editors. Methanol Basic Chem. Energy Feed. Futur. Asinger's Vis. Today, Berlin, Heidelberg: Springer Berlin Heidelberg; 2014, p. 1–22. doi:10.1007/978-3-642-39709-7_1.
[51] Bertau M, Offermanns H, Plass L, Schmidt F. Methanol: The Basic Chemical and Energy Feedstock of the Future. 2014. doi:10.1007/978-3-642-39709-7.
[52] Methanol Institute. Energy - Methanol Institute 2010. http://www.methanol.org/energy/ (accessed July 24, 2018).
[53] Faberi S, Paolucci L. Methanol : a future transport fuel based on hydrogen and carbon dioxide. 2014. doi:10.2861/57305.
[54] Olah GA, Goeppert A, Prakash GKS. Beyond Oil and Gas: The Methanol Economy. 2nd ed. Weinheim, Germany: Wiley-VCH Verlag GmbH & Co. KGaA; 2009. doi:10.1002/9783527627806.
[55] Olah GA, Goeppert A, Prakash GKS. Chemical recycling of carbon dioxide to methanol and dimethyl ether: From greenhouse gas to renewable, environmentally carbon neutral fuels and synthetic hydrocarbons. J Org Chem 2009;74:487–98. doi:10.1021/jo801260f.
[56] Olah GA. Towards oil independence through renewable methanol chemistry. Angew Chemie - Int Ed 2013;52:104–7. doi:10.1002/anie.201204995.
[57] Larminie J, Dicks A. Direct Methanol Fuel Cells. Fuel Cell Syst. Explain., John Wiley & Sons, Ltd; 2013, p. 141–61. doi:10.1002/9781118878330.ch6.
[58] Larminie J, Dicks A. Fuelling Fuel Cells. Fuel Cell Syst. Explain., John Wiley & Sons, Ltd; 2013, p. 229–308. doi:10.1002/9781118878330.ch8.
[59] Shih CF, Zhang T, Li J, Bai C. Powering the Future with Liquid Sunshine. Joule 2018:1–25. doi:10.1016/j.joule.2018.08.016.
[60] Bergins C, Tran K, Koytsoumpa E, Kakaras E, Buddenberg T, Sigurbjörnsson Ó. Power to Methanol Solutions for Flexible and Sustainable Operations in Power and Process Industries. Power-Gen Eur 2015.
[61] Bergins C, Koytsoumpa E-I, Buddenberg T, Wu S, Sigurbjornsson O, Tran KC, et al. The Challenge of Energy Storage in Europe : Focus on Power to Fuel 2017;138:1–10. doi:10.1115/1.4032544.
[62] Héder M. From NASA to EU: The evolution of the TRL scale in Public Sector Innovation. Innov J 2017;22:1–23.
[63] Pérez-Fortes M, Tzimas E. Techno-economic and environmental evaluation of CO2 utilisation for fuel production. Synthesis of methanol and formic acid. 2016. doi:10.2790/981669.
[64] Carbon Recycling International | below50 n.d. https://below50.org/project/carbon-recycling-international/ (accessed May 14, 2018).
[65] Atsonios K, Panopoulos KD, Kakaras E. Investigation of technical and economic aspects for methanol production through CO2 hydrogenation. Int J Hydrogen Energy 2016;41:2202–14. doi:10.1016/j.ijhydene.2015.12.074.
[66] Ledakowicz S, Nowicki L, Petera J, Nizioł J, Kowalik P, Gołębiowski A. Kinetic characterisation of catalysts for methanol synthesis. Chem Process Eng - Inz Chem i Proces 2013;34:497–506. doi:10.2478/cpe-2013-0040.
[67] Hankin A, Shah N. Process exploration and assessment for the production of methanol and dimethyl ether from carbon dioxide and water. Sustain Energy Fuels 2017:1541–56. doi:10.1039/C7SE00206H.
[68] Alvarado M. Methanol. MethanolOrg 2016:1. doi:10.1044/leader.PPL.21022016.20.
[69] The Methanol Industry | Methanol Institute | www.methanol.org n.d. https://www.methanol.org/the-methanol-industry/ (accessed July 19, 2018).

[70] Leung DYC, Caramanna G, Maroto-valer MM. An overview of current status of carbon dioxide capture and storage technologies. Renew Sustain Energy Rev 2014;39:426–43. doi:10.1016/j.rser.2014.07.093.
[71] Matzen M, Demirel Y. Methanol and dimethyl ether from renewable hydrogen and carbon dioxide: Alternative fuels production and life-cycle assessment. J Clean Prod 2016;139:1068–77. doi:10.1016/j.jclepro.2016.08.163.
[72] Institute for Occupational Safety and Health of the German Social Accident Insurance. Dimethyl Ether - IFA GESTIS Substance database n.d.
[73] Dimethyl ether - National Library of Medicine HSDB Database n.d. https://toxnet.nlm.nih.gov/cgi-bin/sis/search/a?dbs+hsdb:@term+@DOCNO+354 (accessed July 3, 2019).
[74] Alternative Fuels Data Center: Dimethyl Ether n.d. https://afdc.energy.gov/fuels/emerging_dme.html (accessed July 3, 2019).
[75] Dimethyl ether DME Fact Sheet n.d. http://www.etipbioenergy.eu/fact-sheets/dimethyl-ether-dme-fact-sheet#app (accessed September 18, 2019).
[76] Lee S, Sardesai A. Liquid phase methanol and dimethyl ether synthesis from syngas 2005;32:197–207. doi:10.1007/s11244-005-2891-8.
[77] Schmidt O, Gambhir A, Staffell I, Hawkes A, Nelson J, Few S. Future cost and performance of water electrolysis : An expert elicitation study. Int J Hydrogen Energy 2017;42:30470–92. doi:10.1016/j.ijhydene.2017.10.045.
[78] Fraile D, Lanoix J-C, Maio P, Rangel A, Torres A. Overview of the market segmentation for hydrogen across potential customer groups, based on key application areas. 2015.
[79] Hydrogen in Industry | Hydrogen n.d. https://hydrogeneurope.eu/hydrogen-industry (accessed July 10, 2019).
[80] Santos DMF, Sequeira CAC, Figueiredo JL. Hydrogen production by alkaline water electrolysis. 2017 Int Conf Adv Comput Commun Informatics, ICACCI 2017 2013;36:1176–93.
[81] Kotowicz J, Jurczyk M, Ecel DW, Ogulewicz W. Analysis of Hydrogen Production in Alkaline Electrolyzers. J Power Technol 2016;96:149–56.
[82] Schalenbach M, Zeradjanin AR, Kasian O, Cherevko S. A Perspective on Low-Temperature Water Electrolysis – Challenges in Alkaline and Acidic Technology 2018;13:1173–226. doi:10.20964/2018.02.26.
[83] Sapountzi FM, Gracia JM, Weststrate CJ (Kee. J, Fredriksson HOA, Niemantsverdriet JW (Hans. Electrocatalysts for the generation of hydrogen, oxygen and synthesis gas. Prog Energy Combust Sci 2017;58:1–35. doi:10.1016/j.pecs.2016.09.001.
[84] Xiang C, Papadantonakis KM, Lewis NS. Principles and implementations of electrolysis systems for water splitting. Mater Horizons 2016;3:169–73. doi:10.1039/c6mh00016a.
[85] Zeng K, Zhang D. Recent progress in alkaline water electrolysis for hydrogen production and applications. Prog Energy Combust Sci 2010;36:307–26. doi:10.1016/j.pecs.2009.11.002.
[86] Ni M, Leung MKH, Leung DYC. Technological development of hydrogen production by solid oxide electrolyzer cell (SOEC). Int J Hydrogen Energy 2008;33:2337–54. doi:10.1016/j.ijhydene.2008.02.048.
[87] O'Brien JE. Thermodynamic Considerations for Thermal Water Splitting Processes and High Temperature Electrolysis 2009:639–51. doi:10.1115/imece2008-68880.
[88] Ursua A, Gandia LM, Sanchis P. Hydrogen Production From Water Electrolysis: Current Status and Future Trends. Proc IEEE 2012;100:410–26. doi:10.1109/JPROC.2011.2156750.
[89] Lin Y, Beale SB. Performance predictions in solid oxide fuel cells. Appl Math Model 2006;30:1485–96. doi:10.1016/j.apm.2006.03.009.
[90] Thyssenkrupp. Hydrogen from large-scale electrolysis - Efficienct solutions for sustainable chemicals and energy storage n.d.
[91] Boretti A. Renewable hydrogen to recycle CO2 to methanol. Int J Hydrogen Energy 2013;38:1806–12. doi:10.1016/j.ijhydene.2012.11.097.
[92] Products • Nel Hydrogen n.d. https://nelhydrogen.com/products/ (accessed July 10, 2019).
[93] Matzen M, Alhajji M. Chemical storage of wind energy by renewable methanol production : Feasibility analysis using a multi-criteria decision matrix 2015;93. doi:10.1016/j.energy.2015.09.043.
[94] Diéguez PM, Ursúa A, Sanchis P, Sopena C, Guelbenzu E, Gandía LM. Thermal performance of a commercial alkaline water electrolyzer: Experimental study and mathematical modeling. Int J Hydrogen Energy 2008;33:7338–54. doi:10.1016/j.ijhydene.2008.09.051.

[95] Sherif SA, Barbir F, Veziroglu TN. Wind energy and the hydrogen economy-review of the technology. Sol Energy 2005;78:647–60. doi:10.1016/j.solener.2005.01.002.
[96] Reiter G, Lindorfer J. Global warming potential of hydrogen and methane production from renewable electricity via power-to-gas technology 2015:477–89. doi:10.1007/s11367-015-0848-0.
[97] Smolinka T. Water Electrolysis: Status and Potential for Development 2014.
[98] Millet P, Grigoriev S. Chapter 2 - Water Electrolysis Technologies. In: Gandía LM, Arzamendi G, Diéguez PM, editors. Renew. Hydrog. Technol., Amsterdam: Elsevier; 2013, p. 19–41. doi:https://doi.org/10.1016/B978-0-444-56352-1.00002-7.
[99] Fuel Cell Today. Water Electrolysis & Renewable Energy Systems. 2013. doi:10.1017/CBO9781107415324.004.
[100] Institute of Engineering Thermodynamics - Research on Electrolysis at the DLR n.d. https://www.dlr.de/tt/en/desktopdefault.aspx/tabid-2911/4400_read-6457/ (accessed July 10, 2019).
[101] Schalenbach M, Tjarks G, Carmo M, Lueke W, Mueller M, Stolten D. Acidic or Alkaline ? Towards a New Perspective on the Efficiency of Water Electrolysis 2016;163. doi:10.1149/2.0271611jes.
[102] Nafion™ membranes - Delivering on the Promise of Clean Energy n.d. https://www.chemours.com/Nafion/en_US/index.html (accessed October 17, 2019).
[103] Nikiforov A, Christensen E, Petrushina I, Oluf J, J. N. Advanced Construction Materials for High Temperature Steam PEM Electrolysers. Electrolysis 2012. doi:10.5772/51928.
[104] Carmo M, Fritz DL, Mergel J, Stolten D. A comprehensive review on PEM water electrolysis. Int J Hydrogen Energy 2013;38:4901–34. doi:10.1016/j.ijhydene.2013.01.151.
[105] Stolten D, Scherer V, editors. Transition to Renewable Energy Systems. Wiley-VCH Verlag GmbH & Co. KGaA; n.d.
[106] Emanuele Taibi and Raul Miranda (IRENA), Wouter Vanhoudt, Thomas Winkel J-CL and FB (Hinicio). Hydrogen From Renewable Power. 2018.
[107] Gabbasa M, Sopian K, Fudholi A. ScienceDirect A review of unitized regenerative fuel cell stack : Material , design and research achievements. Int J Hydrogen Energy 2014;39:17765–78. doi:10.1016/j.ijhydene.2014.08.121.
[108] Buttler A, Spliethoff H. Current status of water electrolysis for energy storage, grid balancing and sector coupling via power-to-gas and power-to-liquids: A review. Renew Sustain Energy Rev 2018;82:2440–54. doi:10.1016/j.rser.2017.09.003.
[109] Millet P, Mbemba N, Grigoriev SA, Fateev VN, Aukauloo A, Etiévant C. Electrochemical performances of PEM water electrolysis cells and perspectives. Int J Hydrogen Energy 2011;36:4134–42. doi:10.1016/j.ijhydene.2010.06.105.
[110] Millet P, Ngameni R, Grigoriev SA, Fateev VN. Scientific and engineering issues related to PEM technology : Water electrolysers , fuel cells and unitized regenerative systems. Int J Hydrogen Energy 2010;36:4156–63. doi:10.1016/j.ijhydene.2010.06.106.
[111] Ni M, Leung MKH, Leung DYC. Energy and exergy analysis of hydrogen production by a proton exchange membrane (PEM) electrolyzer plant 2008;49:2748–56. doi:10.1016/j.enconman.2008.03.018.
[112] Minh NQ, Mogensen MB. Reversible Solid Oxide Fuel Cell Technology for Green Fuel and Power Production. Interface Mag 2013;22:55–62. doi:10.1149/2.F05134if.
[113] Shi Y, Cai N, Li W, Luo Y, Ni M. High Temperature Electrolysis for Hydrogen or Syngas Production from Nuclear or Renewable Energy. Handb Clean Energy Syst 2015:1–19. doi:10.1002/9781118991978.hces146.
[114] Minh NQ. Solid oxide fuel cells for power generation and hydrogen production. J Korean Ceram Soc 2010;47:1–7. doi:10.4191/KCERS.2010.47.1.001.
[115] EG&G Technical Services I. Fuel Cell Handbook. 7th ed. U.S. Department of Energy; 2004.
[116] Stempien JP. Effects of electrode microstructure, operating temperature and exhaust gas recirculation on a Solid Oxide Electrolyzer cell and system performance n.d. doi:10.13140/RG.2.1.2484.0568.
[117] Elder R, Allen R. Nuclear heat for hydrogen production: Coupling a very high/high temperature reactor to a hydrogen production plant. Prog Nucl Energy 2009;51:500–25. doi:10.1016/j.pnucene.2008.11.001.
[118] Hauch A, Mogensen MB. Advances in Medium and High Temperature Solid Oxide Fuel Cell Technology. vol. 574. 2017. doi:10.1007/978-3-319-46146-5.
[119] Guan J, Minh N, Ramamurthi B, Ruud J, Hong J-K, Riley P, et al. High performance flexible reversible solid oxide fuel cell 2006.

[120] Mermelstein J, Posdziech O. Development and Demonstration of a Novel Reversible SOFC System for Utility and Micro Grid Energy Storage. Fuel Cells 2017;17:562–70. doi:10.1002/fuce.201600185.
[121] Gómez SY, Hotza D. Current developments in reversible solid oxide fuel cells. Renew Sustain Energy Rev 2016;61:155–74. doi:10.1016/j.rser.2016.03.005.
[122] Wendel CH, Braun RJ. Design and techno-economic analysis of high efficiency reversible solid oxide cell systems for distributed energy storage. Appl Energy 2016;172:118–31. doi:10.1016/j.apenergy.2016.03.054.
[123] Kazempoor P, Braun RJ. Model validation and performance analysis of regenerative solid oxide cells: Electrolytic operation. Int J Hydrogen Energy 2014;39:2669–84. doi:10.1016/j.ijhydene.2013.12.010.
[124] Wendel CH, Kazempoor P, Braun RJ. Novel electrical energy storage system based on reversible solid oxide cells: System design and operating conditions. J Power Sources 2015;276:133–44. doi:10.1016/j.jpowsour.2014.10.205.
[125] Kazempoor P, Braun RJ. Model validation and performance analysis of regenerative solid oxide cells for energy storage applications: Reversible operation. Int J Hydrogen Energy 2014;39:5955–71. doi:10.1016/j.ijhydene.2014.01.186.
[126] Santhanam S, Heddrich MP, Riedel M, Friedrich KA. Theoretical and experimental study of Reversible Solid Oxide Cell (r-SOC) systems for energy storage. Energy 2017;141:202–14. doi:10.1016/j.energy.2017.09.081.
[127] Er-Rbib H, Kezibri N, Bouallou C. Dynamic simulation of Reversible Solid Oxide Cell (RSOC). Chem Eng Trans 2017;61:1075–80. doi:10.3303/CET1761177.
[128] Simonsen SB, Graves C, Jensen SH, Mogensen MB, Ebbesen SD. Eliminating degradation in solid oxide electrochemical cells by reversible operation. Nat Mater 2014;14:239–44. doi:10.1038/nmat4165.
[129] Liu S-S, Ai N, Chen K, Jiang SP, Koyama M. Why solid oxide cells can be reversibly operated in solid oxide electrolysis cell and fuel cell modes? Phys Chem Chem Phys 2015;17:31308–15. doi:10.1039/c5cp05065k.
[130] Quoilin S, Broek M Van Den, Lemort V, Dewallef P, Declaye S. Techno-economic survey of Organic Rankine Cycle (ORC) systems. Renew Sustain Energy Rev 2013;22:168–86. doi:10.1016/j.rser.2013.01.028.
[131] EXERGY - ORC Generating electricity from low-medium temperature heat sources n.d. http://www.exergy-orc.com/orc (accessed April 11, 2019).
[132] The ORC Technology | TURBODEN n.d. https://www.turboden.com/turboden-orc-technology/1062/the-orc-technology (accessed April 11, 2019).
[133] Macchi E, Astolfi M, editors. Organic Rankine Cycle (ORC) Power Systems. Elsevier; 2017. doi:10.1016/C2014-0-04239-6.
[134] Astolfi M, Martelli E, Pierobon L. 7 - Thermodynamic and technoeconomic optimization of Organic Rankine Cycle systems. In: Macchi E, Astolfi M, editors. Org. Rank. Cycle Power Syst., Woodhead Publishing; 2017, p. 173–249. doi:https://doi.org/10.1016/B978-0-08-100510-1.00007-7.
[135] Februar I. Sunfire supplies Boeing with largest reversible solid oxide electrolyser/fuel cell system. Fuel Cells Bull 2016;2016:1. doi:10.1016/s1464-2859(16)70002-2.
[136] Léonard G, Giulini D, Villarreal-Singer D. Design and Evaluation of a High-Density Energy Storage Route with CO2 Re-Use, Water Electrolysis and Methanol Synthesis. Comput Aided Chem Eng 2016;38:1797–802. doi:10.1016/B978-0-444-63428-3.50304-0.
[137] Léonard G, Toye D, Heyen G. Assessment of solvent degradation within a global process model of post-combustion CO2 capture. Proc. 24th Eur. Symp. Comput. Aided Process Eng. – ESCAPE 24, vol. 33, Elsevier; 2014, p. 13–8. doi:10.1016/B978-0-444-63456-6.50003-X.
[138] Léonard G, Crosset C, Toye D, Heyen G. Influence of process operating conditions on solvent thermal and oxidative degradation in post-combustion CO2 capture. Comput Chem Eng 2015;83:121–30. doi:10.1016/j.compchemeng.2015.05.003.
[139] Yuan X, Cao W, Hu J, Chen X, Zhu Q, Duan Q, et al. Coordinated Control of a Wind-Methanol-Fuel Cell System with Hydrogen Storage. Energies 2017;10:2053. doi:10.3390/en10122053.
[140] Di Giorgio P, Desideri U. Potential of reversible solid oxide cells as electricity storage system. Energies 2016;9. doi:10.3390/en9080662.
[141] Mottaghizadeh P, Santhanam S, Heddrich MP, Friedrich KA, Rinaldi F. Process modeling of a reversible solid oxide cell (r-SOC) energy storage system utilizing commercially available SOC reactor. Energy Convers Manag 2017;142:477–93. doi:10.1016/j.enconman.2017.03.010.

[142] Ferrero D. Design, development and testing of SOEC-based Power- to-Gas systems for conversion and storage of RES into synthetic methane 2016. doi:10.6092/polito/porto/2645377.
[143] Soltanieh M, Azar KM, Saber M. Development of a zero emission integrated system for co-production of electricity and methanol through renewable hydrogen and CO2 capture. Int J Greenh Gas Control 2012;7:145–52. doi:10.1016/j.ijggc.2012.01.008.
[144] Mathieu P, Nihart R. Zero-Emission MATIANT Cycle. J Eng Gas Turbines Power 2008;121:116. doi:10.1115/1.2816297.
[145] Akikur RK, Saidur R, Ping HW, Ullah KR. Performance analysis of a co-generation system using solar energy and SOFC technology. Energy Convers Manag 2014;79:415–30. doi:10.1016/j.enconman.2013.12.036.
[146] Hank C, Gelpke S, Schnabl A, White RJ, Full J, Wiebe N, et al. Economics & carbon dioxide avoidance cost of methanol production based on renewable hydrogen and recycled carbon dioxide – power-to-methanol. Sustain Energy Fuels 2018:1244–61. doi:10.1039/C8SE00032H.
[147] Rivera-Tinoco R, Farran M, Bouallou C, Auprêtre F, Valentin S, Millet P, et al. Investigation of power-to-methanol processes coupling electrolytic hydrogen production and catalytic CO2 reduction. Int J Hydrogen Energy 2016;41:4546–59. doi:10.1016/j.ijhydene.2016.01.059.
[148] Ni M, Leung MKH, Leung DYC. An electrochemical model of a solid oxide steam electrolyzer for hydrogen production. Chem Eng Technol 2006;29:636–42. doi:10.1002/ceat.200500378.
[149] Ni M, Leung MKH, Leung DYC. Parametric study of solid oxide steam electrolyzer for hydrogen production. Int J Hydrogen Energy 2007;32:2305–13. doi:10.1016/j.ijhydene.2007.03.001.
[150] Ni M, Leung MKH, Leung DYC. Parametric study of solid oxide fuel cell performance. Energy Convers Manag 2007;48:1525–35. doi:10.1016/j.enconman.2006.11.016.
[151] Ni M, Zhao TS, editors. Solid Oxide Fuel Cells: From Materials to System Modeling. Cambridge: The Royal Society of Chemistry; 2013. doi:10.1039/9781849737777.
[152] Doherty W, Reynolds A, Kennedy D. Modelling and Simulation of a Biomass Gasification-Solid Oxide Fuel Cell Combined Heat and Power Plant Using Aspen Plus. ECOS 2009 - 22nd Int Conf Effic Cost, Optim Simul Environ Impact Energy Syst 2009:1711–20.
[153] Ferguson JR, Fiard JM, Herbin R. Three-dimensional numerical simulation for various geometries of solid oxide fuel cells. J Power Sources 1996;58:109–22. doi:10.1016/0378-7753(95)02269-4.
[154] Noren DA, Hoffman MA. Clarifying the Butler-Volmer equation and related approximations for calculating activation losses in solid oxide fuel cell models. J Power Sources 2005;152:175–81. doi:10.1016/j.jpowsour.2005.03.174.
[155] Menon V, Janardhanan VM, Deutschmann O. A mathematical model to analyze solid oxide electrolyzer cells (SOECs) for hydrogen production. Chem Eng Sci 2014;110:83–93. doi:10.1016/j.ces.2013.10.025.
[156] Poling BE, Prausnitz JM, O'Connell JP. The properties of gases and liquids. 5th ed. McGRAW-HILL; 2001. doi:10.1021/ja0048634.
[157] Krishna R, van Baten JMM. Investigating the validity of the Bosanquet formula for estimation of diffusivities in mesopores. Chem Eng Sci 2012;69:684–8. doi:10.1016/j.ces.2011.11.026.
[158] Veldsink JW, van Damme RMJ, Versteeg GF, van Swaaij WPM. The use of the dusty-gas model for the description of mass transport with chemical reaction in porous media. Chem Eng J Biochem Eng J 1995;57:115–25. doi:10.1016/0923-0467(94)02929-6.
[159] Welty J, Wicks CE, Rorrer GL, Wilson RE. Fundamentals of Momentum, Heat, and Mass Transfer. 5th ed. Wiley; 2008.
[160] Cunningham RE, Williams RJJ. Diffusion in Gases and Porous Media. 1st ed. New York: Springer; 1980. doi:10.1007/978-1-4757-4983-0.
[161] He W, Lv W, Dickerson J. Gas Diffusion Mechanisms and Models. Gas Transp. Solid Oxide Fuel Cells, 2014, p. 9–17. doi:10.1007/978-3-319-09737-4.
[162] Ni M, Leung MKH, Leung DYC. A modeling study on concentration overpotentials of a reversible solid oxide fuel cell. J Power Sources 2006;163:460–6. doi:10.1016/j.jpowsour.2006.09.024.
[163] Herring JS, Brien JEO, Stoots CM, Hawkes GL, Hartvigsen JJ, Shahnam M. Progress in high-temperature electrolysis for hydrogen production using planar SOFC technology 2007;32:440–50. doi:10.1016/j.ijhydene.2006.06.061.
[164] Barelli L, Bidini G, Cinti G. Airflow Management in Solid Oxide Electrolyzer (SOE) Operation: Performance Analysis. ChemEngineering 2017;1:13. doi:10.3390/chemengineering1020013.
[165] Cai Q, Luna-Ortiz E, Adjiman CS, Brandon NP. The effects of operating conditions on the

performance of a solid oxide steam electrolyser: A model-based study. Fuel Cells 2010;10:1114–28. doi:10.1002/fuce.200900211.
[166] Ursua A, Sanchis P. Static-dynamic modelling of the electrical behaviour of a commercial advanced alkaline water electrolyser. Int J Hydrogen Energy 2012;37:18598–614. doi:10.1016/j.ijhydene.2012.09.125.
[167] Ulleberg Ø. Stand-Alone Power Systems for the Future: Optimal Design, Operation & Control of Solar-Hydrogen Energy Systems. Norwegian University of Science and Technology Trondheim, 1998.
[168] Van-Dal ÉS, Bouallou C. Design and simulation of a methanol production plant from CO2 hydrogenation. J Clean Prod 2013;57:38–45. doi:10.1016/j.jclepro.2013.06.008.
[169] Al-Malah KIM. Aspen Plus®. Hoboken, NJ, USA: John Wiley & Sons, Inc.; 2016. doi:10.1002/9781119293644.
[170] Bussche KM Vanden, Froment GFF. A Steady-State Kinetic Model for Methanol Synthesis and the Water Gas Shift Reaction on a Commercial Cu/ZnO/Al2O3 Catalyst. J Catal 1996;161:1–10. doi:10.1006/jcat.1996.0156.
[171] Mignard D, Pritchard C. On the use of electrolytic hydrogen from variable renewable energies for the enhanced conversion of biomass to fuels. Chem Eng Res Des 2008;86:473–87. doi:10.1016/j.cherd.2007.12.008.
[172] Atsonios K, Panopoulos KD, Kakaras E. Thermocatalytic CO2 hydrogenation for methanol and ethanol production: Process improvements. Int J Hydrogen Energy 2016;41:792–806. doi:10.1016/j.ijhydene.2015.12.001.
[173] Cascetta M, Cau G, Puddu P, Serra F. Experimental investigation of a packed bed thermal energy storage system. J Phys Conf Ser 2015;012018. doi:10.1088/1742-6596/655/1/012018.
[174] Cascetta M, Serra F, Arena S, Casti E, Cau G, Puddu P. Experimental and Numerical Research Activity on a Packed Bed TES System. Energies 2016;9:1–13. doi:10.3390/en9090758.
[175] Berkeley L. Sunfire SOEC steam electrolysis module for Salzgitter Flachstahl. Fuel Cells Bull 2017;2017:12. doi:10.1016/s1464-2859(17)30269-9.
[176] Buonomano A, Calise F, Dentice M, Palombo A, Vicidomini M. Hybrid solid oxide fuel cells – gas turbine systems for combined heat and power : A review. Appl Energy 2015;156:32–85. doi:10.1016/j.apenergy.2015.06.027.
[177] Sengodan S, Lan R, Humphreys J, Du D, Xu W, Wang H. Advances in reforming and partial oxidation of hydrocarbons for hydrogen production and fuel cell applications. Renew Sustain Energy Rev 2018;82:761–80. doi:10.1016/j.rser.2017.09.071.
[178] Agyenim F, Hewitt N, Eames P, Smyth M. A review of materials, heat transfer and phase change problem formulation for latent heat thermal energy storage systems (LHTESS). Renew Sustain Energy Rev 2010;14:615–28. doi:10.1016/j.rser.2009.10.015.
[179] Lonis F, Tola V, Cau G. Renewable methanol production and use through reversible solid oxide cells and recycled CO2 hydrogenation. Fuel 2019;246:500–15. doi:10.1016/j.fuel.2019.02.108.
[180] Petipas F, Brisse A, Bouallou C. Model-based behaviour of a high temperature electrolyser system operated at various loads. J Power Sources 2013;239:584–95. doi:10.1016/j.jpowsour.2013.03.027.
[181] Villareal Singer D. Reversible solid oxide cells for bidirectional energy conversion in spot electricity and fuel markets. 2017. doi:10.7916/D8V988P6.
[182] Al-Kalbani H, Xuan J, García S, Wang H. Comparative energetic assessment of methanol production from CO2: Chemical versus electrochemical process. Appl Energy 2016;165:1–13. doi:10.1016/j.apenergy.2015.12.027.
[183] Im-orb K, Saebea D, Visitdumrongkul N, Arpornwichanop A, Patcharavorachot Y. Flowsheet-based model and exergy analysis of solid oxide electrolysis cells for clean hydrogen production. J Clean Prod 2017;170:1–13. doi:10.1016/j.jclepro.2017.09.127.
[184] Drescher U, Brüggemann D. Fluid selection for the Organic Rankine Cycle (ORC) in biomass power and heat plants. Appl Therm Eng 2007;27:223–8. doi:10.1016/j.applthermaleng.2006.04.024.
[185] Victor RA, Kim JK, Smith R. Composition optimisation of working fluids for organic Rankine cycles and Kalina cycles. Energy 2013;55:114–26. doi:10.1016/j.energy.2013.03.069.
[186] Linstrom P. NIST Chemistry WebBook, NIST Standard Reference Database 69. Natl Inst Stand Technol 1997. doi:https://doi.org/10.18434/T4D303.
[187] FLEXCHX. Review of electrolysis technologies and their integration alternatives - FLEXCHX Flexible combined production of power, heat and transport fuels from renewable energy sources

2018:35.
[188] Pérez-Fortes M, Schöneberger JC, Boulamanti A, Tzimas E. Methanol synthesis using captured CO2 as raw material : Techno-economic and environmental assessment. Appl Energy 2016;161:718–32. doi:10.1016/j.apenergy.2015.07.067.
[189] Sedighnejad H, Iqbal T, Quaicoe J. Compressed air energy storage system control and performance assessment using energy harvested index. Electron 2014;3:1–21. doi:10.3390/electronics3010001.